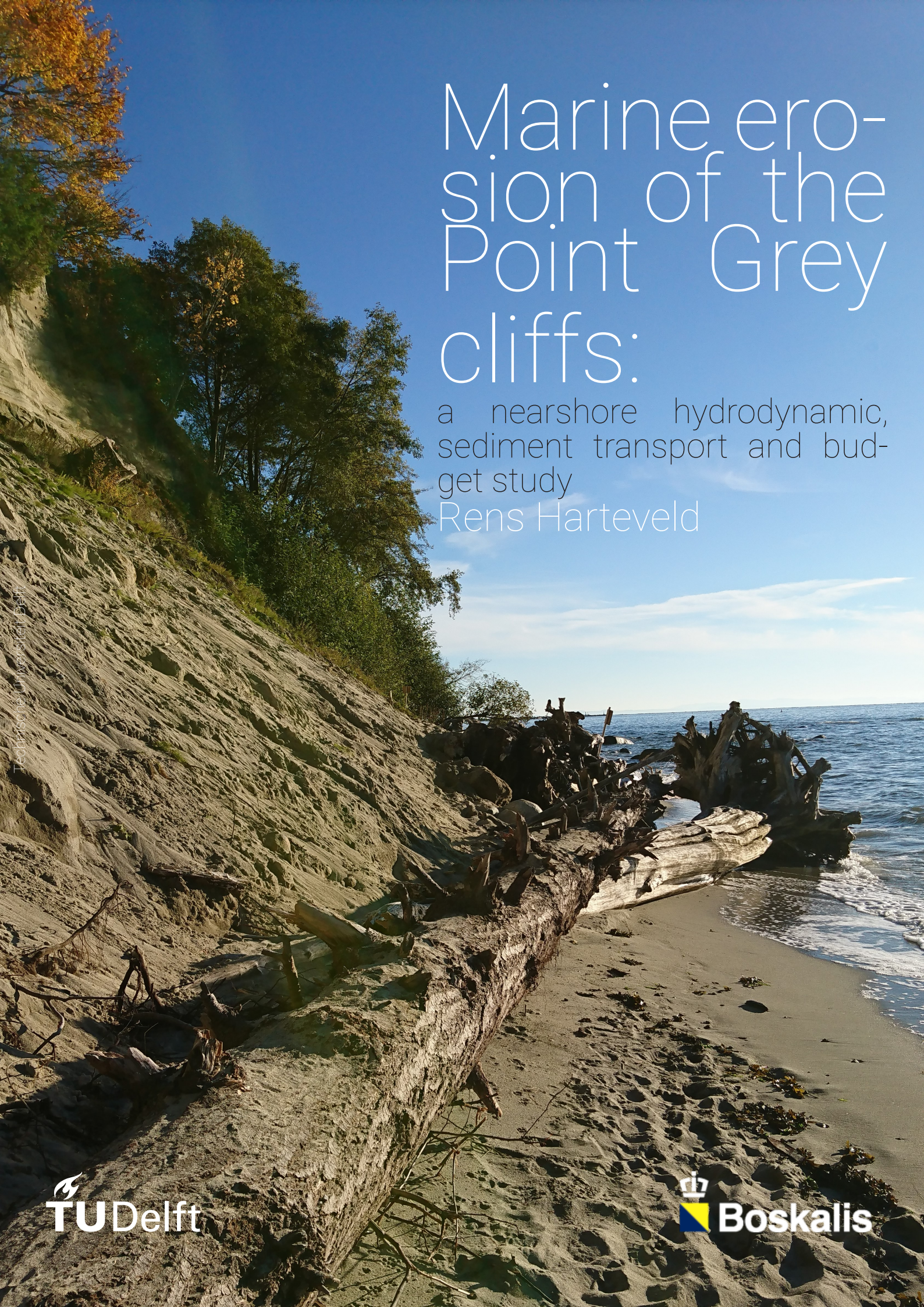

Marine erosion of the Point Grey cliffs:

a nearshore hydrodynamic, sediment transport and budget study

Rens Harteveld

Technische Universiteit Delft

TU Delft

Boskalis

Marine erosion of the Point Grey cliffs:

a nearshore hydrodynamic, sediment transport and budget study

by

Rens Harteveld

to obtain the degree of Master of Science
at the Delft University of Technology,
to be defended publicly on Thursday June 13, 2019 at 10:45 AM.

Student number:	4250990	
Project duration:	July 2, 2018 – June 13, 2019	
Thesis committee:	Prof. dr. ir. S. G. J. Aarninkhof,	TU Delft, chair
	Ir. S. G. Pearson,	TU Delft/Deltares
	Dr. ir. R. J. Labeur,	TU Delft
	Drs. D. Rijks,	Boskalis

An electronic version of this thesis is available at `http://repository.tudelft.nl/`.

TU Delft

Preface

This thesis is the last in completing the Hydraulic Engineering Masters program at the Delft University of Technology. It's part of the *Living Breakwaters* project from the University of British Columbia in Vancouver, Canada. The thesis work was primarily done at Boskalis in Papendrecht.

First of all I would like to show my gratitude towards the following people: Daan, thank you for guidance and support throughout the project and Boskalis. Your ideas and motivation during our many discussions were of great help. Stuart, there is not a better daily supervisor I could have wished for. Always available when I was stuck or to read anything I produced. Your enthusiasm and feedback helped me a lot! Thank you Stefan for chairing the committee and your input during the meetings. Then to Robert Jan for enabling me to think more critically about models. Lastly a special thanks to Pieter Koen from Deltares for helping me to set-up and improve the model during several stages.

Secondly, several people from Canada deserve acknowledgments as well. Kees and Tugce, thank you for support from overseas and during my stay in Vancouver. You made me feel at home right away! Also thanks to Doug for your input and chats during my visit. Lastly to Gabriela and Deanne for their help during the sediment collection and sieving.

Lastly I would like to thank my family and friends for their support during my studies and for making the past 7 years an experience to never forget.

Rens Harteveld
Delft, June 2019

Summary

The Point Grey cliffs, located in Vancouver, Canada, at the edge of the Strait of Georgia, are eroding. The cliff's retreat endangers university facilities and infrastructure on top as well as archaeological treasures hidden inside the cliffs. The geology consists mainly of unconsolidated material, a mix of sands and silts with a mean diameter of ~300 µm. Retreat estimations show that the cliffs have been receding due to marine erosion and sub-aerial processes since 1938. The main sub-aerial processes at the Point Grey cliffs are groundwater seepage and surface water run-off. Wave-induced sediment transport is the key marine erosion mechanism. Together these mechanisms lead to the Point Grey cliff's retreat.

Four marine erosion time scales are identified for the erosion of the Point Grey cliffs, namely: seconds to days, days to months, years to decades and centuries to millennia. During high water levels of high tides together with storm surges, the cliff toe may be directly attacked by waves and wave run-up. The erosion mechanism within the second time scale, days to months, are sediment transports due to local wave-induced or tidal currents. On the third time scale, a sediment budget deficit due to supply changes by nature or induced by coastal interventions in the coastal system. The Fraser River is an important factor on both the sediment transports and budgets. The fourth time scale, centuries to millennia, encompasses climate change effects of sea-level rise and intensified wave conditions. In the near future sea-level rise may happen within decades instead of centuries.

A numerical hydrodynamic model, with sediment transport, was developed to study marine erosion time on the time scale of days to years; investigating the alongshore sediment transport over days and potential sediment deficit to the Point Grey cliff system. Two main reasons to study these time scales are that the literature points to these two time scales as the main causes for the marine erosion, and the time scales can be studied with the same model. The coastal system was then divided into discrete scenarios to analyze the hydrodynamics and sediment transports over cross-sections. The sediment transports can then be manually extrapolated to yearly budgets. The water levels in the model are calibrated, while local currents/waves/sediment transport are not. The model shows high sensitivity to differences in significant wave height and locations of the cross-sections. Other sediment sizes did not prove to affect model results as much. The model serves to improve understanding of the alongshore sediment transport is the main relevant process and whether it is wave-induced.

The coastal system of the Point Grey cliffs is shaped by three important physical processes: the tide, waves, and riverine sediment input. The tide at the Point Atkinson has a mixed semi-diurnal tide with a tidal range of 2 to 5 m. The low energy wave climate is locally generated in the Strait of Georgia. The Point Grey cliffs are most vulnerable for west northwest incoming waves. The significant wave height of regular wave conditions is in the order of 0.5 m with peak wave periods of 7 to 9 s. A five year return period storm has significant wave heights the order of 1.1 m. The storm surge with 1.3 year return period equals 0.6 m. The North Arm Fraser River is the last important component of the coastal system. Its seasonal variability is expressed by the terms: freshet during snow melt in the summer and non-freshet. During freshet 80% of the yearly discharge flows through the North Arm, approximately 1200 $m^3 s^{-1}$. Off-season, this decreases to 375 $m^3 s^{-1}$. Upstream, the river carries $17 - 19 \cdot 10^9$ $kg y^{-1}$ of which 15% is clay, 50% silt, and 35% sand. The North Arm carries 3 to 9% of this sediment to the Strait of Georgia.

Results show flow velocities of ~12 $cm s^{-1}$ during ebb on the shallow shelf in front of the cliffs. The flood tide pulls the river flow northwards. Ebb currents counteract the river outflow and both deflect westwards away from the cliffs. The scenario results show that sediments transport is primarily initiated by waves. Tidal- or river currents did not prove significant enough to initiate transport of the local sands (380 µm median diameter). The modelled wave-driven sediment transport is mainly bed-load transport in the direction of wave propagation. Previous studies state alongshore sediment transport directed northwards to the Spanish Banks, while the sediment budget shows a sediment flow in the opposite direction towards the south. The model does show unforeseen sediment transports from below the Museum of Anthropology towards the North Arm Breakwater. Lastly, the model implies that the North Arm Fraser River is not able to transport any

sediment to the Point Grey cliffs other than silt. Literature states that sands carried by the North Arm Fraser River are flushed westwards to the deep water of the Strait of Georgia. The channelization of the North Arm in 1917 is thought to be the critical factor here. The model was unable to reproduce the sediment outflow.

This study resulted in a substantiated current hydrodynamic overview together with new insights in the sediment transport and budget at the Point Grey cliffs. The model shows a transport path towards the North Arm breakwater not yet described by the literature. A strong indication was found for a structural sediment deficit. In future research, the degree of exposure to direct wave attack should be investigated further. Secondly, the impact of sea-level rise and intensified wave conditions should be studied by using future scenarios. The existing model can be improved by extra data collection, primarily nearshore wave data. With the help of these findings and further research, a start can be made with the technical specifications for a potential marine erosion solution, ultimately saving the Point Grey cliffs.

Contents

List of Figures

List of Tables

1 Introduction

1.1. Problem description

The Point Grey coastal cliffs have been eroding for decades and threaten damaging the buildings, infrastructure, cultural heritage and archaeological findings of the University of British Columbia (UBC) (UBC, 2004, UBC/Pacific Spirit Regional Park Cliff Management, 2000). Located on the western side of Vancouver, Canada, at the edge of the Burrard Peninsula and the Strait of Georgia the 60 m high soft cliffs (see Figure 1.1) span a range of almost 4 km. The top of cliffs houses the UBC on lands formerly inhabited by the First Nation's Musqueam. The Musqueam used the Point Grey cliffs for thousands of years as lookout for any possible intruders and the beach and forests as hunting grounds (UBC/Pacific Spirit Regional Park Cliff Management, 2000). Today the Musqueam are closely involved by the UBC regarding multiple projects, as well as any alterations made on their traditional lands (Lau, 2015, UBC/Pacific Spirit Regional Park Cliff Management, 2000). The beach below the Point Grey cliffs is called Wreck Beach. On the north side Wreck Beach changes over in Acadia Beach (Figure 1.3) with a large sand bank in front of it named Spanish Banks. On the south side Wreck Beach ends at the North Arm breakwater (Figure 1.3). Behind the breakwater a sheltered part called the Booming Ground can be found, where logs are stored before they are transported up the Fraser River to the sawing mills.

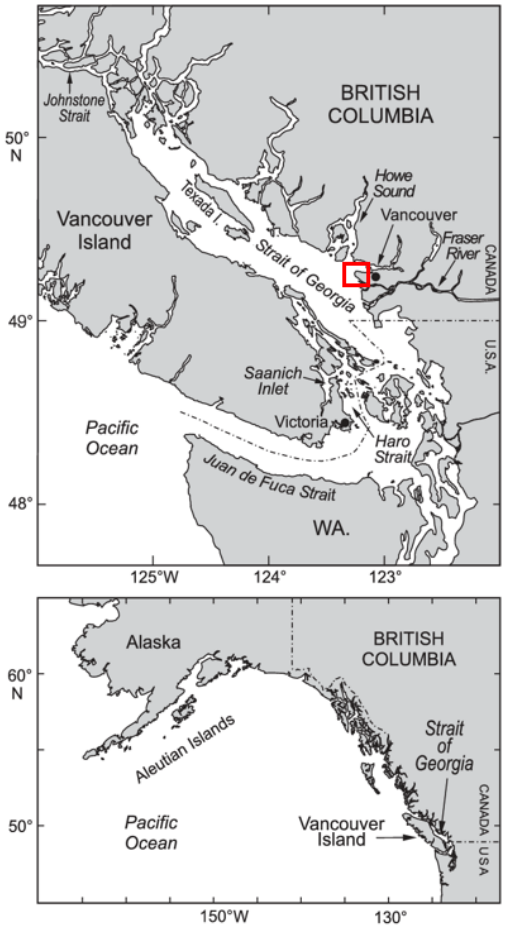

Figure 1.1: The location of the Strait of Georgia with the site of interest, the Point Grey cliffs marked by a red square. From Johannessen and Macdonald (2009).

The estimated average speeds of the coastal cliff's retreat range from 7.5 cm y^{-1} (UBC, 2004, Van Osch, 1990) to a maximum of 50.0 cm y^{-1} (Van Osch, 1990), with local maxima even reaching up to 200 cm y^{-1} (Golder Associates Ltd., 2015). Pool (1975) gives an average recession rate of 30.0 cm y^{-1}.

Figure 1.2 shows a map zoomed map of the Point Grey cliffs with important places mentioned in the paragraphs before. Figure 1.2a shows the different stakeholders in the project area. Figure 1.2b pinpoints priority areas of the Point Grey cliffs erosion along Wreck Beach.

(a) Overview Point Grey lands with UEL (University Endowment Lands). From Cantoni et al. (2019).

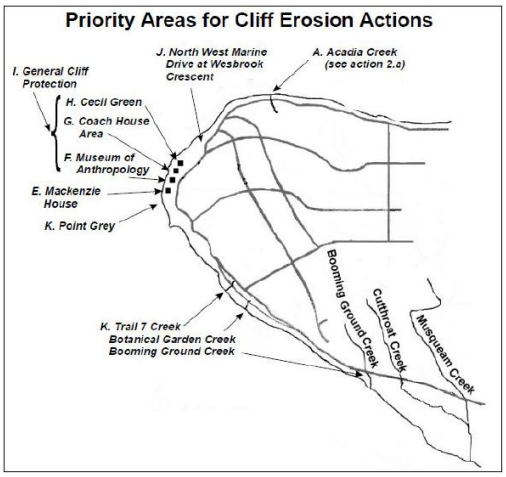

(b) Point Grey priority cliff erosion areas (UBC/Pacific Spirit Regional Park Cliff Management, 2000).

Figure 1.2: Close-up of Point Grey lands with the priority erosion areas.

Sandwell et al. (2004) tried to estimate the recession rates at two different locations with the help of aerial photography and various cliff inspections between 1976 and 2004 (Golder Associates Ltd., 2015). Golder Associates Ltd. (2015) mentions the high uncertainty in the estimates, but can give a good baseline in historical recession rates. Apparently the crest of the cliff at the spiral drain area started eroding faster after installation of test wells (see Figure 1.4a). The toe (Figure 1.4b) started eroding faster in 1979 and after installation of the berm and groynes two years later it slowed down again, but still continues. Here marine erosion is the most significant erosion mechanism (Golder Associates Ltd., 2015, Sandwell et al., 2004).

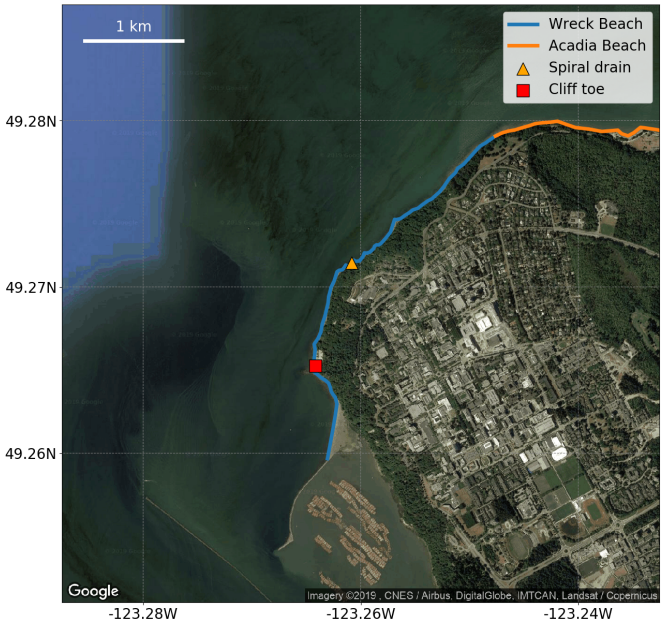

Figure 1.3: Location of spiral drain and cliff toe location.

Pool (1975) gathered results of different BSc. theses and found that the erosion of the cliffs are due to two major contributors: wave action and precipitation. The undercutting due to wave action mainly happens during higher tides and onshore wind periods (Pool, 1975). The logs lying on the beach also help to erode extra cliff material during high tides by smashing into the cliff face (UBC/Pacific Spirit Regional Park Cliff Management, 2000). In total five different reasons for the cliff erosion can be given (Doyle, 2018, UBC/Pacific Spirit Regional Park Cliff Management, 2000), which are listed below:

- Wave alongshore drift.
- Groundwater leakage from cliff aquifers.
- Freeze and thaw processes.
- Wind and rain events.
- Overland flows.

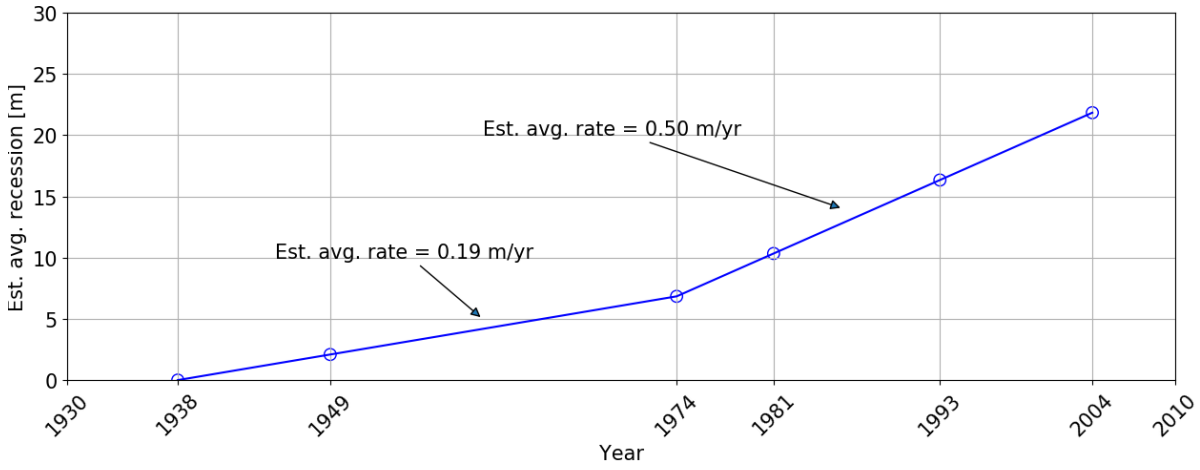

(a) Historic Point Grey cliff crest recession at spiral drain shaft area.

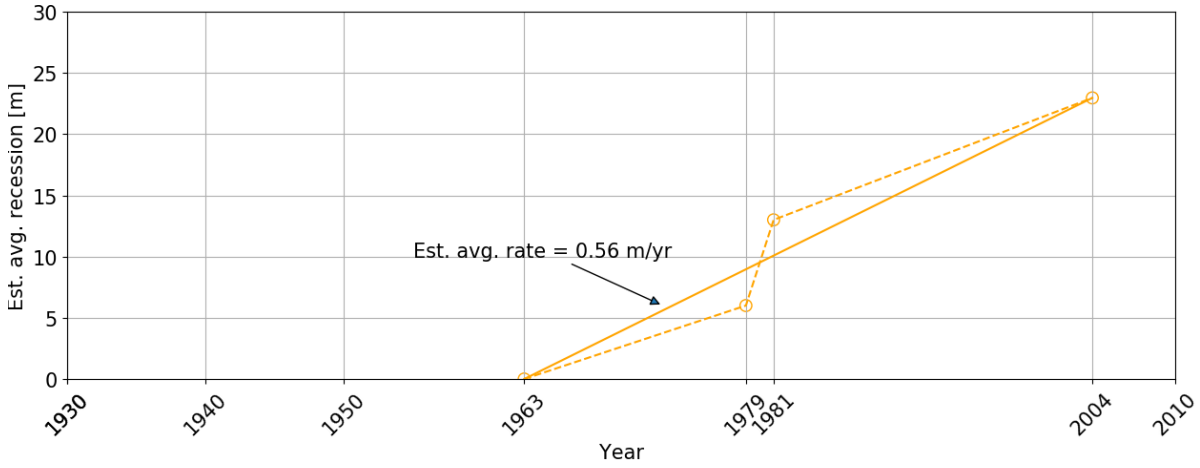

(b) Historic cliff toe recession at Point Grey.

Figure 1.4: Historic estimated average recession rates of two cliff elements at two different locations shown in Figure 1.3. From Sandwell et al. (2004).

Mines, and Resources (Canada) Energy (1980) shows the sediment transport from Point Grey towards the Spanish Banks, located to the north, which strengthens the case sketched by other sources for sediment transport going due north (Figure 1.5). However, this source does not particularly mentions the role of waves. Armstrong (1990), Golder Associates Ltd. (2015), Pool (1975), R. A. Spence Ltd. (1967), UBC (2004), UBC/Pacific Spirit Regional Park Cliff Management (2000) support the notion that the wave-induced alongshore sediment transport being the marine erosion mechanism.

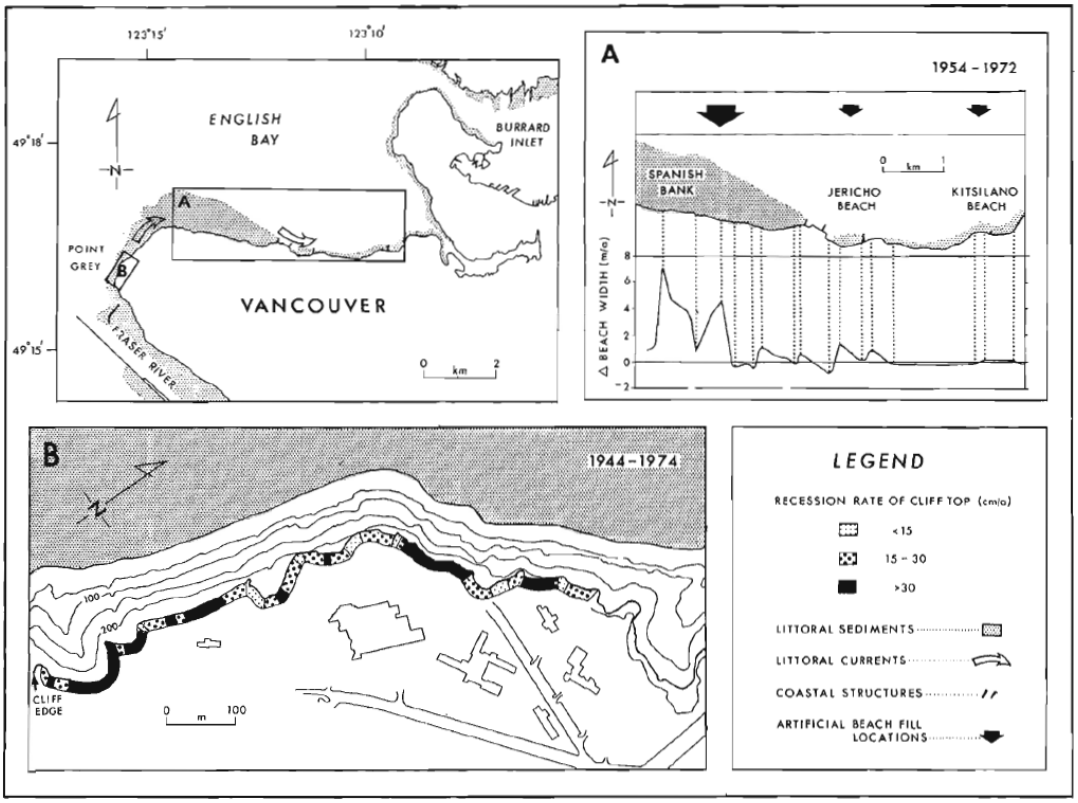

Figure 1.5: Sediment transport from Point Grey cliffs towards Spanish Banks. FromMines, and Resources (Canada) Energy (1980). Originally from Lem (1974) & Lum (1975).

1.2. Objectives

The final goal for the UBC is to stabilize and protect the cliffs from both marine and sub-aerial erosion processes. Earlier interventions have not stopped the recession completely. This study aims to be the basis for a design process to a coastal works mitigating the marine erosion and halt the retreat of the Point Grey cliffs. The goal of this study is to provide deeper insights in the hydrodynamics and the marine erosion at the Point Grey cliffs. Here we outline several key objective and corresponding research questions:

- **Put wave-driven alongshore sediment transport into context in the physical process of cliff erosion and identify any other potential marine erosion mechanisms.**
  1. *How do soft coastal cliffs erode?*
  2. *Which marine erosion mechanisms are important for the Point Grey cliffs?*

- **Get an in-depth understanding of the hydrodynamics and sediment transports and budgets in the Point Grey cliffs coastal system.**
  3. *What are the current hydrodynamics, sediment properties, sediment transport patterns, and human interventions around the coastal system at the Point Grey cliffs?*
  4. *Which physical process initiates the sediment transports at the Point Grey cliffs and how do they influence the sediment budgets?*

- **Provide recommendations to mitigate the marine erosion of the Point Grey cliffs.**
  5. *What further steps need to be taken to reach a solution for the marine erosion at the Point Grey cliffs?*

The objectives are so that firstly a better understanding of the process regarding cliff erosion is reached and to widen the perspective to indicate any other potential marine erosion mechanisms damaging the cliffs. The second objective is to gain insight in the hydrodynamics, sediment transports and human interventions in the Fraser River delta as a starting point for further in-depth study of sediment transports. Finally the results of this report can be used as technical design criteria for further studies together with recommendations to improve the current study.

1.3. Thesis structure

Chapter 1 gives an introduction to the Point Grey cliffs and motivation and approach of this study. Chapter 2 provides background information on coastal cliff erosion with particular focus on marine erosion. Chapter 3 gives an overview of the coastal system and all its components, such as hydrodynamics, sediments, human interventions etc. Next, Chapter 4 will present key findings during the site visit at the Point Grey cliffs. Chapter 5 presents the methodology used to model the hydrodynamics, sediment transport and budgets. It combines the information found in previous chapters to reach test scenarios to study the coastal system of the Point Grey cliffs in more detail. Chapter 6 guides the reader through the set-up and elements of the hydrodynamic model. Chapter 7 presents the results of the model and Chapter 8 puts these results into context of found literature and other data. Chapter 9 puts the conclusions of the research forward, together with recommendations for further improving this study. The appendices (A - G) show the results of data studies (LiDAR, wave/wind data, nautical charts, pebble counts) and additional model (calibration) results.

2

Coastal cliff erosion and its time scales

2.1. Coastal cliff erosion

Coastal cliffs are sharp interfaces between the shoreline and elevated lands. Due to marine, terrestrial, and human activities, coastal cliffs are in constant threat of retreating landward (Hampton et al., 2004). About 80% of the world's coastline consists of coastal cliffs (Emery and Kuhn, 1982). In certain cases, as with the Point Grey cliffs, the retreat of coastal cliffs is problematic considering the high-value property and infrastructure on top of the cliffs.

According to Lee and Clark (2002), Moore and Davis (2014) the erosion process of coastal cliffs can be divided in four steps (see Figure 2.1). At first the cliff material is detached from the cliff face by slope sliding, groundwater seepage, surface erosion, and wave attack. Also Edil and Vallejo (1980), Hampton et al. (2004), UBC/Pacific Spirit Regional Park Cliff Management (2000) highlight aforementioned mechanisms as primary causes of cliff erosion. Weathering and mass movement (gravity) are the last two detachment processes, which will not further discussed. Subsequently the material is transported down the slope after which it settles on the foreshore, stabilizing the slope and creating a talus protecting the cliff foot. The material can then be transported alongshore or cross-shore away from the original position. When the toe material is gone, the sequence repeats itself making the cliff retreat even more.

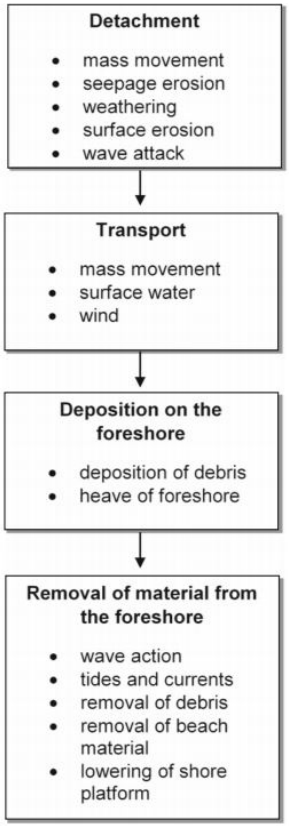

Figure 2.1: General steps of cliff erosion by Moore and Davis (2014). Originally from Lee and Clark (2002).

2.1.1. Detachment

Surface erosion

Surface erosion is a mechanism for cliff recession by which water or wind detach small sediment particles from the cliff face (Lee and Clark, 2002). After detaching the particles can be transported down the cliff slope onto the foreshore. Especially soft and unvegetated cliffs are prone to this kind of cliff face erosion.

Figure 2.2 shows the formation of gullies on a cliff face due to surface water run-off at the Point Grey cliffs. These are clear indicators of surface water run-off being a significant contributor to the recession of a cliff.

Seepage erosion

Howard and McLane (1988) states that seepage of groundwater through the cliff face can erode by destabiliz-

ing forces and water flows down the cliff face. These water flows carry sediment down the slope and, again, depositing it on the foreshore. Landslides are of concern for slopes with seepage problems. From Figure 2.3 can be seen that seepage induced landslides show rough surfaces, while landsliding due to wave attack leaves a smoother cliff face.

Figure 2.2: Gully formation in Point Grey cliff due to surface water run-off. Photo courtesy of S. G. Pearson.

Wave attack

The last mechanism follows from wave attack down at the cliff foot. (Sunumura, 2015) states waves can undercut, thus oversteepen, and take away material by abrasion, quarrying and scouring the cliff face (Lee and Clark, 2002). Collins and Sitar (2008) state that 82% of cliff failures can be related to wave action, although undercutting does not occur significantly at soft cliffs. It only takes a small undercut before material from the upper cliff face slides down, forming a talus.

Figure 2.3: Left: Cliff failure due to groundwater seepage. Right: Cliff failure due to wave attack. Both images from Collins and Sitar (2008).

Sunumura (2015) focuses more on the erosion of the cliff foot and shows the whole process in Fig. 2.4. According to Sunumura (2015) there are three influences to cliff toe erosion (see Fig. 2.4). Firstly, the water

level dictates which waves can directly attack the cliff foot. The water level is influenced by the tide, seasonal change, and sea-level change.

Secondly, the beach and nearshore morphology also control the wave energy reaching the cliff toe. A talus, which is fallen debris covering the cliff toe from direct wave attack, is often a sign of absence of marine erosion. In the case of apparent marine erosion, a talus will be very short-lived (Emery and Kuhn, 1982).

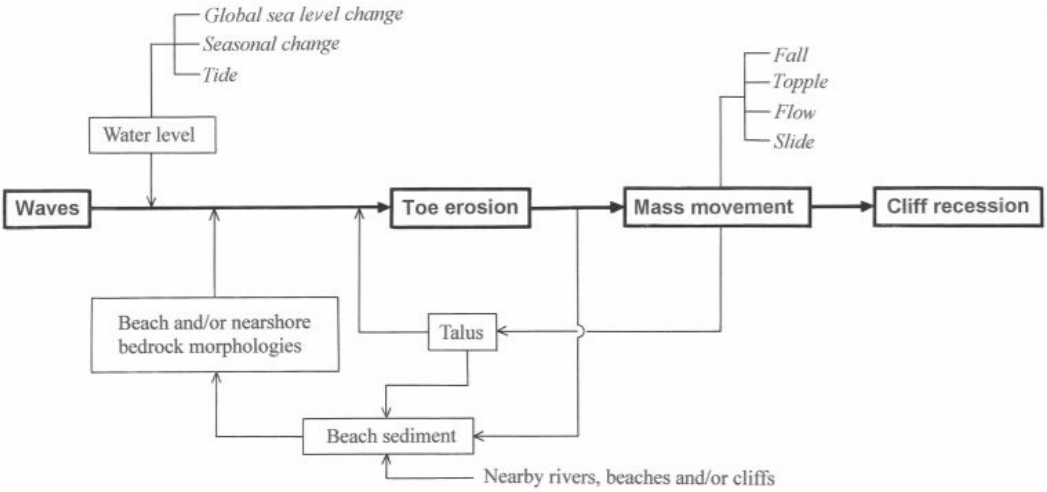

Figure 2.4: Overview of interactions concerning cliff toe erosion. From Sunumura (2015).

A second contribution of waves to cliff toe erosion is given by Lee (2008). He adds the mechanism of wave run-up to the erosion of the cliff toe (see Figure 2.5). The small layer of water travels up and down the beach slope, transporting sediments cross-shore. This sediment then enters the nearshore and can potentially be transported alongshore.

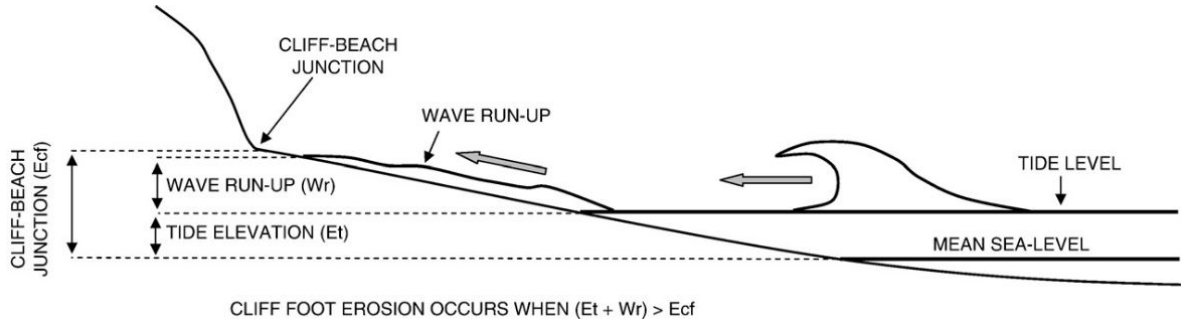

Figure 2.5: Cliff toe erosion due to wave run-up. From Lee (2008), adapted from Ruggiero et al. (2001).

2.1.2. Transport & deposition on the foreshore

The main transport mechanisms, which forces sediment to come down from the cliff face, are gravity (which induces landslides), surface water run-off and sometimes wind (Lee and Clark, 2002). The material then forms a talus structure on the foreshore, which acts as a temporary cliff toe protection. This deposited material is then prone of being picked up and transported away.

2.1.3. Removal of material from the foreshore

Talus material on the foreshore can be transported to other locations due to currents, leaving the cliff foot exposed again. The loss of talus material results in that cliffs slope will never reach a stable slope, since the process of coastal cliff erosion will repeat its cycle (Figure 2.1). Potential alongshore currents originate from the tides and oblique incoming waves. It is also possible for storm waves to transport the material cross-shore.

2.2. Time scales

Coastal processes can be divided into different spatial- and temporal scales. Figure 2.6 shows the relation between different temporal scales and their corresponding spatial scales.

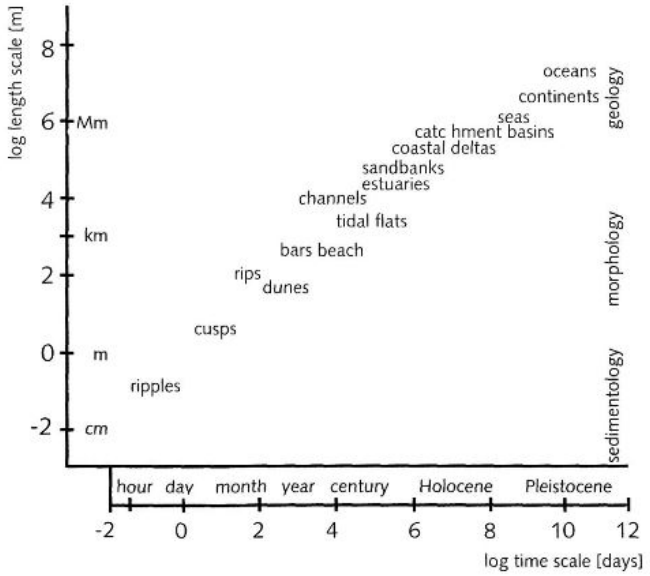

Figure 2.6: Spatial- & temporal scales with their corresponding morphological processes. From Dronkers (2005).

It is important to keep note of the considered time scale when assessing erosion in a coastal system. Gracia et al. (2005) states four timescales for coastal erosion, namely the very short, the short, the long and the very long term coastal erosion. Each temporal scale has its own corresponding spatial scales together with a different coastal erosion type. Gracia et al. (2005) used these time scales to divide erosion contributors to sandy shorelines. However, these time scales are also suitable to find erosion mechanisms for the Point Grey cliffs in a more general sense.

In Sections 2.1 and 2.2 four temporal scales are mentioned together with their corresponding shoreline erosion mechanisms. The four time scales and cliff erosion steps can be found in Figure 2.7 given by Lee (2008), showing the relations between them. The focus of this study is on the marine erosion, consisting of the system drivers, primary responses, in the top of Figure 2.7. The first example is time scale $\mathcal{O}(100-1000\text{ y})$ (Section 2.2.4). The climate and geological factors induce changes in sea-level rise and wave climate. These changes affect the sediment budgets of a coastal system (time scale $\mathcal{O}(1-10\text{ y})$, Section 2.2.3). Subsequently the changes in sediment budgets, wave climates and sea-level rise result in changes of the shoreline system in terms of sediment transports (time scale $\mathcal{O}$(1 d - 1 m), Section 2.2.2). Sediment transports can cause losses of sediment to adjacent coastal systems. The four steps of coastal cliff erosion are described by the interactions between the 'Shoreline system' and 'Cliff system'. The finest time scale, $\mathcal{O}$(1 s - 1 h), can be described by the wave energy reaching the cliff toe (foot).

The sub-aerial cliff erosion processes can be found in the lower half of the diagram. The groundwater seepage, surface water run-off, etc. can be found in the precipitation primary response factor.

2.2.1. Time scale $\mathcal{O}$(1 s - 1 h)

The first and smallest scale we call time scale $\mathcal{O}$(1 s - 1 h), which corresponds to spatial variations in the order of centimeters to meters. This time scale is called 'very short term' and is in the order of seconds to minutes to hours (Gracia et al., 2005). The main source of forcings come from storms (Gracia et al., 2005). Storm surges can raise the water level enabling waves to directly attack the cliff toe. This time scale fits with the detachment step from Figure 2.1, specifically the direct wave attack. Wave attack, direct and wave run-up, at the cliff toe is described by Ruggiero et al. (2001), Sunumura (2015) in the 'Wave attack' section.

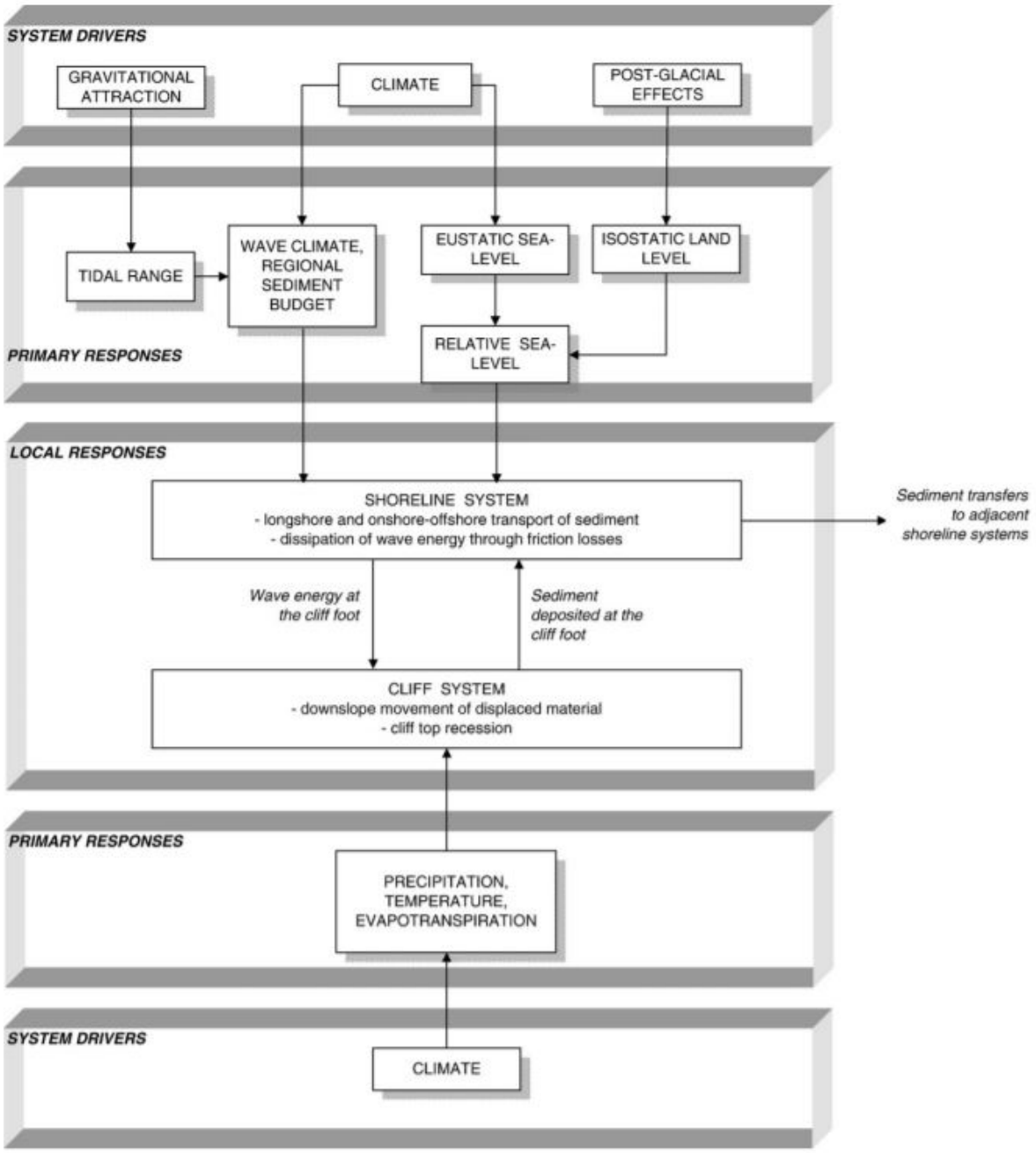

Figure 2.7: Influences on a shoreline and cliff coastal system. By Lee (2008).

2.2.2. Time scale $\mathcal{O}$(1 d - 1 m)

The 'short term' time scale (Gracia et al., 2005), time scale $\mathcal{O}$(1 d - 1 m), includes the spatial variations in the order of meters to kilometers. The temporal scales range from days to months. The sources of short term variations are longer storms than in the earlier timescale, strong littoral currents and due to coastal works (Gracia et al., 2005). Strong littoral currents may be caused due to tidal activity and obliquely-incoming waves. The last cliff erosion step (Figure 2.1) of 'Removal of material from the foreshore' can be allocated to this temporal scale.

Figure 2.8 shows the different directions for sediment transport. The alongshore current is, mostly, the direction with the most impact on the shoreline. The flows parallel to the coast are induced by the obliquely incoming waves and tidal currents.

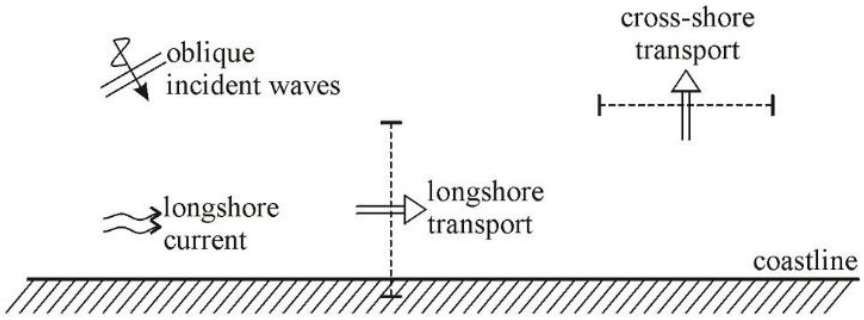

Figure 2.8: Alongshore- and cross-shore sediment transport due currents initiated by oblique incoming waves. From Bosboom and Stive (2015).

2.2.3. Time scale $\mathcal{O}(1-10\,\mathrm{y})$

Time scale $\mathcal{O}(1-10\,\mathrm{y})$, the 'long term' scale by Gracia et al. (2005), encompasses shoreline variations from years to decades with according spatial scales larger than kilometers to tens of kilometers. The causes of this type of erosion follow from human interventions (coastal works) and natural changes (sediment supply of river, higher storm frequency). (Gracia et al., 2005). These factors have an impact on the sediment budget of a system. A deficit in sediment means that a coast is an eroding state, while a sediment surplus causes a system to accrete.

Atkins et al. (2016) state that due human interventions, like coastal works and dredging, alter the sediment flows and budgets in the Fraser River delta. Coastal works inhibit sediment transports, like North Arm breakwater and jetty. The jetty causes a deflection of flow and sediment at the North Arm Fraser River (Atkins et al., 2016). The dredging in the Fraser River alters the natural deliverance of sediment to the Fraser River delta (Church, 2010). Dredging is also the likely cause of the erosion of the marsh at the Fraser River delta (Atkins et al., 2016).

2.2.4. Time scale $\mathcal{O}(100-1000\,\mathrm{y})$

The fourth time scale, time scale $\mathcal{O}(100-1000\,\mathrm{y})$, accompanies variations in spatial scales to the global level initiated by geological or climatic changes (Gracia et al., 2005). She calls this time scale the 'very long term' scale. The temporal scales are in the order of centuries to millennia.

From 1910 until 2014 the average sea-level rise at Vancouver was 0.37 $\mathrm{mm\,y^{-1}}$ (Environmental Reporting British Columbia, 2017). The same source also states that the further sea-level rise until 2099 is in between 0.26 and 0.98 m, which is in agreement with the Intergovernmental Panel on Climate Change (Church et al., 2013). This means an average sea-level rise of 3 to 12 $\mathrm{mm\,y^{-1}}$. With current climate change, man could see sea-level rise on smaller time scales than the geological time scale.

For soft coastal cliffs sea-level rise is one of the factors in their recession (Lee, 2008). Johannessen and Macdonald (2009), Shaw et al. (1998) indicate the high sensitivity of the Point Grey cliffs' shoreline to sea-level rise as presented in Figure 2.9. Not only sea-level rise is an effect of climate change. Johannessen and Macdonald (2009), Lee (2008), Shaw et al. (1998) mention the storm intensity following from climate changes. The increased storm intensities could cause waves with higher energies to reach the coast of Point Grey. The combination of sea-level rise and increased wave intensity result in a need for sediment for the shoreline to adjust itself to the new boundary conditions.

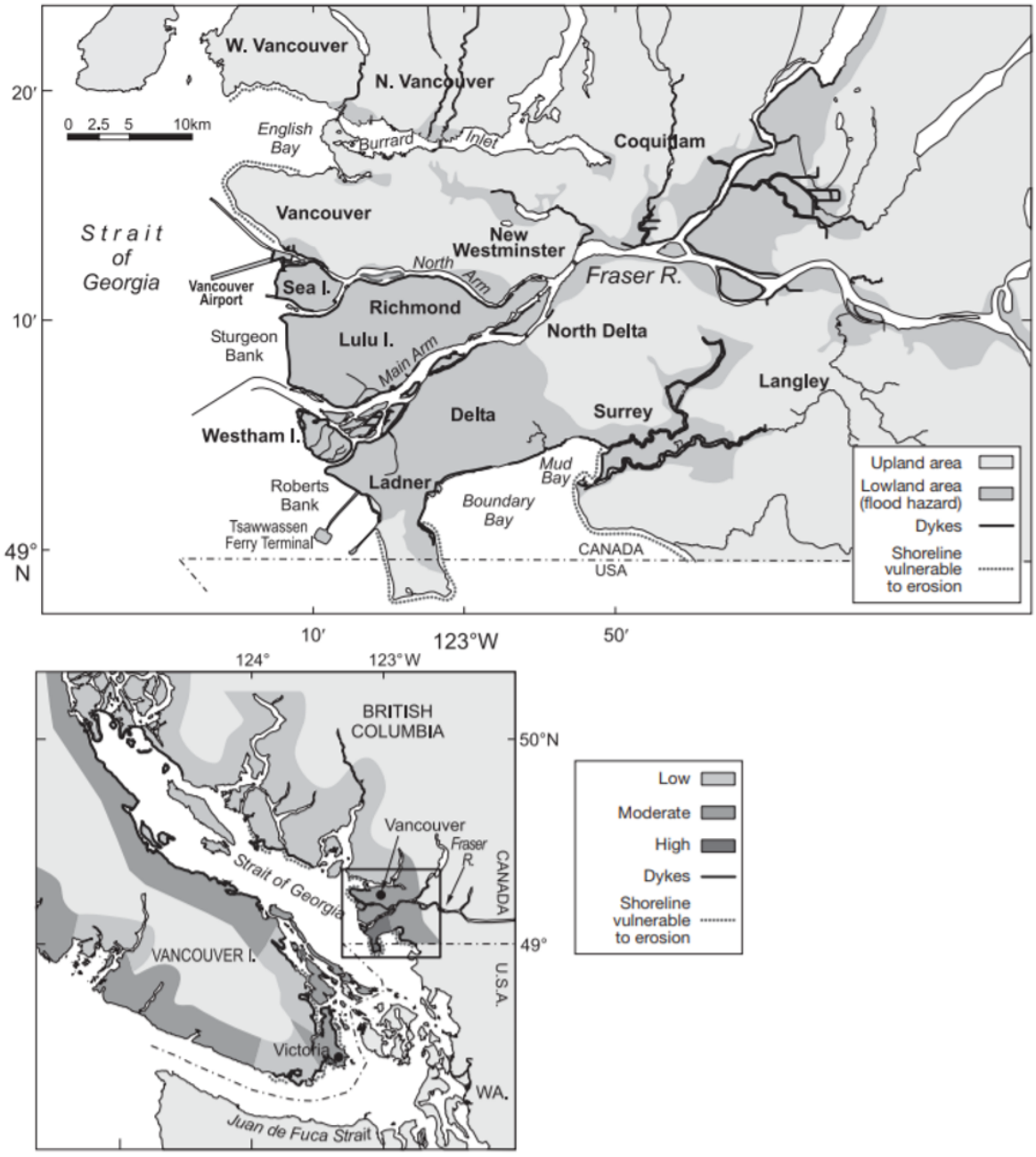

Figure 2.9: Sensitivity of Point Grey to sea-level rise. From Johannessen and Macdonald (2009), Shaw et al. (1998).

3

Point Grey: the coastal system

The Point Grey cliffs are the edge of the Burrard Peninsula reaching into the Strait of Georgia. The Strait of Georgia is approximately 220 km long and 28 km wide. The average depth is about 155 m with maxima going over 400 m. The Strait of Georgia is connected by two entrances to the Pacific Ocean. Due to Vancouver Island on the western side, the Strait of Georgia is sheltered from sea swell waves (Thomson, 1981).

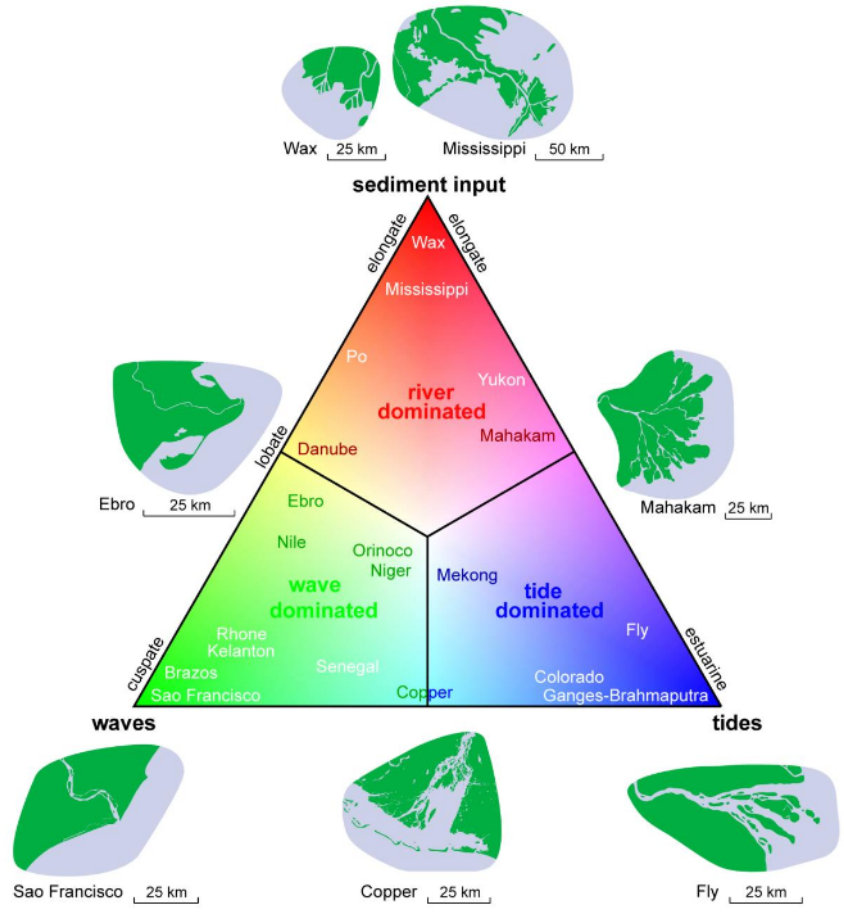

Figure 3.1: Triangular system classification diagram by William Galloway. The colors indicate the relative importance of waves (green), tide (blue), river sediment input (red). From Bosboom and Stive (2015). Originally from Galloway (1975).

Coastal systems in the world can be assessed by three physical processes as seen in Figure 3.1: wave energy, tidal energy and river sediment input. Ayranci (2014) describes the Fraser River delta is a river dominated delta with tidal influences. This specific chapter looks at the three specified processes and tries to gain deeper insight in each of the three components. Other properties of the coastal system are also identified, such as the geology, prior coastal works and dredging operations.

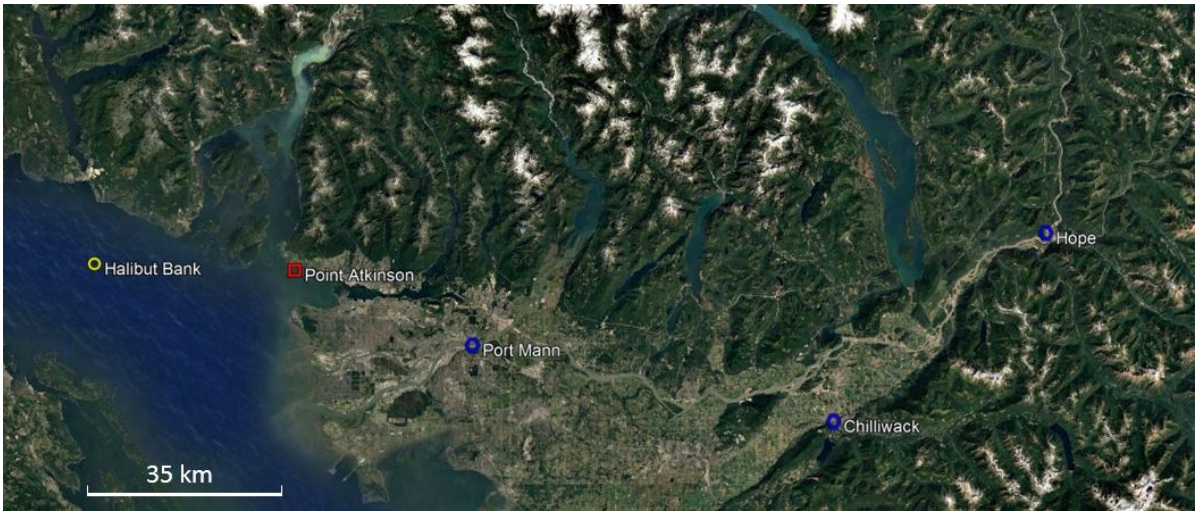

Figure 3.2: Overview of different measurement stations in the vicinity of the Grey Point cliffs.

Both Figures 3.2 and Table 3.1 give an overview of the different data sources used to obtain the data for this analysis. Point Atkinson is a tidal station, from which water level measurements are obtained. Chilliwack, Hope, and Port Mann report the discharge of the Fraser River. Halibut Bank is a wave-buoy in the Strait of Georgia.

Table 3.1: Measuring stations used in the hydrodynamic data gathering and analysis.

Station	Station ID	Type	Years	Lat.	Long.
Chilliwack	08MH001	Discharge (river)	1983 - 1992, 2007 - 2016	49.097222°	-121.967222°
Halibut Bank	C46146	Wind & waves	2008 - 2017	49.340000°	-123.730000°
Hope	08MF005	Discharge (river)	1983 - 1992, 2007 - 2016	49.385833°	-121.454167°
Point Atkinson	#7795	Water level (tidal)	2008 - 2017	49.333300°	-123.250000°
Port Mann	08MH126	Discharge (river)	1983 - 1992	49.217778°	-122.824444°

3.1. Geology

About 50,000 years ago an early Fraser River deposited a delta consisting of clay, silt, and sand out into the Strait of Georgia. This clay is now underneath the whole Burrard Peninsula (Piteau Associates, 2002). A typical cliff lay-out is given in Figure 3.3. From beach level four distinct layers can be identified: first a Quadra sand layer, a second layer of silt, and on top of that another Quadra sand layer. Lastly, glacial deposit called till was left when the ice sheet melted (Clague, 1976, Piteau Associates, 2002, Pool, 1975). The cliffs are thus primarily made of soft sediment material with mean diameters of the sedi-

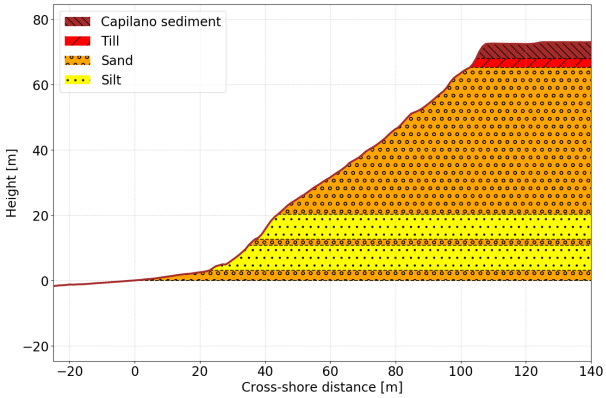

Figure 3.3: Cross-section of typical composition of the Point Grey cliffs.

ments in the cliff ranging from 200 to 300 µm (Piteau Associates, 2002). The cliff tops are about 50 to 80 meters above mean sea-level (MSL) (Piteau Associates, 2002, Pool, 1975).

The list below gives extra information on the different layers presented in Figure 3.3 (Piteau Associates, 2002).

- Sand Q1: Fine to coarse sand, with minor peat and gravel.
- Silt Q2: Interbedded silt, fine sand and minor peat.
- Till V1: Sandy, loamy lodgment till (mixture between dense sands, silt and clay).
- Capilano sediments: Beach gravels and or silt to clay loam.

3.2. Tidal characteristics

There are considerable tidal ranges inside the Strait of Georgia. At the Point Grey cliffs, the tidal range is about 2.8 m (Thomson, 1981). Just north of the Grey Point cliffs is the tidal station of Point Atkinson located (see Figure 3.2). Through personal communication[1] official water level data is retrieved from the Fisheries and Oceans Canada consisting of the years 2008 up to and including 2017.

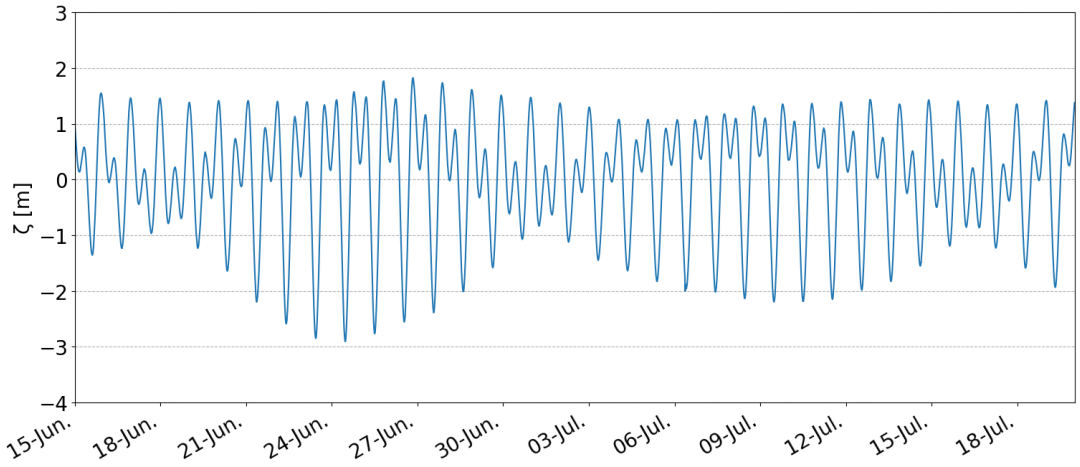

(a) Summer 2017.

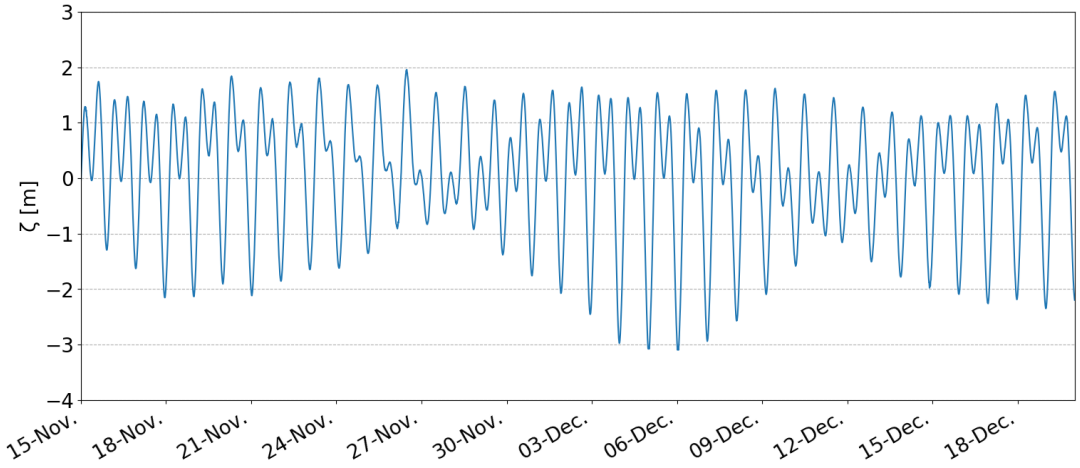

(b) Winter late 2017.

Figure 3.4: Tidal signals during summer and late 2017 at Point Atkinson.

The tidal form factor (Equation 3.1) gives a value of 1.0 which means a mixed tidal signal, with mostly semi-diurnal characteristics (Bosboom and Stive, 2015). This behavior can be seen in Figure 3.4. The Mean Higher High Water (MHHW) around Point Atkinson is 1.1 m, Mean Lower High Water (MLHW) 0.9 m, Mean Higher

[1] With Jenny Chiu of Fisheries and Oceans Canada on 3 October 2018.

Low Water (MHLW) -0.1 m, Mean Lower Low Water (MLLW) is -1.8 m. A zoomed version of Figure A.1a and the marked water levels discussed previously can be found in Figure 3.5. All values are given in respect to MSL.

$$F = \frac{(K_1 + O_1)}{(M_2 + S_2)} = \frac{75.9 + 40.9}{91.8 + 22.0} = 1.0 \tag{3.1}$$

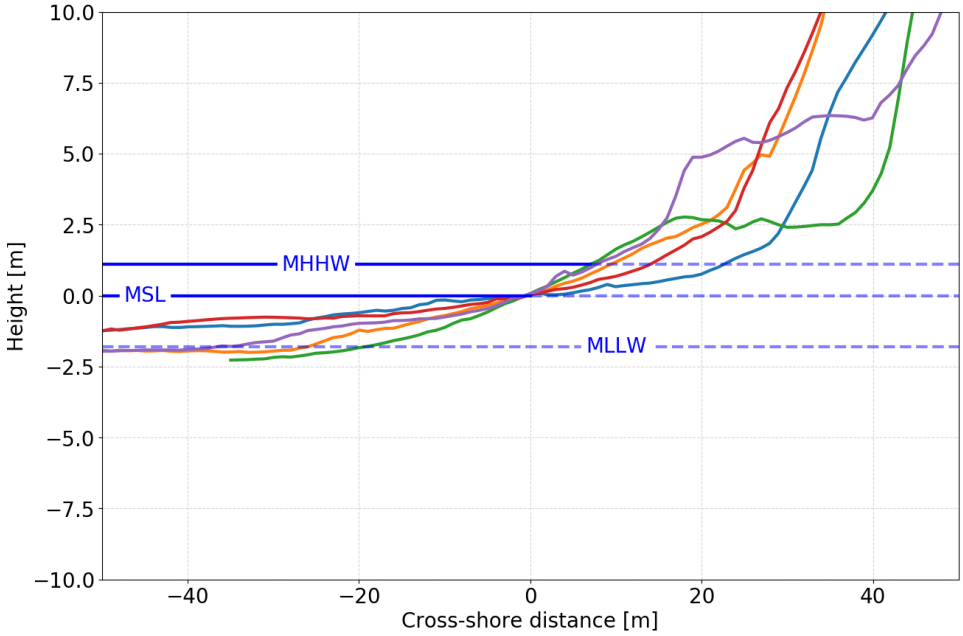

Figure 3.5: The cliffs cross-sections with MHHW, MSL and MLLW water levels. The axis are not equally scaled.

The tidal range, as seen in Figure 3.6, varies over the year. The tidal range per day over the years is plotted. The black line shows the mean per day over those ten years. During the winter and summer the tidal range is generally higher than in the fall or spring. Since the tidal range occasionally surpasses the 4 m mark, the tidal environment may be considered macro-tidal.

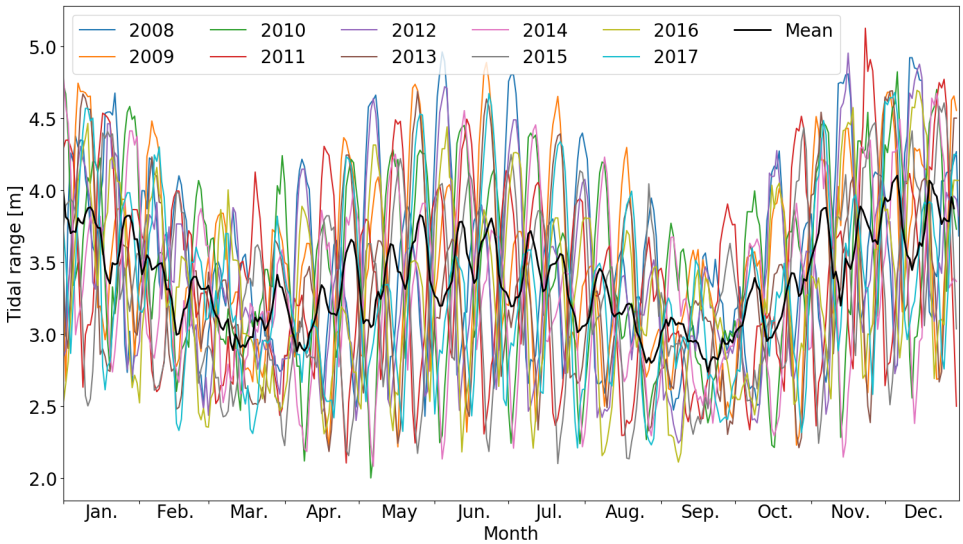

Figure 3.6: Tidal ranges at Point Atkinson through the years 2008 to 2017.

3.3. Wind & waves

The waves in the Strait of Georgia are mainly wind generated waves. Especially the waves formed during the winter season with fetches of approximately 100 km from the northwest are important to the erosion of the Point Grey cliffs (Pool, 1975). She describes five fetch limited wave fields which affect the Point Grey cliffs. These are waves (and thus winds) from the southwestern through northwestern part of the Georgian Strait. The significant wave height of storms in the Strait of Georgia are normally less than 2.1 m and the largest maximum is 3.3 m (Barrie and Currie, 2000, Milliman, 1980).

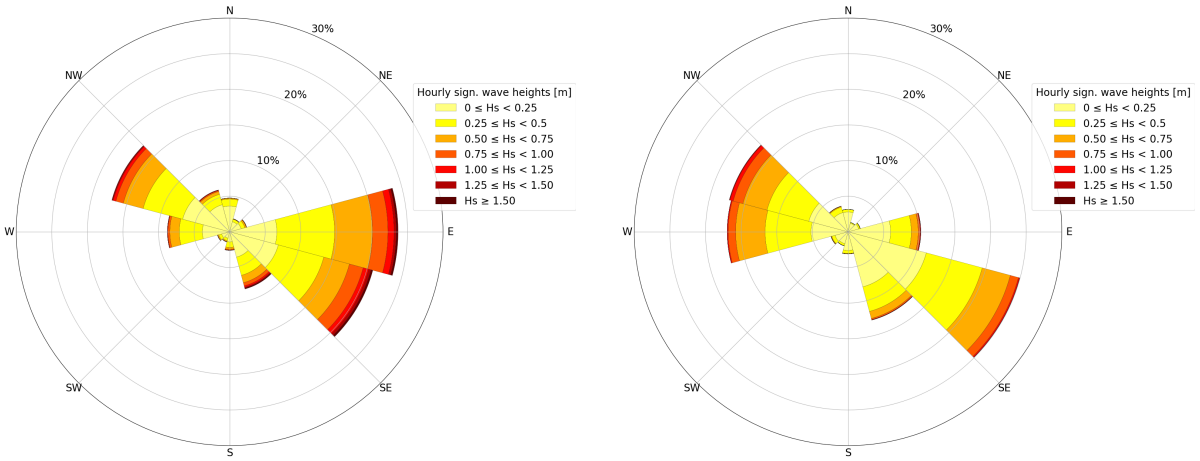

(a) Non-freshet wave rose.

(b) Freshet wave rose.

Figure 3.7: Wave roses during two distinct periods, the freshet and non-freshet, at Halibut Bank.

The winds and waves over the Strait of Georgia are monitored by the Halibut Bank buoy located 35 km west northwest of the site. This buoy measures the wind speed, wind direction, significant wave heights, peak wave periods. The orientation is given from degrees north clockwise and gives where the wind is coming from. The buoy does not measure the direction of the waves. Since the Strait of Georgia is sheltered by Vancouver Island thus almost no swell waves from distant storms are present, the wind direction is imposed on the significant wave height. In Figures 3.7 and 3.8 the distribution of direction and magnitude over ten years of both waves and wind respectively are plotted.

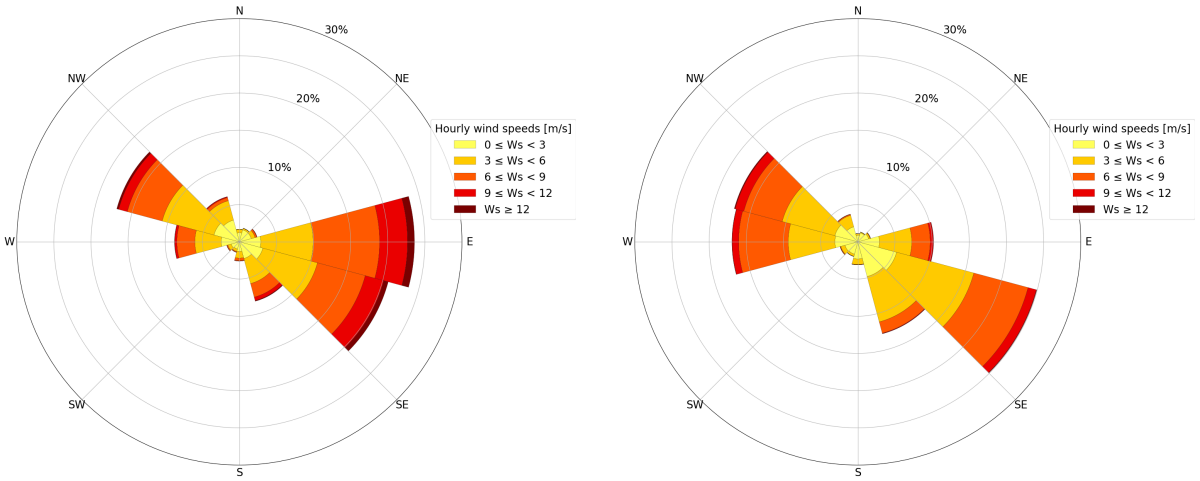

(a) Non-freshet wind rose.

(b) Freshet wind rose.

Figure 3.8: Wind roses during two distinct periods, the freshet and non-freshet, at Halibut Bank.

3.4. Storm surges

At the tidal station of Point Atkinson storm surges may appear during large storm events. Storm surges are the result of differences in atmospheric pressure and the pushing of water to onshore areas. Tinis (2017) states that at Point Atkinson a storm surge of 0.6 m has a Return Period of 1.3 years. The choice for a 1.3 year Return Period follows from a comparison the author makes in his report. The data the author used for his analysis is presented in Table 3.2. The data can be used for an extreme value analysis for storm surges in later studies to achieve similar Return Periods.

Adding this storm surge to the water levels presented in Figure 3.5 one can see that adding the storm surge to high water levels due to the tide exposes the cliff toes to potential direct wave attack.

Table 3.2: Maximum annual storm surge levels at Point Atkinson out of the past 53 years. Only the years since 1997 are shown here. From Tinis (2017).

Year	Rank	Surge [m]
1998	1	1.031
2006	4	0.91
2002	7	0.891
2015	8	0.85
2016	9	0.85
2011	10	0.84
2005	13	0.82
2007	20	0.79
2001	27	0.739
2009	29	0.72
2012	33	0.68
1997	36	0.655
2010	38	0.65
2004	44	0.571
2003	45	0.571
2013	49	0.549
1999	50	0.533
2000	51	0.455
2008	53	0.44

3.5. Fraser River

The largest river flowing into the Strait of Georgia is the Fraser River. Its mean annual outflow is $115 \cdot 10^9$ $m^3 y^{-1}$ at Port Mann with an approximate sediment load of $19 \cdot 10^9$ $kg y^{-1}$ (Johannessen et al., 2003, Thomas and Bendell-Young, 1999). Einsele (2013) states a modern annual sediment discharge of $17.3 \cdot 10^9$ $kg y^{-1}$ determined also at Port Mann. Milliman (1980) gives a range in between 10 and $30 \cdot 10^9$ $kg y^{-1}$. The Fraser River sediment load is distributed in the following way: 35% sand, 50% silt and 15% clay and about 37% ($6.4 \cdot 10^9$ $kg y^{-1}$) is left on the sub-aerial Fraser delta (Milliman, 1980). Attard et al. (2014) studied the sediment load of the Fraser River at Mission from 2010 and compared these with data between 1966-1986. He concluded a relatively stable sediment load over the years.

Figure 3.9 is constructed by using the method presented by Pawlowicz et al. (2017), since no up-to-date data is available at the Port Mann station. Therefore Pawlowicz et al. (2017) takes the discharge at the station Hope together with the Chilliwack station. This is fitted to the data from Port Mann between 1983 to 1992. The resulting regression is given below ($r^2 = 0.97$, mean error $\pm 272 m^3 s^{-1}$):

$$Q_{PortMann} = Q_{Hope} + 6.32\, Q_{Chilliwack} + 426 \tag{3.2}$$

The Fraser River discharges fresh water and sediment divided over several arms into the Strait of Georgia. The Main Arm of the river takes account for 85% of the total discharge. The North Arm receives the remaining 15% due to the finished trifurcation works in 1975 (Milliman, 1980, Thomson, 1981). 91-97% of the sediment load goes to the Main Arm (Isfeld et al., 1996), only three to nine percent flows through the North Arm (Golder Associates Ltd., 2015). The Middle Arm of the Fraser River discharges about four percent of the total discharge with little to no sediment (McLaren and Ren, 1995).

The river outflow shows a clear seasonal variation with high discharges in the summer due to snow melt. The typical winter fresh water discharge of the Fraser River is 2000 $m^3 s^{-1}$ (Pawlowicz et al., 2017). In the analysis in this report a mean non-freshet discharge of 2500 $m^3 s^{-1}$ is found and will be used in further sections. This discharge corresponds to the months of August through April. From the same analysis, the mean freshet discharge (mid-May to mid-July) at Port Mann is 8008 $m^3 s^{-1}$. The sediment load during freshet (May through July) is 80% of the mean annual sediment load. Most of the sediment is suspended material, namely 95% (Milliman, 1980).

Table 3.3: Sediments in Fraser river. From McLean et al. (1999).

Grain size	Sediment load [$t y^{-1}$]
Suspended	
Clay	$2.7 \cdot 10^6$
Silt	$8.3 \cdot 10^6$
Sand (< 177 µm)	$3.1 \cdot 10^6$
Sand (> 177 µm)	$3.0 \cdot 10^6$
Bed load	
Sand (> 177 µm)	$0.2 \cdot 10^6$

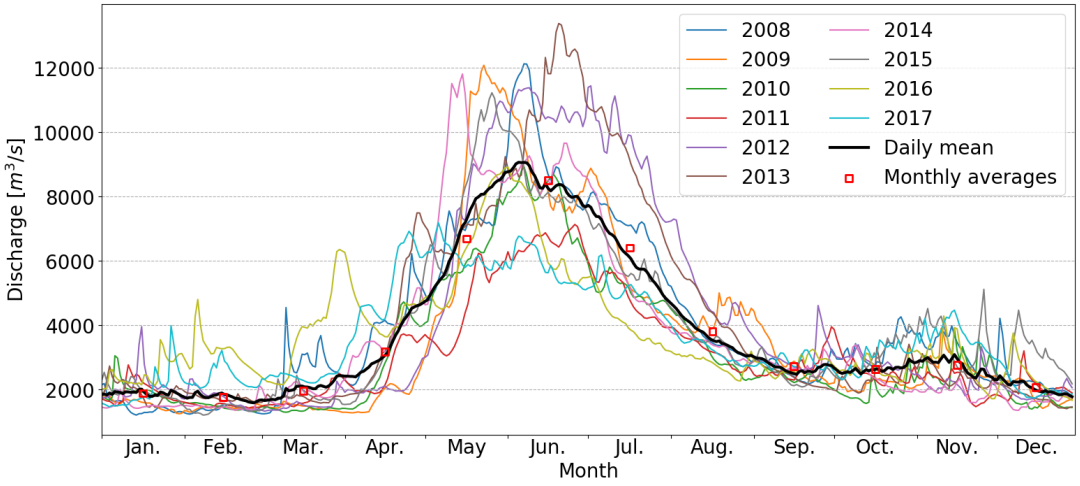

Figure 3.9: Fraser River discharges through the years 2007 to 2016.

Attard et al. (2014), McLean et al. (1999) both provide the distribution of the annual sediment load, which agrees reasonably well with Milliman (1980). The portion of sand with a mean grain size greater than 177 µm is said to be in intermittent suspension (McLean et al., 1999). The D_{50} of the largest sand class is 320 µm with a D_{10} of 200 µm Northwest Hydraulic Consultants (2002). The median grain size for the smaller sand class is not as easy to compute, it is part of the suspended material. Therefore an estimation of 123 µm is used; the average of the upper limit of 177 µm and lower limit of 68 µm. The latter is also true for the silt part. For this sediment type a median grain size of 40 µm is used. In the transport model just the silt and sand particles are taken into account, since the soil samples in the area mostly consist of silt or sand (Ayranci, 2014).

3.6. Human Interventions

In the delta of the Fraser River many human interventions have taken place in the past and present, which influence properties of the coastal system of the Grey Point cliffs. Two different impacts can be distinguished: the marine works in the coastal delta and the dredging in the Fraser River.

3.6.1. Marine works

During the last century numerous works and events took place, which altered the coastal system in any way. These measures are listed in Table 3.4. The major marine works are the three jetties constructed in 1912, 1917, and 1961. These jetties obstruct the natural sediment distribution over the marshes. Furthermore the table shows that no other attempts to protect the cliffs have been made since 1981. As the sediment discharges from the Fraser River, it is guided offshore or to the south in the case of the Main Arm. At the North arm its guided offshore immediately, or trapped in the Booming Grounds due to the constructed breakwater in 1953. This only holds when there is any natural transport northwards due to waves or the tide.

Berm & groyne system

In 1974 the first marine measures were taken to diminish incoming wave energy (Pool, 1975). The measures included a rubble-mound groyne system together with a cobble berm at Towers Beach (see 3.10). The berm was to protect the cliff toe from direct wave attack, while the groynes were placed to trap alongshore sediment transports. The following statement from McLean (1975) shows the a statement about these measures:

"During the summer of 1974 a 3200 foot sand fill and cobble core berm and groin system was constructed at Towers Beach, University of British Columbia to prevent marine erosion along Point Grey cliffs. During the following winter the berm was partially successful in protecting the cliff base, however, along the western beach the sand fill was severely eroded by W and NW storm waves. By the end of February the berm had failed over a 1500 foot length allowing storm waves to undercut the cliff base during high tides. Throughout the study period the groynes were very ineffective in stabilizing the sand fill, allowing a large amount of material to move eastward by littoral drift. The useful life of the berm is probably less than two years. Remedial measures will probably be required in the future."

Table 3.4: Human interference in Fraser River delta. Inspired by Atkins et al. (2016).

What	**When**	**Relevance to coastal system and Point Grey cliffs**	**Source**
Dredging in Fraser River began	1800s to present	Less sediment supply to river delta.	Bros (2007), Ferguson (1991), Golder Associates Ltd. (2015)
Largest documented flood	1894	Large sediment pulse to delta.	nhc (2008)
Dyke construction	1906 to present	Flood prevention and flood sediment distribution restricted.	Richmond (2000)
Steveston Jetty construction	1912	Northward marshes isolated from sediment.	Levings (1980)
North Arm dredging	1913	Channel deepened, less sediment reaching Wreck beach annually.	Fraser Estuary Management Program (2006)
Construction of North Arm Jetty	1917	Protecting Booming Grounds from SW waves.	Levings (1980)
South jetty construction.	1930s	Northward marshes isolated from sediment.	Levings (1980)
Steveston Jetty extension.	1935	Westward extension. Guiding more sediment offshore.	Levings (1980)
Flood of record	1948	Large sediment pulse to delta.	nhc (2008)
Extension of North Arm Jetty	1951	Westward extension. Guiding more sediment offshore.	Golder Associates Ltd. (2015)
Construction of North Arm Breakwater	1953	Protecting Booming Grounds from N/NW/W waves.	Golder Associates Ltd. (2015), UBC/Pacific Spirit Regional Park Cliff Management (2000)
Nechako diversion	1954	Less discharge through Fraser River.	French and Chambers (1997)
Construction of Iona jetty/causeway	1961	Alteration of sedimentation regime.	Levings (1980)
Large flood event	1972	Large sediment pulse to delta.	nhc (2008)
Trifurcation works (split Main Arm and North Arm) in Fraser River	1973-1975	Less sediment entering the Fraser River North Arm.	Atkins et al. (2016), Golder Associates Ltd. (2015)
Berm installed at Towers Beach	1974	Protecting Point Grey cliffs from wave attack.	Golder Associates Ltd. (2015), Pool (1975)
Berm damaged	1975	Berm no longer effective protecting cliffs against wave attack.	Pool (1975)
Dredged sediment of North Arm placed at Wreck Beach adjacent to North Arm Breakwater.	1977	Nourishment to Wreck Beach to provide shelter against wave attack.	Golder Associates Ltd. (2015), UBC/Pacific Spirit Regional Park Cliff Management (2000)
Steveston Jetty reconstruction	1978 to present.	Discharge and sediment distribution altered.	Levings (1980)
Cobble berm and groynes installed between Tower 1 and 2.	1981	Attempts to mitigate marine alongshore erosion of Wreck Beach.	Golder Associates Ltd. (2015), UBC/Pacific Spirit Regional Park Cliff Management (2000)
Extension of North Arm Breakwater	1987	Further sheltering of Booming Grounds from N/NW/W waves.	Golder Associates Ltd. (2015)
Borrow dredging reduced	Late 1990s	Sediment removal from Fraser River reduced.	Bros (2007)
Large flood event	2007	Large sediment pulse to delta.	nhc (2008)

McLean (1975) states the ineffectiveness of the total system and that the sand fill can be flushed out through the cobbles. In 1981 the berm was heightened to MSL+3.2 m (CD+6.2 m) with the addition of groynes (Downie and Saaltink, 1983). In Figure 3.5 transect three clearly shows this berm in front of the cliff foot. Figure 1.4b shows that after alteration of the existing berm the erosion rate of the toe became slower. Today one can see that the berm has positioned itself perpendicular to the main incoming wave direction (Golder Associates Ltd., 2015)[2].

The mean diameters of the material at two locations in the berm were 25.2 - $43.6 \cdot 10^3$ µm. The use of larger rocks was a choice to minimize reflection of incoming waves (Downie and Saaltink, 1983).

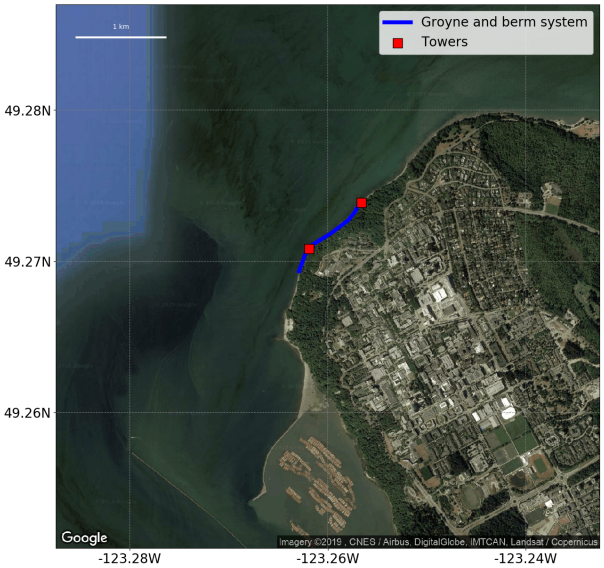

Figure 3.10: Location of groyne and berm system on Tower beach.

Jetties & breakwater

The jetties built in 1912, 1917, 1935, and 1961 canalize the Fraser River and move the mouth of this river further towards the Strait of Georgia. The canalization is to concentrate the flow with higher velocities for which the river keeps a lower bed level, which minimizes the amount of dredging needed. However, this also stops any possible natural sediment transport over these blockades (Atkins et al., 2016, Isfeld et al., 1996, Milliman, 1980).

An extra obstruction, the North Arm breakwater constructed in 1953, traps a large part of the sediment outflow of the North Arm in the Booming Grounds. The combination of the two forces a concentrated outflow of the North Arm Fraser River into the Strait of Georgia. This results in a deflection of the natural (sediment) flow as stated earlier.

Trifurcation works

In 1975 the trifurcation works were completed at New Westminster (Table 3.4). This river alteration changed the division of discharge and sediment through the two arms of the Fraser River. The key is that less sediment is passed through the North Arm Fraser River and thus less sediment can ultimately reach the Point Grey cliffs (Atkins et al., 2016, Fraser Estuary Management Program, 2006).

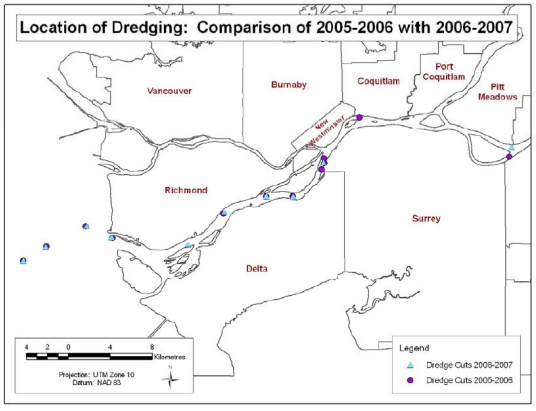

(a) Dredging locations.

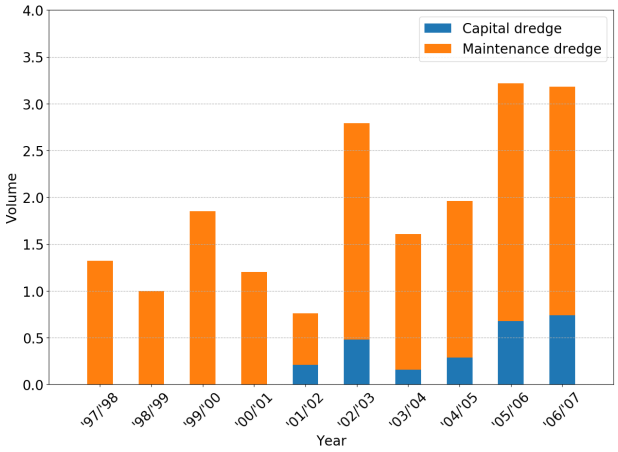

(b) Amount of dredged material in 10^6 m^3.

Figure 3.11: Dredging locations and amount of dredged material lower Fraser River (FREMP, 2007).

[2]Also seen in personal observation on 5 November 2018.

3.6.2. Dredging

In the lower part of the Fraser River's South Arm annual dredging occurs to maintain the possibility for sea ships to enter this part of the river. FREMP (2007) provides an overview of where and how much is dredged from this lower part of the Main Arm Fraser River all shown in Figure 3.11. Church (2010) states that $2.9 \cdot 10^6$ ty^{-1} is dredged from the Fraser Main Arm. Hart (2018) states approximately the same, namely $3.1 \cdot 10^6$ ty^{-1}. 80% of this dredged material is used for other projects. The remaining 20% is disposed in the ocean (FREMP, 2007). Church (2010) says the dredging leaves about $1.3 \cdot 10^6$ ty^{-1} of >177 µm sand (Table 3.3) for the coastal system. All of the numbers above apply to >177 µm sand class, as Attard et al. (2014) all the finer classes are generally not found on the river bed. From Table 3.3 can be found that of the >177 µm sand class 5% can be considered bed load, while the rest is of this class is considered to be suspended material.

According to Pool (1975) from 1964 to 1974 the average annual dredged material of 183,500 $m^3 y^{-1}$ is removed from the mouth which leaves about 68,800 $m^3 y^{-1}$ for the Point Grey cliff sedimentation processes. However, Bros (2007) states about 20,000 $m^3 y^{-1}$ per five years. Due to this dredging all of the sediment flow will go through the North Arm and nothing through the Middle Arm. Nowadays the dredging in the North Arm has completely stopped (Hart, 2018), which means no more dredging interference leaving more sediments for the natural process in the North Arm and probably Point Grey.

3.7. Conceptual sediment budgets

Golder Associates Ltd. (2015), Pool (1975) state that only the North Arm of the Fraser River is a potential source of sediment, thus reducing the sediment input to only the North Arm of the Fraser River. The Main Arm gives the highest sediment influx into the Fraser delta. However, the coarse sand will be deposited very close to its mouth. Only the fine sand, silt, and clay will be transported northwards by the plume (Barrie and Currie, 2000, Pawlowicz et al., 2017). Figure 3.13 shows the sediment flow of sand proposed by Armstrong (1990). The figure give rise to the assumption that also sediment from south of the North Arm jetty enters the Point Grey area.

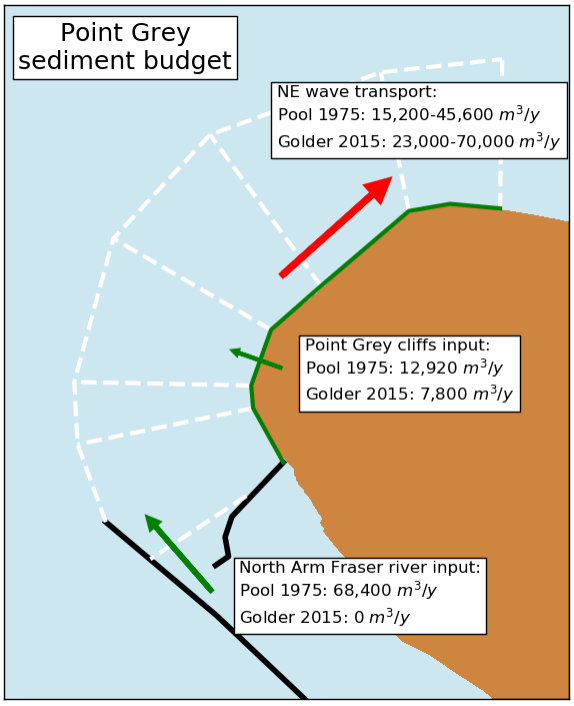

Figure 3.12: The visualization of conceptual sediment transports the North Arm/cliff input and the wave alongshore transport. (Table 3.5).

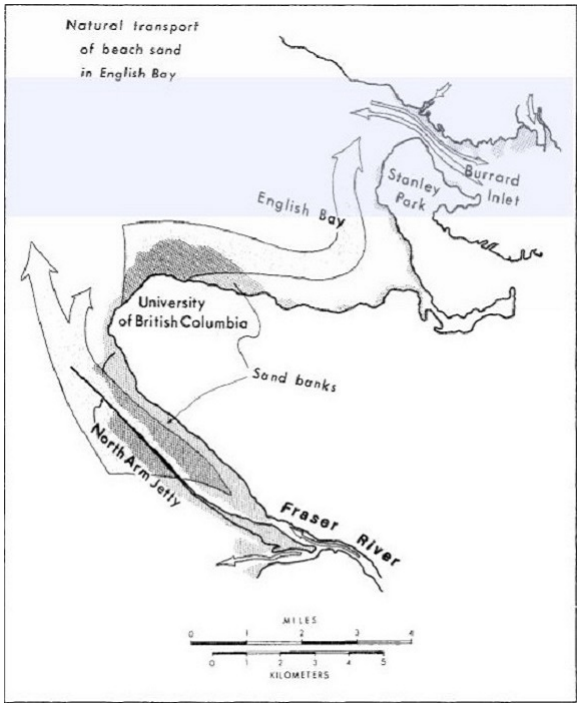

Figure 3.13: Transport of sand along Wreck Beach and Point Grey cliffs. From Armstrong (1990).

Using data presented by Golder Associates Ltd. (2015), Pool (1975) conceptual sediment budgets can be constructed. The results of the data is presented in Table 3.5 and Figure 3.12. Together they estimate a north-

westward wave-induced sediment transport of 15,200 to 70,000 $m^3 y^{-1}$ based on empirical formulae. Then, Pool (1975) states an input of sediment from the North Arm Fraser, while Golder Associates Ltd. (2015) does not. 30 years apart the there is not much difference in coastal works (Table 3.4). However, in the time of Pool (1975) dredging took place. while this has stopped by the time of Golder Associates Ltd. (2015). Contradictory is that Golder Associates Ltd. (2015) states no sediment input from the North Arm, while the conditions are better than during the time of Pool (1975). According to Golder Associates Ltd. (2015) this is mainly due to the North Arm jetty and thus the channelization of the North Arm.

Table 3.5: Estimated budgets for the Point Grey cliff coastal system taken from values of Golder Associates Ltd. (2015) and Pool (1975). All figures are given in $m^3 y^{-1}$.

Case	Wave sediment transport NE		Gross N.A. Fraser River input	Dredging	Net N.A. Fraser River input	Point Grey cliff input	Net sediment budget	
	Lower bound	Upper bound					Lower bound	Upper bound
Pool (1975)	-15,200	-45,600	+250,800	-182,400	+68,400	+12,920	+66,120	+35,720
Golder Ltd. (2015)	-23,000	-70,000	negl.	negl.	negl.	+7,800	-15,200	-62,200

4

Site visit

On the 26th and 28th of October 2018 an initial site survey was done to identify different sections of Wreck Beach beneath the Point Grey cliffs. This identification serves to get an insight in the coastal zone and which different sections, or Shore Units (SU) following Howes et al. (2018), are inside a specific coastal system. Differences in shore morphology, prominent sediments and dominant processes lead to different SUs. Figure 4.1 shows the division of SUs in the Point Grey cliff coastal zone.

Figure 4.1: Coastal zone of Point Grey cliffs with individual SUs. Adapted from Golder Associates Ltd. (2015).

The beach starting at the breakwater down south all the way through SU6 is called Wreck Beach. At the north (SU-6) Wreck Beach turns into Acadia Beach. Wreck Beach has a small intermediate beach consisting of SUs 3 and 4, which is called Tower Beach.

On the 5th of November fieldwork was done to obtain sediment samples for a grain size diameter analysis. The field work started at 8:00 am to be on time before the lowest water level of the day (at 09:39 am) to obtain intertidal sediment samples. For this fieldwork a permit was requested and obtained from the Metro Vancouver Regional Parks. In total 16 different locations (Table 4.1) were sampled on that day. The following day, the

6th of November, pebble counts were done to determine the nominal diameter of the berm placed on Tower beach in 1984. All the locations are shown in Figure 4.2. The samples with codes containing 1s (e.g. T1, M1, etc.), with the exception of N1, are taken from the cliff toe. Samples with 2s are taken from the shoreline and 3s from the intertidal area.

Table 4.1: Coordinates where sediments are taken along Wreck Beach.

No.	Sample code	Lat.	Long.
1	N1	49.261524°	-123.262386°
2	N2	49.261419°	-123.262542°
3	N3	49.261759°	-123.263106°
4	T1	49.265903°	-123.264042°
5	T2	49.265811°	-123.264286°
6	T3	49.265734°	-123.264814°
7	M1	49.270211°	-123.262366°
8	M2	49.270385°	-123.262337°
9	M3	49.270409°	-123.262479°
10	P1	49.275253°	-123.253297°
11	P2	49.275455°	-123.253340°
12	P3	49.275608°	-123.253632°
13	H2	49.278185°	-123.249528°
14	H3	49.278420°	-123.249827°
15	S2	49.279664°	-123.241213°
16	S3	49.280159°	-123.240842°
	PC1	49.269612°	-123.262979°
	PC2	29.273854°	-123.256790°

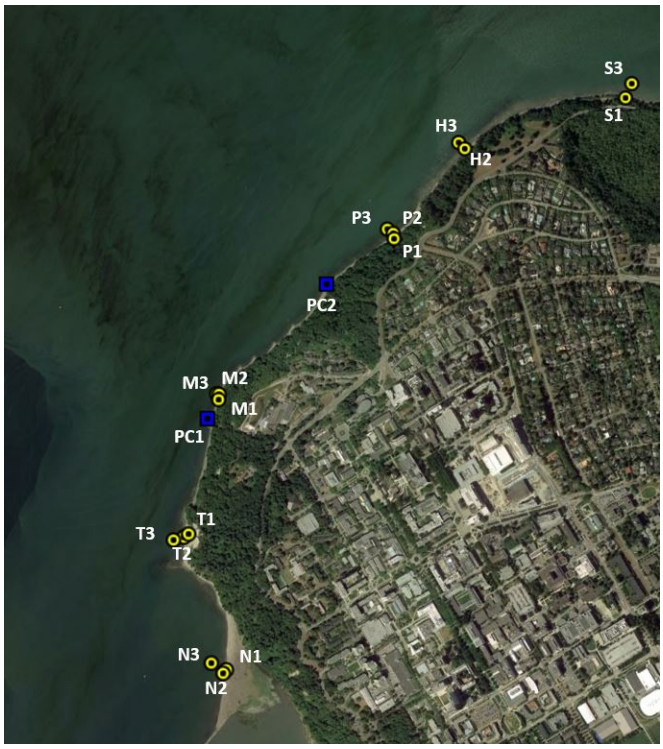

Figure 4.2: Overview of volumetric and surface sampling locations.

4.1. SU1 - North Arm Breakwater to exposed cliffs

A large portion of SU1 is a wide sandy beach which is formed by the placement of the North Arm breakwater and also the sheltering of the North Arm Jetty (Golder Associates Ltd., 2015). The nourishment done in 1979 (see Table 3.4) is also partly responsible for the wide beach. Said beach protect the cliff from marine erosion to a large extent. This beach is probably the result of the nourishment done in 1977 (Table 3.4). On the north end of this SU, there might be some marine erosion. On top of the beach near the breakwater large logs can be found. The intertidal area of SU1 consisted mainly of sand except for the northern part. In other SUs the upper-intertidal is also very rocky.

(a) Sample N1.

(b) Sample N2.

(c) Sample N3.

Figure 4.3: All three samples taken at transect N. Taken on 05/11/2018.

Transect N is located on the widest beach at the most southern point of Wreck Beach and at the far end the breakwater is located. In this transect three samples were taken (N1, N2, N3).

4.2. SU2 - Exposed cliffs

SU2, just north of SU1, is one of the most exposed and active cliff faces of the area. Due to the lack of vegetation and frequent wave attack during high tides, this cliff is easily wave undercut with collapsing of the upper cliff face as a result. Two online articles report about large cliff failures (CBC News, 2013, 2014) with one even resulting in death. The latter collapse can be observed from the satellite image on Google Earth. The time stated by Google Earth of the two pictures in Figure 4.4 is 02:00 am on both days. If this is correct, the tide difference between the two pictures is about 0.7 m[1]. The difference in the tidal elevation explains the seaward extension of the beach in Figure 4.4a in respect to Figure 4.4b.

(a) Before cliff collapse, on 13 September 2014.

(b) After cliff collapse, on 15 September 2014.

Figure 4.4: Before and after cliff collapse at SU2 mid September 2014.

Figure 4.5: Cliff at transect T. Taken on 03/11/2018

Figure 4.5 shows the bare cliffs in SU2. The large talus in front of cliffs are slumping, due to the combination of marine erosion forces together with human influences. Transect T is located at the just north of transect

[1]Obtained from Department of Fisheries and Oceans: www.pac.dfo-mpo.gc.ca/science/charts-cartes/obs-app/observed-eng.aspx?StationID=07795

N. At this location the cliffs are very unstable, since almost no vegetation is on the cliff face. At this location again three samples were taken (T1, T2, T3 in Figure 4.6).

(a) Sample T1.

(b) Sample T2.

(c) Sample T3.

Figure 4.6: All three samples taken at transect T. Taken on 05/11/2018.

4.3. SU3 - Below MacKenzie House

The cliffs of SU3 are less prone to collapse due to more apparent vegetation. Although signs of wave undercutting can still be seen. The beach of SU3 is generally sand. The north border is the first groyne to be encountered when coming down from trail 4. Figure 4.8 shows the view when looking south and north when standing atop the southernmost groyne. Golder Associates Ltd. (2015) states that in this SU sand accumulates, which originates from the cliffs in SU2.

(a) Sample M1.

(b) Sample M2.

(c) Sample M3.

Figure 4.7: All three samples taken at transect M. Taken on 05/11/2018.

In SU3 the first part of the berm and groyne system which was constructed in the 1980s. The berm provides an extra protection against marine erosion by adding extra elevation to the cliff toe. In this section the installed berm is the most effective and is only inundated during the highest of tides (Golder Associates Ltd., 2015). Figure 4.8b shows large logs laying on the top of the berm, which are left there by high water and simultaneously wave action. These logs, together with wave attack, can still harm the cliff toe during high water events. On the other hand the logs may function as extra protection against lower waves.

(a) View directed south.

(b) View directed north.

Figure 4.8: Photos at southernmost groyne. Taken on 28/10/2018.

At the third transect three samples were taken. This is on the berm in between the groynes. As with the transects before, three samples were taken. An important note at this transect is that the material is coarser overall. Also, sample M3 was found difficult to obtain due to the scarcity of fine sediment. Although small patch of sediment was found from which it was taken (see Figure 4.7c). Besides a volumetric sample an attempt to determine size of the berm material was done by ways of a pebble count.

4.4. SU4 - Tower Beach

The berm/groyne system continues onwards from Tower 1 to the north. The reason for this distinction between SU3 and SU4 is the orientation of the shore line. In between the groynes at SU5 the shoreline has adjusted to the dominant wave direction. The latter is clearly illustrated in Figure 4.9. According to Golder Associates Ltd. (2015) due the groyne spacing and scarcity of updrift sediment, no further beach stabilization has occurred. At the northern edge of SU4, at Tower 2, a second pebble count was done. In the same figure in can be clearly seen that in between the groynes the shoreline has adjusted itself perpendicular to incoming waves.

Figure 4.9: The adjustment of the shore line in SU4 (northeast) in comparison to SU3 (south). From Google Earth 23/7/2018.

4.5. SU5 - Tower 2 to Acadia Beach

Just behind the constructed berm and groyne system SU5 starts. In this SU more sand is present again. In the upper-intertidal area larger rocks (gravel, boulders) can be found with strips of sand in between these rocks. This may be signs of deposition of sand taken from upstream parts. The sediment samples were taken from these sand strips. In this SU the infrastructure, Marine Drive NW and the sewage system, is already very close to the current cliff top. Further recession of the cliff puts these structures at risk.

(a) Sample P1. (b) Sample P2. (c) Sample P3.

Figure 4.10: All three samples taken at transect P. Taken on 05/11/2018.

(a) Sample H2. (b) Sample H3.

Figure 4.11: Both samples taken at transect H. Taken on 05/11/2018.

Transect P is located at the part of beach where sand is becoming more apparent again in stead of the pebble berm. The sediment in the samples (P1, P2, P3) appear to be darker than at transect N and T. At transect H only two samples were taken, namely H2 and H3. One underwater sample and one on the beach. No cliff sample was taken here.

4.6. SU6 - First part of Acadia Beach

SU6 is the start of Acadia Beach and is not as prone to marine erosion as the other SUs are. The intertidal area in front of the beach is a large sandbank called Spanish Bank. These banks are an extra barrier against wave energy, which protects this part of the coast.

Figure 4.12: Sample S3. Taken on 05/11/2018.

Transect S is located at the start of Spanish Banks at Acadia Beach. Two similar samples were taken as at transect H. The water at this transect seemed to be cloudier than at other locations. Whether this is due to the higher water or finer sediment is not known. No photo of sample S2 in the field is made.

4.7. Results volumetric sieving

The sediment samples collected from the site survey are were studied in the lab. The samples were dried and large organic material, like shells, was removed. The samples were then ready to be sieved through sieves with openings from 125 µm to 8000 µm . The results are shown in the Figure 4.13 and Table 4.2. Results from the pebble counts are given in Appendix B.

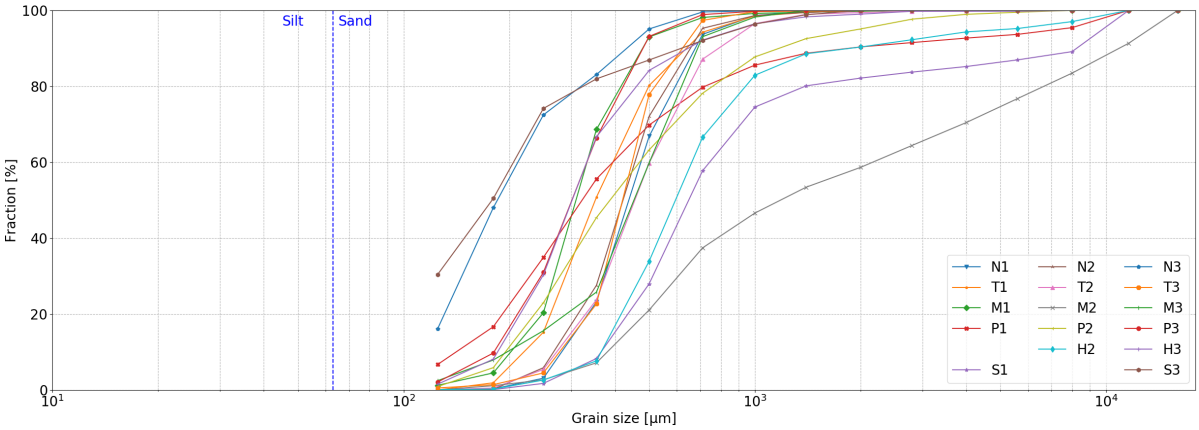

Figure 4.13: Grading diagrams of the volumetric sediment samples obtained at the Point Grey cliffs.

The cumulative grading diagram is constructed from the data obtained from the sieving process and shown in Figure 4.13. From these the diagrams the median grain diameter can read at 50% mark. This median grain diameter is needed for the sediment transport model. Sample M2 really stands out from the rest with the highest median grain diameter of 1200 µm. This can be due to the fact that the sample was actually taken from the core material of the man-made berm. The average median grain diameter, which can be read from Table 4.2, is 440 µm. However, neglecting the contribution of sample M2 to the average median grain diameter this value drops to 380 µm, which will be the final value used in further model computations.

Overall the intertidal samples are finer than other samples. This can be explained by flushing out of finer particles, while coarser particles cannot be transported. The median grain diameter of cliff toe samples T1, M1 and P1 are comparable to the grain diameters of cliff material found in earlier studies mentioned in Section 3.1. Figure 4.14 shows the median grain diameter plotted spatially. At Point Grey (SU2 and SU3) the material is coarser than at the North Arm breakwater and Spanish Banks. A possible explanation is that the two locations are sheltered from waves, while Point Grey is not.

Table 4.2: Median grain sizes (D_{50}) of volumetric samples along Wreck Beach.

No.	Sample Code	Weight [g]	D_{50} [µm]
1	N1	140.62	443.75
2	N2	97.14	427.62
3	N3	118.28	185.73
4	T1	69.66	351.70
5	T2	82.74	460.39
6	T3	88.42	426.39
7	M1	129.58	313.89
8	M2	112.15	1200.00
9	M3	106.66	457.94
10	P1	84.73	325.93
11	P2	103.05	391.65
12	P3	136.81	305.88
13	H2	80.82	603.44
14	H3	137.97	306.31
15	S2	142.48	655.42
16	S3	78.07	178.81
	Avg.	106.82	439.68

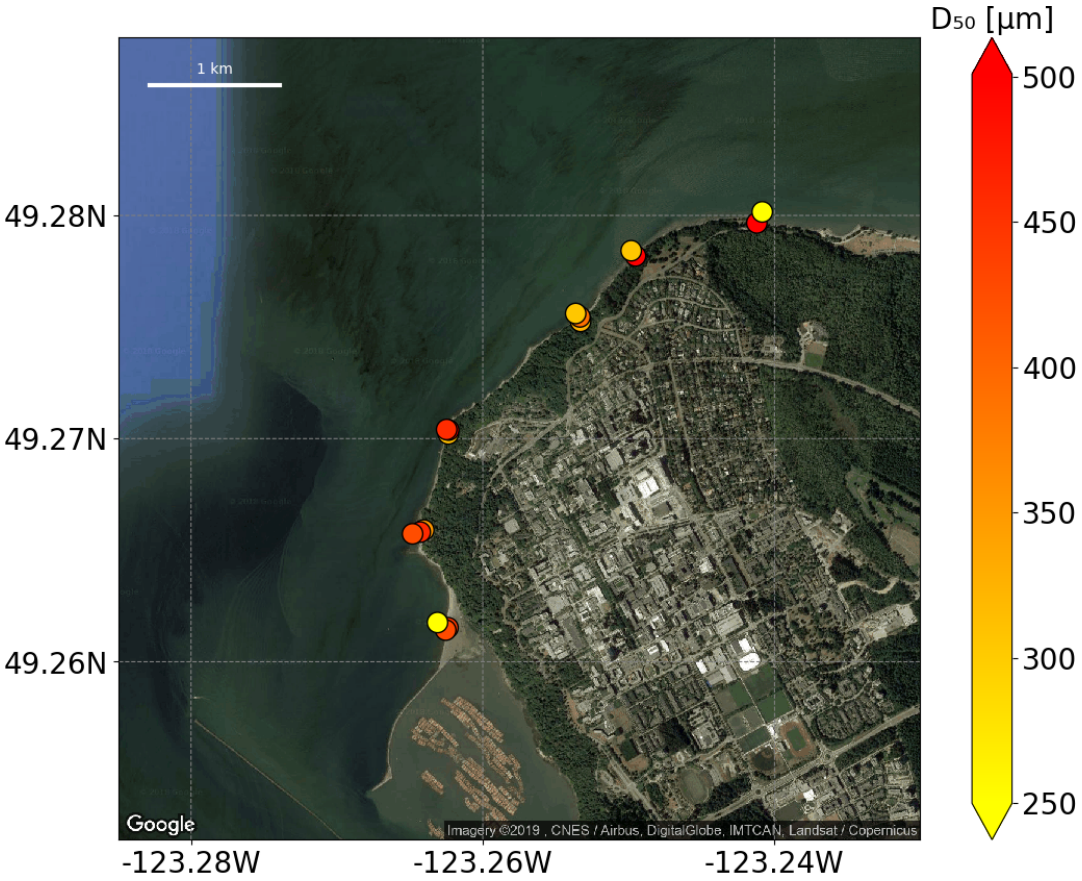

Figure 4.14: Median grain diameters (D_{50}) of samples at several locations along Wreck Beach.

5

Methodology

5.1. Scope

In Chapter 2 potential marine erosion mechanisms over different time scales were identified and are shown in Figure 5.1. Sources state that the wave-induced alongshore sediment transport is the main marine erosion mechanism. Therefore this time scale is chosen to be further investigated. This time scale can then be extrapolated estimate sediment budgets in the system.

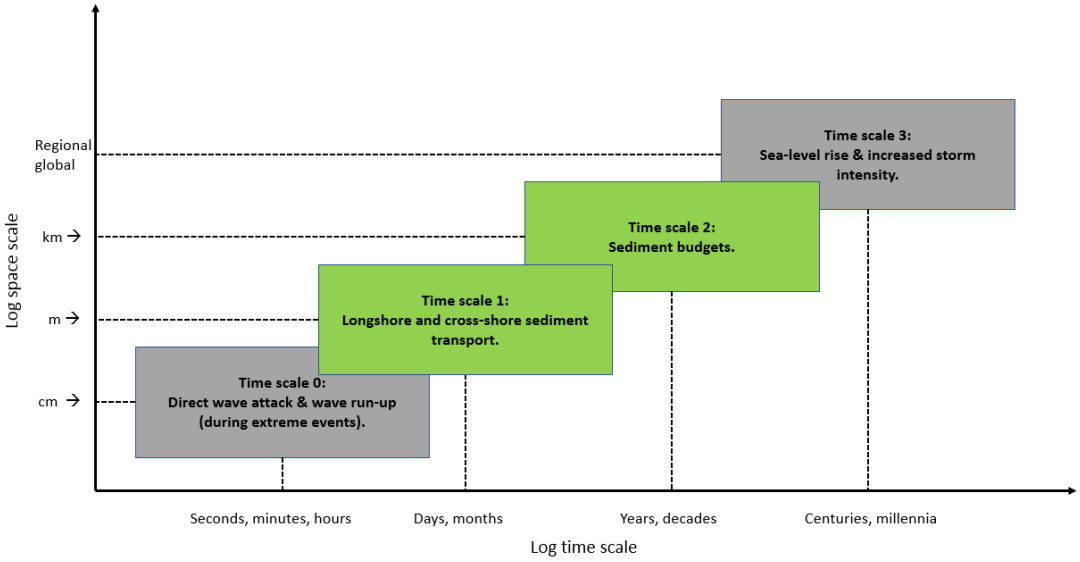

Figure 5.1: Visualized time scales and their marine erosion mechanisms important to coastal cliffs and shoreline erosion. Highlighted in green are the time scales further investigated in this study.

The system will be divided into representative hydrodynamic conditions, which will give an overview of the flows around the Point Grey cliffs. These can be used to see whether sediment will indeed be transported under certain conditions. The representative conditions can then be extrapolated to yearly periods.

5.2. Choice of model

As stated before, the hydrodynamics and sediment transports need to be analyzed. Since the area has two main directions, a two-dimensional (2D) model is needed at minimal. In this case a 2D depth-averaged model is thought to suffice as this study is focuses on general properties of the system and not at three-dimensional (3D) detail processes (e.g. undertow). Choosing for a 3D will give much more detail, but it will increase

computational times considerably. The increased detail also increases the model's complexity, which makes these models harder to set-up, calibrate and validate.

The model needs to represent the tide and river outflow at the Point Grey coastal system, together with wave propagation. This is what Delft3D-FLOW coupled together with Delft3D-WAVE can do perfectly. This coupling can model the interaction between currents and waves, which is very convenient in this model study. While the program is called Delft3D, it must be said noted a 2D situation will be modelled to take away any confusion.

5.3. Scenarios

To analyze the Point Grey coastal system and to distinguish the effect of three main components of the system (tide, river and waves) several scenarios are proposed to model. From Chapter 3 one can see that the hydrodynamics of the system can be divided into two main periods, the freshet and non-freshet of the Fraser River (see Figure 3.9). Then, Figure 3.7 shows that within these two periods two main wave directions can be seen, approximately west northwest and east southeast. For the tide a representative tidal range is chosen, which is about 80% of the spring tide in Figure 3.4 equaling to ~4 m. Lastly, a comparison is made between regular conditions and storm conditions with a return period of five years.

In all the scenarios listed in this Section, no storm surge is modelled. The Delft3D-FLOW module only calculates storm surges with the help of input wind field files. No use was made of this capability, since it was incorrectly assumed that Delft3D models storm surge with just a single wind condition in stead of a wind field file. However, incorporating the representative storm surges can be added by means of an additional constant water level in the area.

5.3.1. Test scenarios

The differentiation between scenarios, discussed in Section 5.3, give the resulting scenarios presented in Table 5.1. As the Point Grey cliffs face the to the northwest the choice is made to exclude waves coming from the east southeast from the model as these waves have limited effect on the sediment transports. In the next two paragraphs the boundary conditions of the river and waves are listed.

Table 5.1: Proposed present-time model scenarios.

Scenario ID	Period	Tidal range	River discharge	Waves
1	Aug. - Apr.	~4 m	Non-freshet	WNW
2	Aug. - Apr.	~4 m	Non-freshet	-
3	Aug. - Apr.	~4 m	Non-freshet	Only storm wind (5 year RP)
4	May - Jul.	~4 m	Freshet	Western storm (5 years RP)
5	May - Jul.	~4 m	Freshet	WNW
6	May - Jul.	~4 m	Freshet	-

The scenarios listed in Table 5.1 are all run with bottom sediment available with a median grain diameter of 380 µm. Also the morphological scale factor is set to almost zero, because the goal is not to model to morphological changes but sediment transports. The effect is an unlimited supply of sediment from the bottom.

Waves & wind

In the tables below (Tables 5.2 & 5.3) the parameters to represent wave and wind climates are shown. These values are obtained through a statistical analysis presented in Appendix C. No wave condition boundaries are used during eastern wave conditions since only the waves from the west are thought to be relevant for this model study. The tables list the wind speed, wind direction, significant wave height, wave direction and peak period of the representative wave condition.

For the storm conditions an extreme value analysis is done. The results are shown in Table 5.4. The extreme

value analysis method can, again, be found in Appendix C. As with the eastern wave conditions in Tables 5.2 and 5.3 the storm waves from the east direction are not included in the simulations. The table lists the wind speed, wind direction, significant wave height, wave direction and peak period corresponding to the representative storm condition.

Table 5.2: Non-freshet wind & wave conditions.

Direction	**West (Scenario 1)**	**East (Scenario 2)**
u_w [m s^{-1}]	5.3	7.7
Wind dir. [°]	295	108
H_s [m]	0.46	-
Wave dir. [°]	295	-
T_p [s]	7.22	-

Table 5.3: Freshet wind & wave conditions.

Direction	**West (Scenario 5)**	**East (Scenario 6)**
u_w [m s^{-1}]	5.2	5.6
Wind dir. [°]	287	119
H_s [m]	0.48	-
Wave dir. [°]	287	-
T_p [s]	8.89	-

Table 5.4: Storm (5 years RP) wind & wave conditions.

Direction	**West (Scenario 4)**	**East (Scenario 3)**
u_w [m s^{-1}]	11.2	13.4
Wind dir. [°]	297	117
H_{ss} [m]	1.94	-
Wave dir. [°]	297	-
T_p [s]	4.71	-

Fraser River discharges

The Fraser River discharge is treated in Section 3.5. The total discharge of the Fraser, the distribution of the discharge, and the seasonality of the discharge are all explained there. The average discharges over 10 years per Fraser River arm is shown in Table 5.5. The total discharge (Q_T) is the discharge found at Port Mann before the Fraser River splits into the North- (Q_N) and Main Arm (Q_M). The discharges presented here are the result of an average of 10 years and are indicative for a single year. Per year these discharges can vary significantly, especially during freshet. The maximum found in Figure 3.9 is 12,000 m^3 s^{-1}, which is an increase of 50% compared to the total discharge during freshet in Table 5.5.

Table 5.5: Fraser River discharges per river arm during freshet and non-freshet conditions [m^3 s^{-1}].

	Q_T	Q_M	Q_N
Non-freshet (Scenarios 1, 2, and 3)	2500	2125	375
Freshet (Scenarios 4, 5, and 6)	8008	6807	1201

5.3.2. Fraser River transport capability

Besides the scenarios presented in Table 5.1 an additional model test is set-up. This model functions to check whether the North Arm of the Fraser River is capable of transporting any sediment to the Point Grey cliffs. For this the sediment load of the river needs to be known. In Section 3.5 information about the sediment load is presented together with grain classes with indicative grain diameter. Also, as with the discharges, the

seasonality sediment load is known as well as the distribution of sediment between Fraser River arms. The model needs a concentration to be set at inflow boundaries, which are explained in further sections.

In this model there will be no bottom sediment available and contains only sediment fractions found in Section 3.5 at the inflow boundary of the North Arm.

Fraser River sediment concentrations

The first step to find approximate sediment concentrations is to calculate the sediment discharges per river arm. In Table 3.3 the total sediment content of the Fraser River at Port Mann is given per year. As mentioned before, 80% of the sediment is discharged during freshet conditions (mid-May to mid-July) during approximately 62 days. The last 20% is discharged divided over the remaining 303 days. The North Arm is thought to take account for 6% of the total sediment load. The Main Arm gets the remaining 94%. Now that the sediment volumes together with the time it takes to discharge these amount is known, the average discharges per second can be calculated. The dredging activity presented in Section 3.6.2 is included in the sediment discharges of the Main Arm. The average sediment discharges can be found in Tables 5.6 and 5.7. $Q_{s,T}$ is the sediment transport at Port Mann. $Q_{s,M}$ and $Q_{s,N}$ is the sediment load in the Main- and North Arm respectively.

Table 5.6: River sediment discharges per river arm during freshet conditions [kg s^{-1}].

Sediment fraction	$Q_{s,T}$	$Q_{s,M}$	$Q_{s,N}$
Silt	1239.5	1165.1	74.4
Sand [< **177** µm]	463.0	435.2	27.8
Sand [> **177** µm]	448.0	421.1	26.9
(Dredging)		(37.3)	

Table 5.7: River sediment discharges per river arm during non-freshet conditions [kg s^{-1}].

Sediment fraction	$Q_{s,T}$	$Q_{s,M}$	$Q_{s,N}$
Silt	63.4	59.6	3.8
Sand [< **177** µm]	23.7	22.3	1.4
Sand [> **177** µm]	22.9	21.5	1.4
(Dredging)		(9.7)	

Now, by using the discharges from Table 5.5 the sediment loads from Tables 5.6 and 5.7 can be transformed into concentrations. The resulting concentrations are shown below in Tables 5.8 and 5.9, which will be used in the model as transport boundary conditions. $c_{s,M}$ and $c_{s,N}$ are the sediment concentrations of the Main- and North Arm respectively.

Table 5.8: River sediment concentration per river arm during freshet conditions [kg m^{-3}].

Sediment fraction	$c_{s,M}$	$c_{s,N}$
Silt	$1.71 \cdot 10^{-1}$	$6.19 \cdot 10^{-2}$
Sand [< **177** µm]	$6.39 \cdot 10^{-2}$	$2.31 \cdot 10^{-2}$
Sand [> **177** µm]	$6.19 \cdot 10^{-2}$	$2.24 \cdot 10^{-2}$
(Dredging)	$(5.48 \cdot 10^{-3})$	

Table 5.9: River sediment concentration per river arm during non-freshet conditions [kg m^{-3}].

Sediment fraction	$c_{s,M}$	$c_{s,N}$
Silt	$2.80 \cdot 10^{-2}$	$1.01 \cdot 10^{-2}$
Sand [< **177** µm]	$1.05 \cdot 10^{-2}$	$3.73 \cdot 10^{-3}$
Sand [> **177** µm]	$1.01 \cdot 10^{-2}$	$3.73 \cdot 10^{-3}$
(Dredging)	$(4.56 \cdot 10^{-3})$	

5.3.3. Base- & sensitivity cases

To compare model results from the scenarios described above with model results using other parameters, base- and sensitivity cases are setup. All of the base- and sensitivity cases are done with scenario 1 in Table 5.1. The first two base cases of scenario 1 are ones with either the wind or waves being disabled.

In total five sensitivity cases for scenario 1 are chosen. Two parameters are changed: the significant wave height of the incoming waves and the mean grain diameter of the bottom sediment. Both parameters have one situation with a decrease of that parameter of 34% and the other increased with 34%. The last sensitivity case is the change in location of cross-sections in the model (see Fig. 7.16).

6

Delft3D model

This chapter will guide the reader through the setup of the hydrodynamic model with all its components. First a small introduction to what the models, Delft3D-FLOW and Delft3D-WAVE themselves do. Afterwards all individual components of the model are discussed. The last section takes the reader through the water level calibration of the models.

In total three separate 2D-models were made to acquire hydrodynamic conditions around the Point Grey coastal system. Figure 6.1 gives an overview of the conceptual model flow together with each of their inputs.

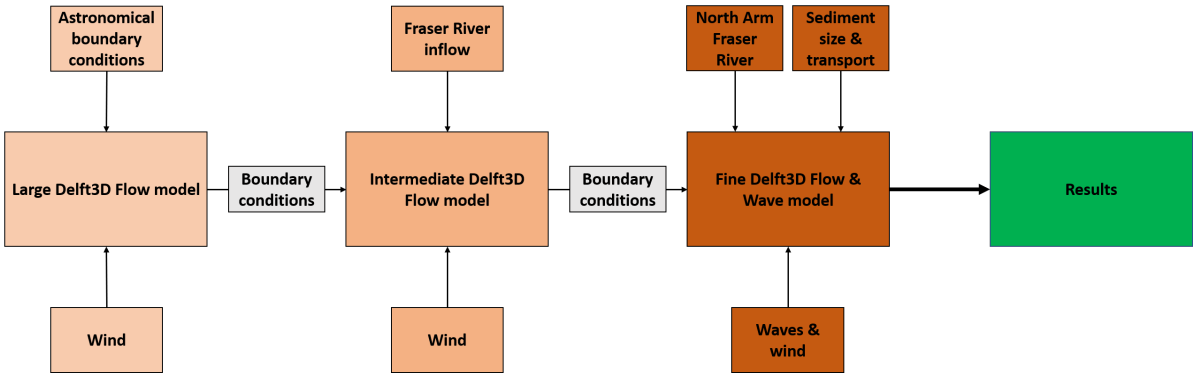

Figure 6.1: Set-up for Point Grey hydro- morphodynamic model.

6.1. Delft3D-FLOW

Delft3D-FLOW forms the hydrodynamic basis of the all of the other program packages, such as transports and short wave propagation. In this case the FLOW-module is used to approximate the hydrodynamic behavior around the Point Grey cliffs. The model solves three different equations: the momentum equation in both x- and y-direction:

$$\underbrace{\frac{\partial v}{\partial t}}_{[1]} + \underbrace{u\frac{\partial u}{\partial x}}_{[2]} + \underbrace{v\frac{\partial u}{\partial y}}_{[3]} + \underbrace{g\frac{\partial \zeta}{\partial x}}_{[4]} \underbrace{- fv}_{[5]} + \underbrace{\frac{\tau_{bx}}{\rho_w(d+\zeta)}}_{[6]} \underbrace{- \frac{F_x}{\rho_w(d+\zeta)}}_{[7]} \underbrace{- \nu(\frac{\partial^2 u}{\partial x^2} + \frac{\partial^2 u}{\partial y^2})}_{[8]} = 0 \qquad (6.1)$$

$$\underbrace{\frac{\partial v}{\partial t}}_{[1]} + \underbrace{v\frac{\partial v}{\partial y}}_{[2]} + \underbrace{u\frac{\partial v}{\partial x}}_{[3]} + \underbrace{g\frac{\partial \zeta}{\partial y}}_{[4]} \underbrace{+ fu}_{[5]} + \underbrace{\frac{\tau_{by}}{\rho_w(d+\zeta)}}_{[6]} \underbrace{- \frac{F_y}{\rho_w(d+\zeta)}}_{[7]} \underbrace{- \nu(\frac{\partial^2 u}{\partial x^2} + \frac{\partial^2 u}{\partial y^2})}_{[8]} = 0 \qquad (6.2)$$

and the depth-averaged continuity equation:

$$\frac{\partial \zeta}{\partial t}^{[9]} + \frac{\partial (d+\zeta)u}{\partial x}^{[10]} + \frac{\partial (d+\zeta)v}{\partial y}^{[11]} = 0 \tag{6.3}$$

in which:

u, v	=	flow velocities in x-, y-direction.
g	=	gravitational constant.
f	=	coriolis parameter.
$\tau_{bx,y}$	=	bed shear stress.
ρ_w	=	density of water.
d	=	water depth.
ζ	=	water level from reference point.
$F_{x,y}$	=	external forces.
v	=	horizontal eddy viscosity.
U	=	absolute magnitude of flow velocity.
C	=	Chézy coefficient.
n	=	Manning coefficient.
h	=	total water depth.

The terms in Equations 6.1, 6.2, and 6.3 represent the following factors:

[1]	velocity gradient in time.
[2,3]	advective terms.
[4]	barotropic pressure gradient.
[5]	Coriolis force.
[6]	bottom stresses.
[7]	external forces (e.g. wind).
[8]	viscosity term.
[9]	water level gradient in time.
[10]	input volume x-direction.
[11]	input volume y-direction.

The bottom roughness in this model is defined in the Manning coefficient. For the depth-averaged flow the shear stresses due to the bottom friction can be written as:

$$\tau_{bx} = \rho_w g(\frac{|U|u}{C^2})$$

$$\tau_{by} = \rho_w g(\frac{|U|v}{C^2})$$

With the Chézy coeffient (C) calculated by:

$$C = \frac{\sqrt[6]{h}}{n}$$

The equations presented before are solved for every point on a computational grid, presented in Figures 6.3a through 6.3d. Delft3D-FLOW uses a staggered grid, which means the water levels and velocities calculated on specific points are not the same (see Figure 6.2).

For more additional information about the Delft3D-FLOW model a reference is made to the Delft3D-FlOW: User Manual (Deltares, 2011a).

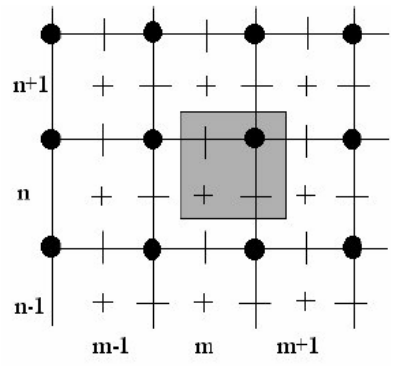

Figure 6.2: Staggered grid of Delft3D Flow (Deltares, 2011a).

6.2. Delft3D-WAVE

The second module used in the model is the Delft3D-WAVE, which is coupled online every 30 simulation minutes with the Delft3D-FLOW model. This means the short waves are computed with the hydrodynamics output of the FLOW-model and then updated with the results from the Delft3D-WAVE model.

The Delft3D-WAVE model is based upon the SWAN model (for more info see Booij et al. (1999), Deltares (2011c)). The SWAN model solves the wave spectrum change over a computational grid with the following action balance:

$$\underbrace{\frac{\partial}{\partial t}N}_{[1]} + \underbrace{\frac{\partial}{\partial x}c_x N}_{[2]} + \underbrace{\frac{\partial}{\partial y}c_y N}_{[3]} + \underbrace{\frac{\partial}{\partial \sigma}c_\sigma N}_{[4]} + \underbrace{\frac{\partial}{\partial \theta}\sigma_\theta N}_{[5]} = \underbrace{\frac{S}{\sigma}}_{[6]} \tag{6.4}$$

The factor N is the action density, which is the energy density of a spectrum divided by the relative frequency. Term [1] stands for change of action density in time, [2,3] state the propagation of action in geographical space, [4] for the relative frequency shift due to changes in depth and current, [5] for the depth-induced and current-induced refraction. Term [6] is the source term for wind-generation, dissipation and others. $c_{x,y,\sigma,\theta}$ are the wave propagation speeds in their respective space (Deltares, 2011c).

6.3. Computational grids

In total three different numerical grids were needed. The large model covers an area from the North Pacific west of Vancouver Island into the Strait of Georgia. The second grid covers the central Strait of Georgia. The last and finest grid forms around the Point Grey cliffs. The grids and their environments are shown in Figure 6.3. The grids are first generated with the help of Delft Dashboard.

For the numerical grids it is suggested to fulfill three criteria (Deltares, 2011a):

1. Orthogonality, the angle between grid lines, should be less than 0.02.

2. Aspect ratio, ratio between grid size in x- and y- direction, should be [1,2].

3. Ratio of grid size in either x- or y-direction of neighboring cells (also called smoothness) should be less than 1.2 in the area of interest.

The orthogonality and smoothness is thoroughly checked for all three model grids. However, the aspect ratio is not thoroughly checked. The model grids are found to be sufficient for this project. In Table 6.1 some grid parameters are shown for the three grids.

Table 6.1: Overview of the grid properties.

Parameters	**Grid**		
	Large	**Intermediate**	**Fine**
$[n_x, n_y]$	[492, 263]	[535,318]	[340,183]
$[\Delta x_{max}, \Delta x_{min}]$ [m]	[2010, 594]	[216,88]	[226,10]
$[\Delta y_{max}, \Delta y_{min}]$ [m]	[2818,886]	[294,134]	[97,5]

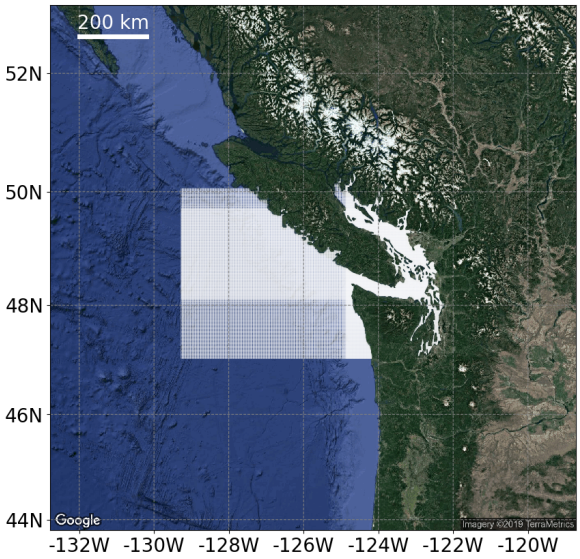

(a) Large grid.

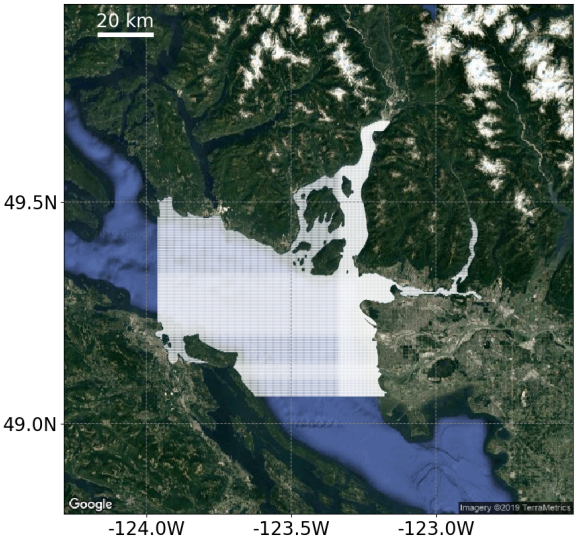

(b) Intermediate grid.

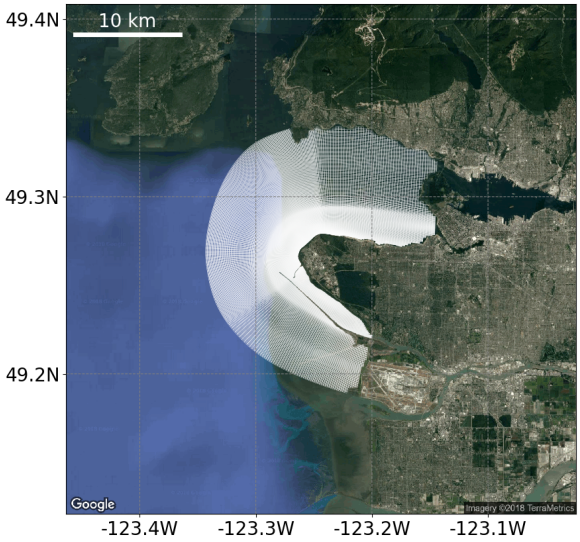

(c) Fine grid.

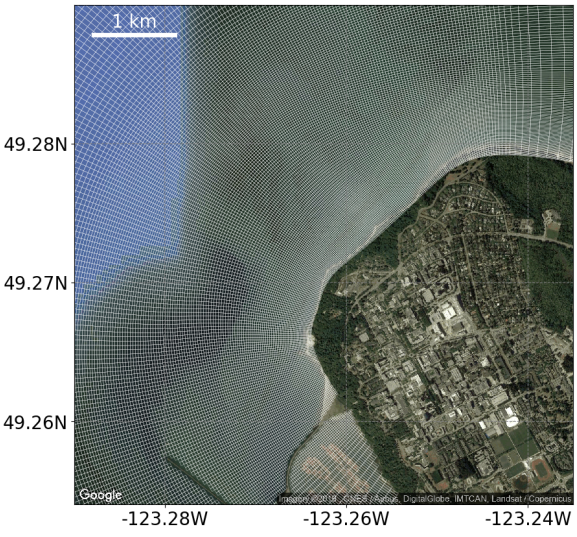

(d) Fine grid zoomed in.

Figure 6.3: Three computational grids and a close-up of the finest grid. The mean grid sizes $[\Delta x, \Delta y]$ are [1300,1852] m for the largest grid in Figure 6.3a, [304,214] m for the intermediate grid (Figure 6.3b), and [118,51] m for the finest grid (Figures 6.3c and 6.3d). Maxima and minima can be found in Table 6.1.

6.4. Bathymetry

The depths of the different grids are from a variety of sources. The depth file in the large model (Figure 6.4a) is from the NOAA[1] with partly additions from the Delft Dashboard GEBCO-08 satellite database. The depths in the intermediate model are again partly from the NOAA depth samples, but also more detailed additions of nautical charts of Point Grey and the Fraser Main Arm (see Appendix D) are implemented. Both these admiralty charts are in Figures D.1 & D.2 of Appendix D.

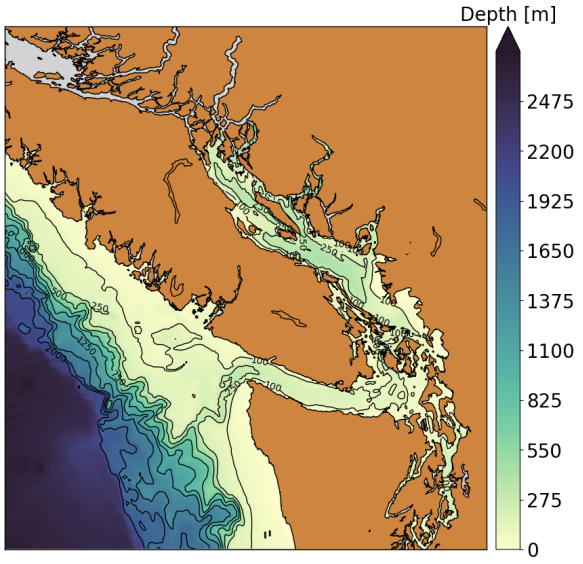

(a) Depth large grid.

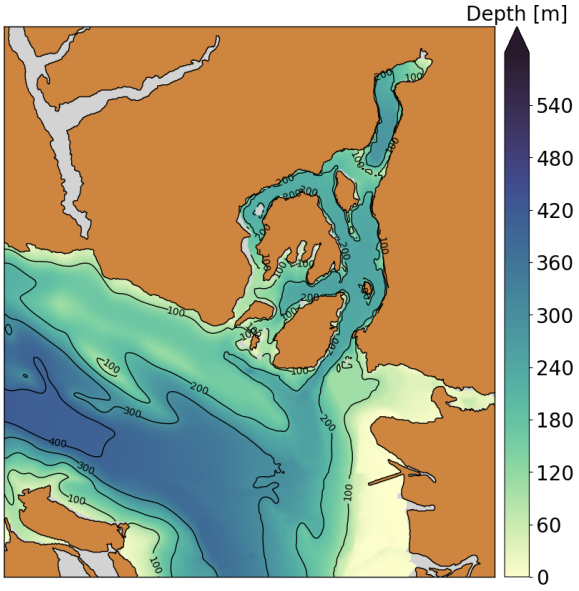

(b) Depth intermediate grid.

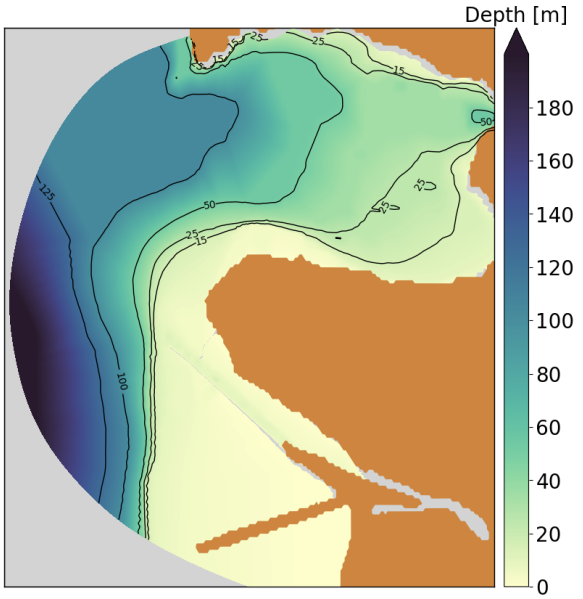

(c) Depth fine grid.

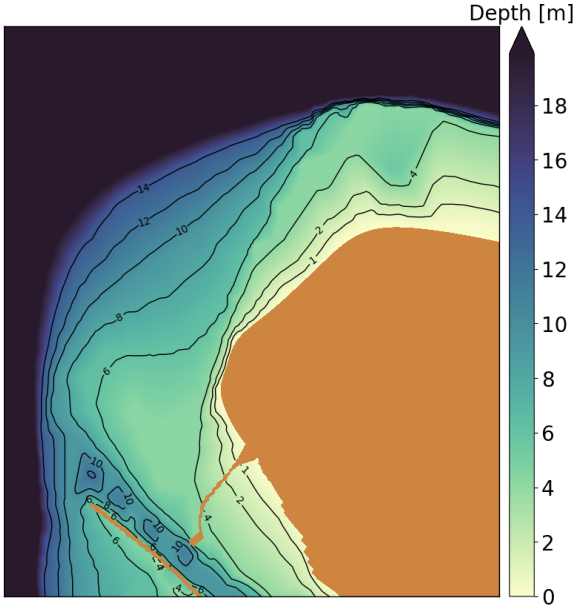

(d) Fine model depth zoomed in.

Figure 6.4: Depths used in the three model simulations.

The resulting bathymetries are shown in Figure 6.4. In the zoomed bathymetry (Figure 6.4d) a wide shallow shelf can be distinguished. As well as the deeper North Arm river bed, cut through the mentioned shallow

[1] National Oceanic and Atmospheric Administration.

parts.

6.5. Boundary- & initial conditions

The large model (Figure 6.3a & 6.4a) has astronomical boundary conditions (M2, S2, N2, K2, K1, O1, P1, Q1, Mf, MM, M4, MS4, MN4) for the western side of the grid, north and south at the North Pacific Ocean generated with the help of Delft Dashboard. All the boundaries around the Strait of Georgia are closed boundaries. Also the northern end is a closed boundary, while in reality this is not the case. However, the model produced realistic results. By means of nesting, the simultaneous models retrieve their water level/flow velocity boundary conditions as seen in Figure 6.1. The other boundary conditions, the river outflows, can be found in Tables 5.2 through 5.5. In Figure 6.5 the different boundary conditions are shown. A blue boundary means a water level boundary. Red stands for a velocity boundary and green for a discharge boundary. A full line represents either an astronomical or constant boundary. A striped line represents a time series boundary prescribed by earlier models. A striped-dot line is again a time series boundary, but with incoming waves.

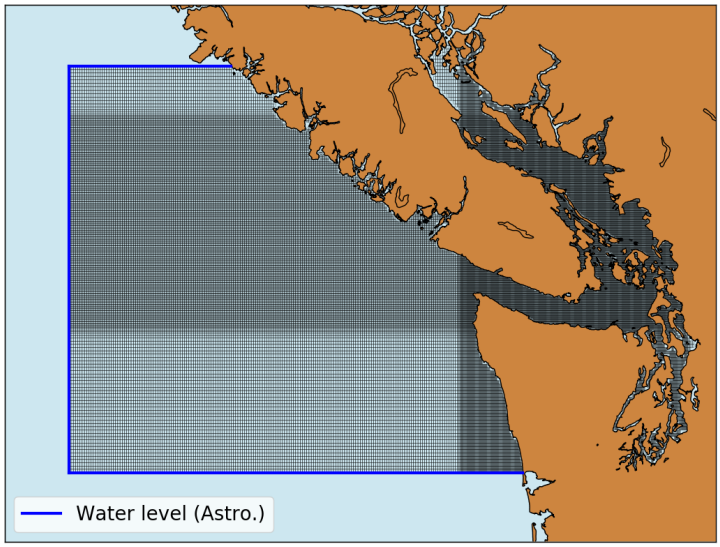

(a) Large boundaries.

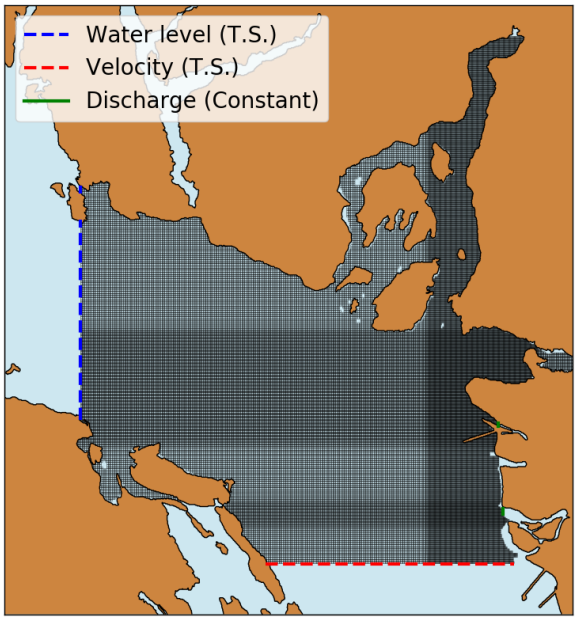

(b) Intermediate boundaries.

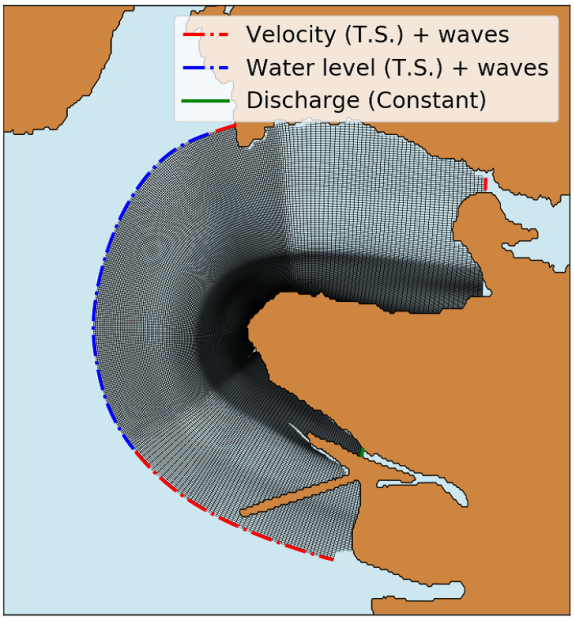

(c) Fine boundaries.

Figure 6.5: All boundaries on the different grids.

The models are run from zero initial conditions, a so-called cold start. The maximum spin-up time for the models is about two days. The spin-up time is the time needed for the eigenmodes, generated by the offset between initial conditions and boundary conditions, to be damped.

6.6. Time step

Running the proposed models each have their own stability limit in terms of the time step. This stability limit is described by the Courant number in Equation 6.5 (Deltares, 2011a). On the one hand, the time step must be as high as possible to reduce model run time. On the other hand, the time step must be chosen such that the model is stable and produces appropriate accurate results.

$$C_f = 2\Delta t\sqrt{gH}\sqrt{\frac{1}{\Delta x^2}+\frac{1}{\Delta y^2}} \tag{6.5}$$

in which:

Δt = time step.
g = gravitational constant.
H = total water depth.
Δx = cell size in x-direction.
Δy = cell size in y-direction.

Table 6.2 shows the time steps chosen for the model runs as well as the maximum resulting Courant numbers using the maximum Δx and Δy for each model from Table 6.1. The fine model needed a lower Courant number to facilitate the high outflow velocities of the Fraser River.

Table 6.2: Overview of model time steps with maximum Courant numbers.

Model	**Time step** [s]	$C_{f,max}$
Large	30	12.5
Intermediate	15	18.2
Fine	3	7.9

6.7. Cross-sections

During the site analysis and visit (Appendix 4) the Point Grey can be divided into several Shore Units (SUs) based on expert judgment. The dissimilarity of the SUs is sought in characteristic like shoreline orientation and shoreline sediment material. In later sections will show that the choice of these boundary locations can be significant. In the fine model cross-sections the SU boundary will be defined as cross-sections which determine flows and sediment transports over the boundaries of said SUs (see Figure 6.6). The calculated sediment transport can be used to set-up and extrapolate sediment flows from one SU to another.

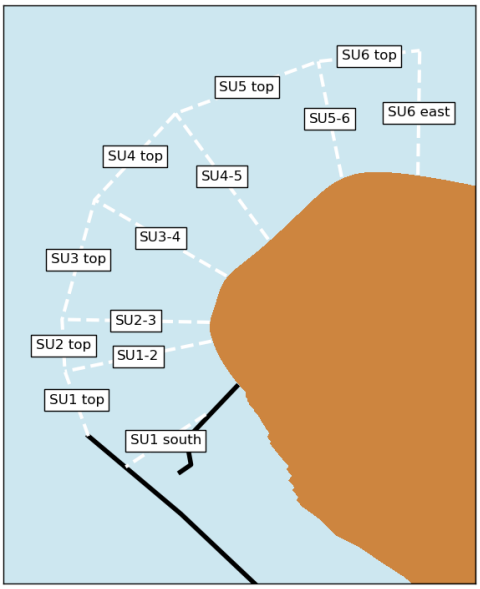

Figure 6.6: Assumed borders of the Shore Units (SUs) in the coastal zone of the Point Grey cliffs.

6.8. Thin dams & dry points

To mimic the presence of the jetties and breakwater, thin dams and dry points are implemented in the model. Thin dams inhibit any flow through a cell

boundary as is the case with jetties and breakwater. Marking cells as dry points means that the cell will be flagged as land and will be exempt during model calculations.

In the fine model with waves enabled, these structures are also implemented as dams. This way the waves are not able to pass over or through these structures.

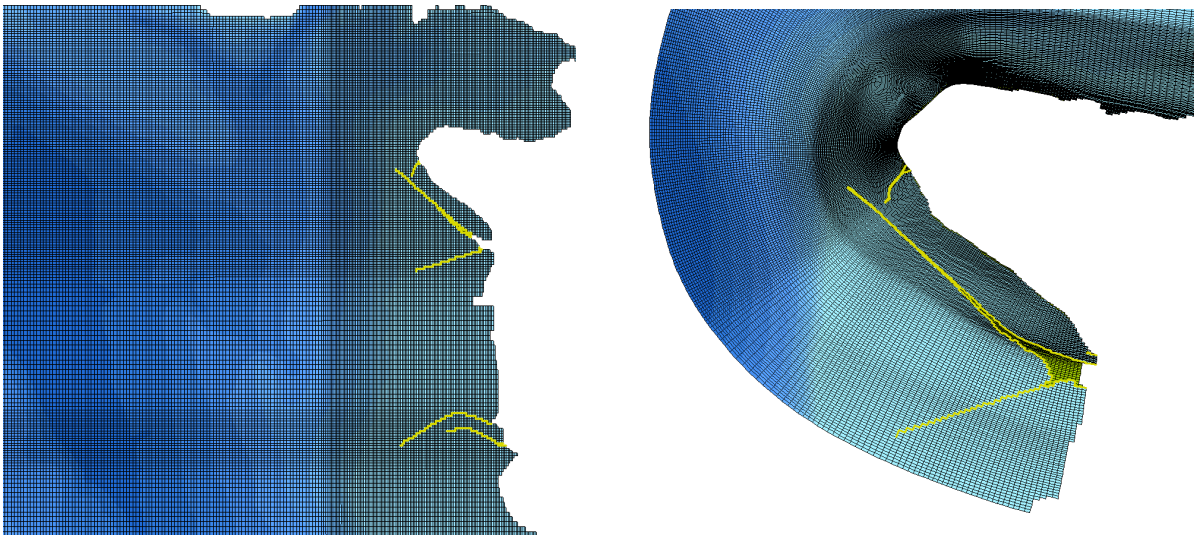

(a) Thin dams and dry points in intermediate model.

(b) Thin dams and dry points in fine model.

Figure 6.7: Impression of the use of thins dams (yellow lines) and dry points (green cells) in the models.

6.9. Calibration

To qualitatively assess the performance of the models the reproduction of the tidal wave into the basin of the Georgian Strait is checked. In the largest grid several International Hydrographic Organization (IHO) tidal stations are imported into the model grid. From the IHO database the water level signals are extracted and compared to the model results.

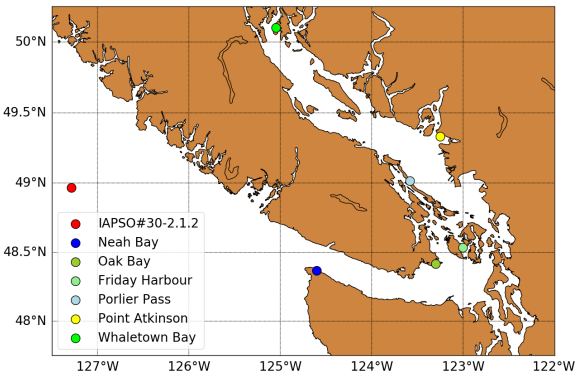

Figure 6.8: Locations of tidal stations used in calibration.

Table 6.3: Coordinates of tidal stations.

Tide station	**Lat.**	**Long.**
IAPSO#3-2.1.2	48.9662°	-127.2830°
Neah Bay	48.3672°	-124.600°
Oak Bay	48.4167°	-123.300°
Friday Harbour	48.5355°	-123.002°
Porlier Pass	49.0166°	-123.583°
Point Atkinson	49.3330°	-123.250°
Whaletown Bay	50.100°	-125.050°

The calibration is done in two steps. The first step is to fit the model results as closely as possible to the database signals by an iterative process. This is done by changing two model settings: the bottom friction, the Manning co-efficient n, and the horizontal eddy viscosity. In the end the friction parameters were set to 0.051 $m^{1/3}s^{-1}$ for both flow directions for all models. The horizontal eddy viscosities, and in case of sediment transport simulation the horizontal eddy diffusivity, were set to 87, 30, 20 $m^2 s^{-1}$ for the large, intermediate and fine models respectively.

In this iterative process Delft3D-TIDE (Deltares, 2011b) was used to analyse the water level signals (see Figures 6.9 & E.1). Delft3D-TIDE can fit a certain set of given tidal constituents to a given tidal signal by means of a Taylor series (Equation 6.6). The approximation by a Taylor series is given by:

$$h(t) = A_0 + \sum_{i=1}^{n} A_i \cos(\omega_i - \varphi_i) \tag{6.6}$$

in which the $h(t)$ is the water level in time, A_0 the mean water level, and A_i, ω_i, φ_i, are the amplitude, frequency, and phase of tidal constituent i respectively. To distinguish tidal constituents from each other, a certain time range is needed. For this analysis a time series of 32 days is chosen. This time series is not long enough to separate K2 from S2 and P1 from K1. Therefore these four constituents are coupled in the analysis (Deltares, 2011b, Luijendijk, 2001). The results of the Delft3D-TIDE analysis can be found in Figure E.2.

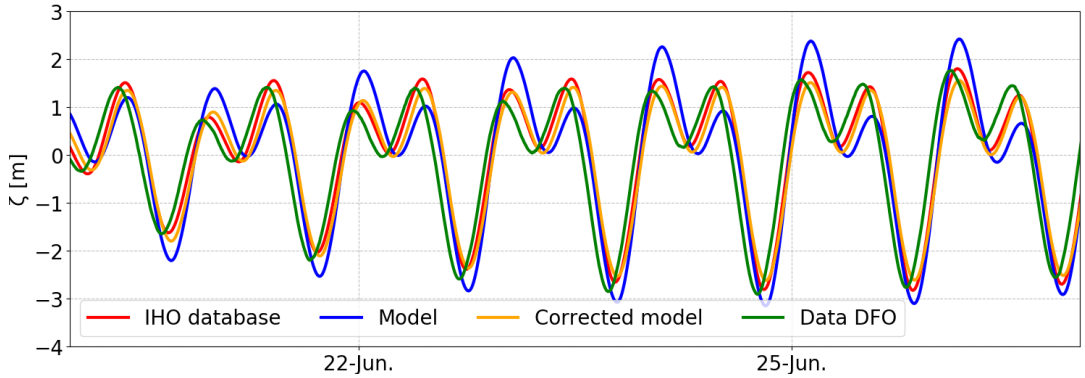

(a) Point Atkinson (best fit).

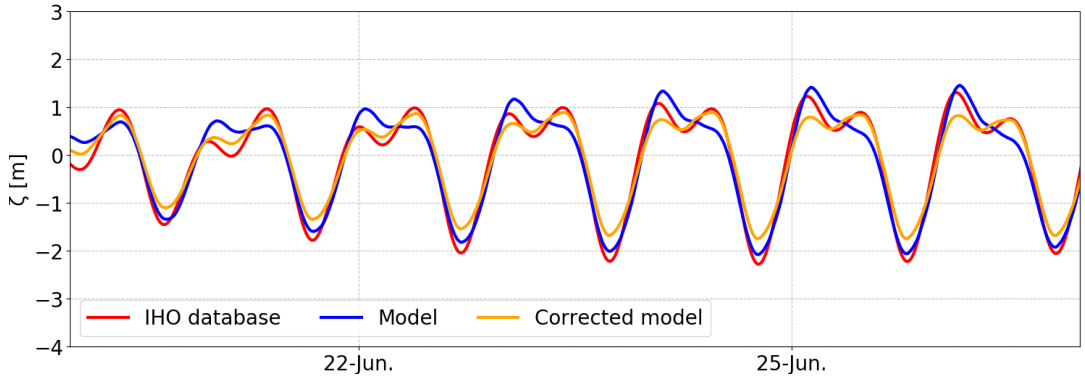

(b) Friday Harbour (worst fit).

Figure 6.9: Water levels best and worst model fits inside the Strait of Georgia.

The resulting models do not represent the reality perfectly. Figures 6.9 and 6.10 show the best and worst fit of the model inside the Strait of Georgia to reality. In case of a perfect model the modeled water levels should perfectly match the water levels of the data. When plotted, the points would lying exactly on one line. Figure 6.10 shows the plot of measured water levels to the modelled water levels and the linear regression lines obtained by minimizing the Root Mean Squared Error (RMSE). The RMSEs are 0.15 m and 0.18 m for Point Atkinson and Friday Harbour respectively. Figure 6.11 shows the tidal amplitudes and phases of the most important tidal constituents for both the best and worst fit again. Possible explanations for the error made in the model might be the complex geometry. Friday Harbour is located at the narrow passages from the Juan de Fuca Strait and the Strait of Georgia. In these passages the tidal propagation is not modelled properly. Finer

grids might help to model the water levels more accurately.

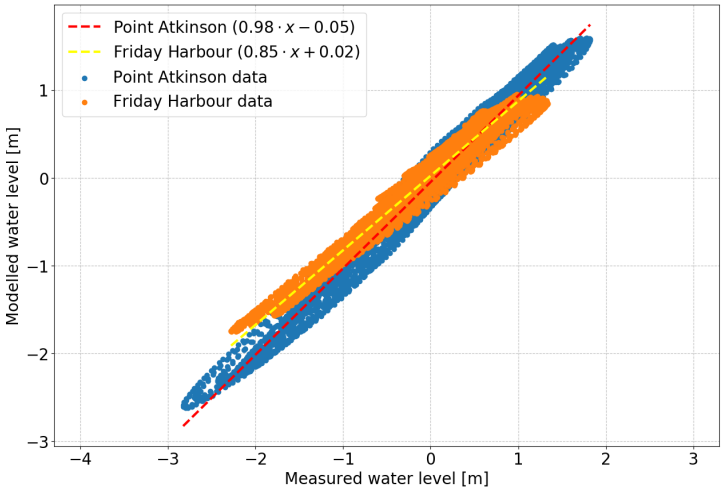

Figure 6.10: Scatter plot of measured data versus modelled data and their respective linear regression functions of Point Atkinson (blue dots, striped red line) and Friday Harbour (orange dots, striped yellow line) tidal stations.

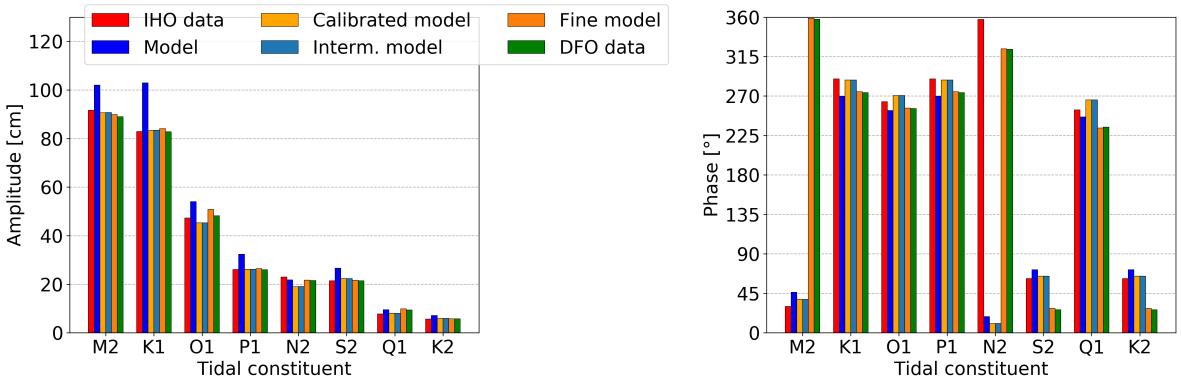

(a) Point Atkinson (best fit).

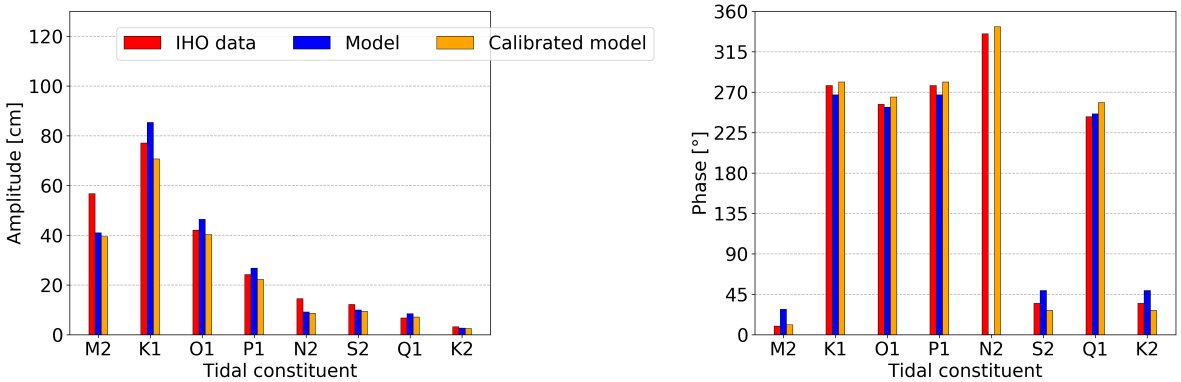

(b) Friday Harbour (worst fit).

Figure 6.11: Amplitudes and phases best and worst fits.

The second step is to 'force' an even better fit to the Point Atkinson tidal station by applying corrections to the modeled tidal constituents. A factor of multiplication is applied to the amplitudes and an additive to the tidal phases. After this step the model is thought to be calibrated sufficiently.

Table 6.4: Amplitude ratio between DFO data and corrected model. The ratio is the eventual multiplication factor for amplitude correction.

Tidal const.	**DFO data** [cm]	**Calibrated model** [cm]	**Ratio** [-]
MM	1.505	0.802	1.877
MF	5.383	4.069	1.323
O1	48.218	45.262	1.065
Q1	9.380	7.993	1.174
K1	82.820	83.377	0.993
P1	26.006	26.180	0.993
N2	21.495	19.000	1.131
M2	88.962	90.647	0.981
S2	21.457	22.299	0.962
K2	5.708	5.931	0.962
MN4	0.235	0.298	0.789
M4	0.783	0.704	1.112
MS4	0.257	0.622	0.413

Table 6.5: Phase difference between DFO data and corrected model. The difference will be the additive correction to the phases in the model.

Tidal const.	**DFO data** [°]	**Calibrated model** [°]	**Difference** [°]
MM	189.3	94.4	+94.9
MF	277.9	102.2	+175.7
O1	255.8	270.6	-14.8
Q1	234.6	265.5	-30.9
K1	273.9	288.2	-14.3
P1	273.9	288.2	-14.3
N2	323.3	10.6	+312.7
M2	357.6	38.2	+319.4
S2	26.3	64.5	-38.2
K2	26.3	64.5	-38.2
MN4	169.2	255.1	-85.9
M4	198.8	296.4	-97.6
MS4	153.0	312.4	-159.4

6.10. Model parameters

In earlier sections the practical model settings are presented. Under the hood of Delft3D-FLOW and WAVE many more parameters or coefficients are set. Table 6.7 lists the parameters used by the model, but which are not yet mentioned in this chapter. Most of the settings shown in Table 6.7 have not been altered and are thus the initial settings. This especially holds for the factors on sediment transports, such as the wave-related suspensed sediment transport factor and others in that list. These are calibration parameters to improve model results. However, these factors have not been changed due to missing exact data.

In Table 6.6 the remaining settings of the Delft3D-WAVE model are given. Again, Table 6.6 lists coefficients which have not been altered due to missing data for validation. The breaker and bed friction coefficients are possible calibration parameters which affect the location where waves break. Due to missing wave data, this could not be calibrated.

Table 6.6: Overview of all model settings used in the Delft3D-WAVE model.

Parameter	**Description**	**Value**
Spectral		
DirSpace	Directional space	circle
NDir	Number of directions	36
FreqMin	Default minimum frequency [Hz]	0.05
FreqMax	Default maximum frequency [Hz]	1
NFreq	Number of frequency bins	24
Hydrodynamics		
FlowWaterLevel	Use of FLOW water level results	Use and extend
FlowVelocity	Use of FLOW current results	Use and extend
FlowBedLevel	Use of FLOW bed level results	Use and extend
FlowWind	Use of FLOW wind results	Use and extend
Physical parameters		
Gravity	Gravitational acceleration [$m\,s^{-2}$]	9.81
WaterDensity	Density of water [$kg\,m^{-3}$]	1025
NorthDir	Direction of north relative to x axis [°]	90
MinimumDepth	Minimum water depth below which points are excluded from computations [m]	0.05
Processes		
GenModePhys	Generation mode of physics	3
Breaking	Wave breaking	Yes
BreakAlpha	Alpha coefficient for wave breaking	1
BreakGamma	Gamma coefficient for wave breaking	0.73
Triads	Include triads	No
BedFriction	Bed friction type	JONSWAP
BedFricCoef	Bed friction coefficient [$m^2\,s^{-3}$]	0.067
Diffraction	Include diffraction	No
WindGrowth	Include wind growth	Yes
WhiteCapping	Inclusion of white capping	Komen
Quadruplets	Include quadruplets	Yes
Refraction	Include refraction	Yes
FreqShift	Include frequency shifting in frequency space	Yes
WaveForces	Method of wave force computation	Radiation stresses

Table 6.7: Overview of all model settings used in the Delft3D-FLOW model.

Parameter	**Description**	**Value**
General		
Coordinate system		Spherical
Number of layers		1
Dryflp	Drying and flooding check	Grid cell centres and faces
Dryflc	Threshold depth drying and flooding [m]	0.2
Dpsopt	Depth at grid cell centres	Mean
Dpuopt	Depth at grid cell faces	Mean
Dco	Marginal depth [m]	-999
Tlfsmo	Smoothing time [min]	60
Trasol	Advection scheme for transport	Cyclic
Momsol	Advection scheme for momentum	Cyclic
Forfuv	Horizontal Forrester filter	Yes
Htur2d	Flag for HLES sub-grid model	No
Physical constants		
Ag	Gravitational acceleration [$\mathrm{m\,s^{-2}}$]	9.81
Rhow	Water density [$\mathrm{kg\,m^{-3}}$]	1025
Rhoa	Air density [$\mathrm{kg\,m^{-3}}$]	1
Wind drag coefficients	First breakpoint (u_w = 0 $\mathrm{m\,s^{-1}}$)	0.00063
	Second breakpoint (u_w = 100 $\mathrm{m\,s^{-1}}$)	0.00723
	Third breakpoint (u_w = 100 $\mathrm{m\,s^{-1}}$)	0.00723
Roughness		
Rouwav	Stress formulation due to waves	Fredsoe
Irov	Wall slip condition	Free
Sediment		
Cref	Reference density for hindered settling [$\mathrm{kg\,m^{-3}}$]	1600
SedTyp	sand	
RhoSol	Specific density [$\mathrm{kg\,m^{-3}}$]	2650
CDryB	Dry bed density [$\mathrm{kg\,m^{-3}}$]	1600
IniSedThick	Initial sediment layer thickness at bed [m]	5
Morphology		
MorUpd	Update bathymetry during FLOW simulation	No
DensIn	Include effect of sediment on fluid density	No
EqmBc	Equilibrium sand concentrations at inflow boundaries	No
MorFac	Morphological scale factor	10^{-11}
MorStt	Spin-up interval before morphological changes [min]	720
Thresh	Threshold sediment thickness for transport and erosion reduction [m]	0.05
Transport formulation	Van Rijn (2000)	
IopKCW	Flag for determining source of current- and wave-related roughness height	1
AksFac	Reference height	1
RWave	Multiplication factor for wave-related roughness	2
AlfaBs	Streamwise bed gradient factor for bed load transport	1
AlfaBn	Transverse bed gradient factor for bed load transport	1.5
Sus	Multiplication factor for suspended sediment reference concentration	1
Bed	Multiplication factor for bed-load transport vector magnitude	1
SusW	Wave-related suspended sed. transport factor	1
SusB	Wave-related bed-load sed. transport factor	1
SedThr	Minimum water depth for sediment computations [m]	0.1
ThetSD	Factor for erosion of adjacent dry cells	0
FWFac	Vertical mixing distribution according to van Rijn (overrules k-epsilon model)	1

7

Results

7.1. Flow fields & velocities

The first results of the model are the flow fields during the six regular scenarios (Table 5.1). Figures 7.1 through 7.2 give overviews of the flow fields at flood and ebb for scenarios 1 and 5. In front of the shelf the largest flood currents are found in the order of 20 cms^{-1}. On top of the shelf the flood velocities are about a factor two lower. However, on top of the shelf higher ebb velocities are found compared to off the shelf. This is the general picture over all the scenarios. The figures are a snapshot at a specific time during the tidal variation in the area. This is shown in the embedded graphs inside the figures, where the dotted line represents the flow velocity and the blue line the water level. These values are retrieved from a measuring station in the middle of the shallow shelf.

Also influence of the higher discharge of the North Arm is clearly visible in the model. During freshet the outflow can reach up to 110 cms^{-1}, at ebb to 70 cms^{-1} (Figure 7.2). During non-freshet conditions the flow contraction in between the jetty and the breakwater results in a maximum ebb flow of 70 cms^{-1} and 40 cms^{-1} during flood conditions (Figure 7.1). Close to the water line high flow velocities are absent.

All of the scenarios show counter flow from the ebb currents against the outflow of the North Arm Fraser River. On top of the undeep spit the flows push each other towards the undeep water. During flood the North Arm outflow is pulled northwards by flood currents. The currents then curl back towards the shoreline just after passing the undeep spit where the flow velocities decrease significantly.

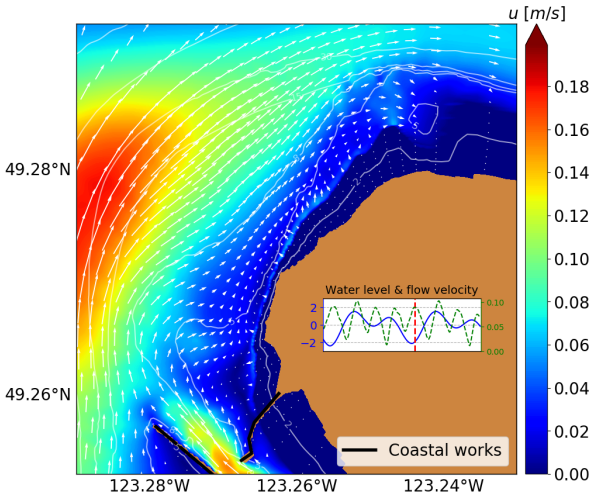

(a) During flood.

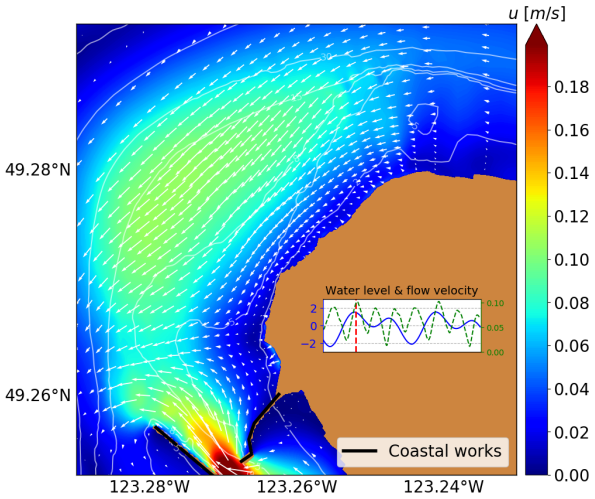

(b) During ebb.

Figure 7.1: Flow velocities and direction during flood and ebb conditions of scenario 1 (low river discharge, waves enabled).

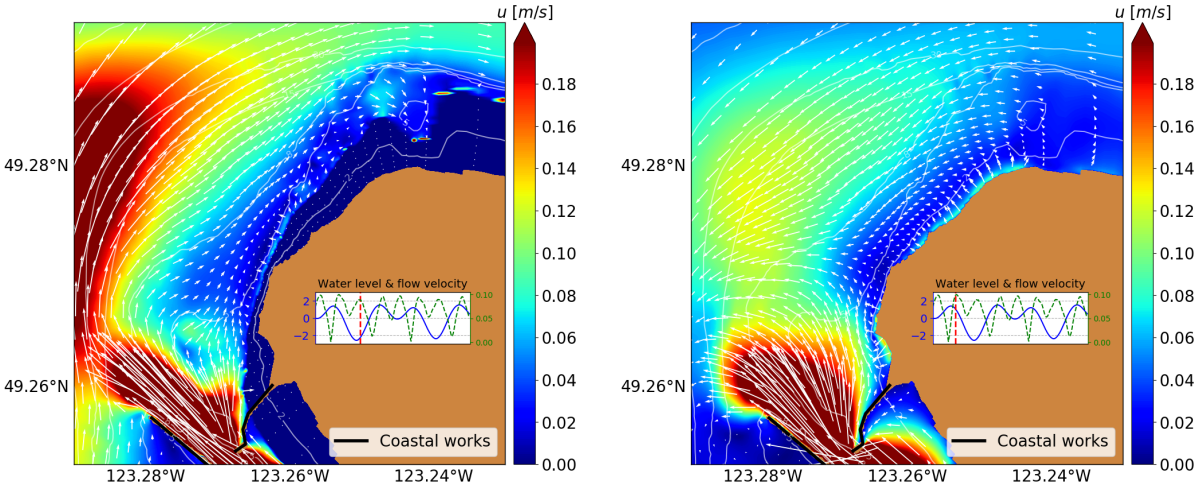

(a) During flood. (b) During ebb.

Figure 7.2: Difference in flow pattern during flood and ebb conditions of scenario 5 (high river discharge, waves enabled).

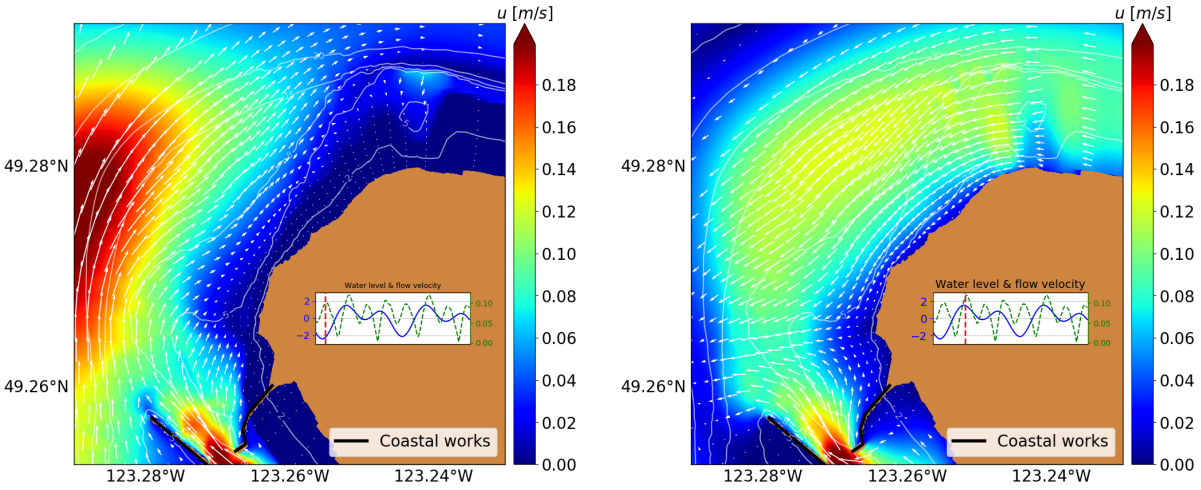

(a) During flood. (b) During ebb.

Figure 7.3: Flow velocities and direction during flood and ebb conditions of scenario 2 (low river discharge, waves disabled).

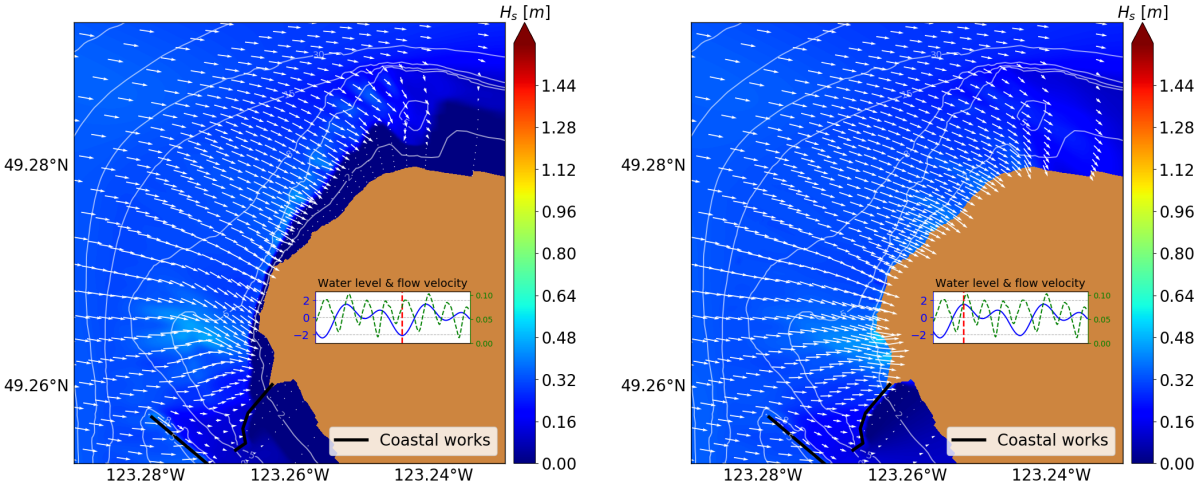

(a) During low water. (b) During high water.

Figure 7.4: Difference in significant wave heights during high and low waters of scenario 1 (low river discharge, waves enabled).

Figures 7.3 presents the periods during non-freshet without any waves, which are assumed coming out of the east. Comparing the flow fields of scenarios 1 and 2 shows that without waves higher ebb flow velocities are found at the Spanish Banks directed southwest.

7.2. Waves

Figures 7.4 and 7.5 show the numerical results of the significant wave height around the Point Grey cliff system. Per scenario a snapshot of the low- and high water conditions is given. From these plots a clear difference in the wave propagation extend can be seen. During low water the waves break far further off-shore, while at high water the waves can reach all the way towards the water line.

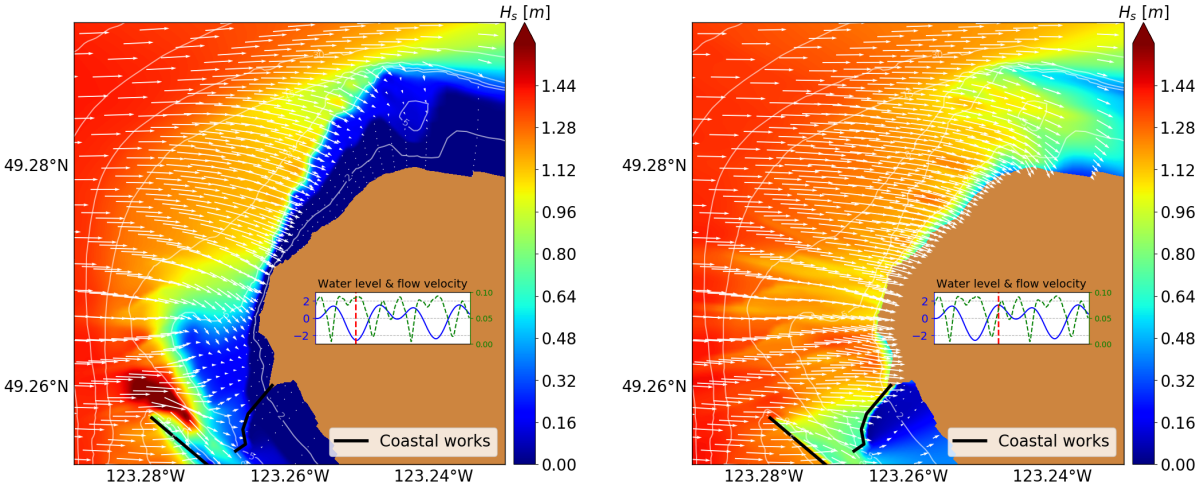

(a) During low water.

(b) During high water.

Figure 7.5: Difference in significant wave heights during high and low waters of scenario 4 (high river discharge, storm wind and waves enabled).

Regular waves coming from the west show wave focusing on the Point Grey location, as well on the northern side of Tower Beach. The significant wave height of these waves is in the order of 0.5 m (Figure 7.4b). The same holds for the waves in scenario 5, so therefore the wave field for that scenario is presented in Appendix F. During a western storm with a return period of five years, these waves reaching the cliff foot can be in the order of one meter (Figure 7.5b). At low water the storm waves break a lot earlier on the shallow bathymetry just north of the breakwater (Figure 7.5a).

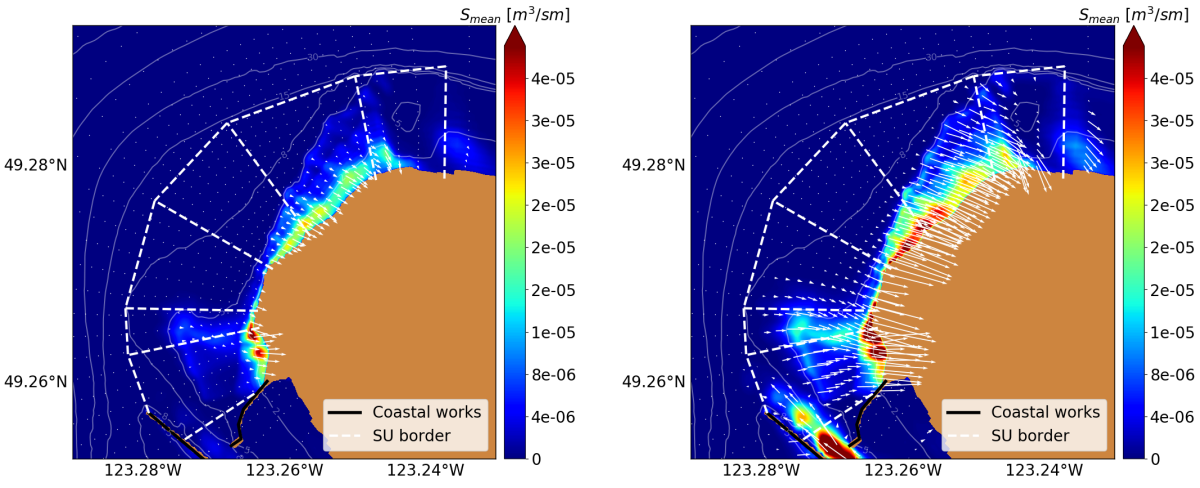

(a) Scenario 1
(low river discharge, waves enabled).

(b) Scenario 5
(high river discharge, waves enabled).

Figure 7.6: Mean sediment transport magnitude and direction over a two days modeling period.

7.3. Sediment transports

To study the sediment transports the mean sediment transports are visualized in Figure 7.6. The highest sediment transports are located close to the shoreline of the Point Grey cliffs. The direction of these transport corresponds to the direction of the waves presented in Figure 7.4. The general direction of the sediment is towards the shore. Also two alongshore directions can be seen: from Tower Beach to the north and from Point Grey to the south.

Over the implemented cross-sections sediment transports can be calculated per second. An example of output is given in Figure 7.7. In this figure the instantaneous transport of the bottom sediment can be seen. For our analysis the mean value is taken over the simulation period to be used in the sediment budget calculation. In Chapter 8 the spikes seen in the figure are discussed. In Appendix F the remaining figures concerning sediment transport over SU boundaries are given.

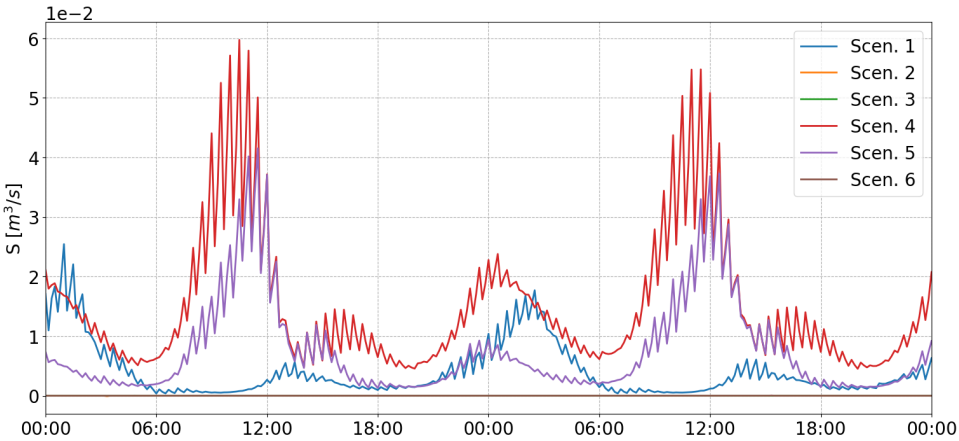

Figure 7.7: Boundary SU1 & SU2.

After extracting all the mean sediment transport from each of the six scenarios (Table 5.1) the contribution of each scenario can be calculated. A general sediment budget of one year is chosen. The scenarios are divided over two periods by the Fraser River (see Figure 3.9): freshet (63 days) and non-freshet (302 days). Within these periods the percentage of occurrence is known for each of the wave conditions through the wave roses (Figure 3.7). The storm scenario happens once every five years on average. Per year these scenarios contribute a factor 0.2 of their total magnitude to a yearly budget. A storm duration of two hours is assumed. In later studies an average storm duration can be obtained through using the wind data presented in this study. Furthermore, all sorts of storms are possible to occur, e.g. a 10 year Return Period storm. This is not taken into account in this study. The contribution of each scenario to the sediment transport over SU1-2 boundary is presented in Table 7.1. All other tables for each single SU boundary can be found in Appendix F.

Table 7.1: Yearly sediment transport computation over cross-section SU1-2.

	Mean transport $[m^3\,s^{-1}]$	**Days**	**Coefficient**	**Occur.**	**Total transport** $[m^3\,y^{-1}]$
Scenario 1	$3.97 \cdot 10^{-3}$	302	1	0.339	35,116
Scenario 2	$-2.06 \cdot 10^{-7}$	302	1	0.661	-4
Scenario 3	$9.60 \cdot 10^{-8}$	0.083	0.2	-	0
Scenario 4	$1.49 \cdot 10^{-2}$	0.083	0.2	-	21
Scenario 5	$7.56 \cdot 10^{-3}$	63	1	0.405	16,666
Scenario 6	$7.39 \cdot 10^{-8}$	63	1	0.595	0
Total	-	-	-	-	51,799

With Tables 7.1 and the tables presented in Appendix F the total sediment transport over the SU boundary can be calculated per year. The results of every SU boundary is shown in Figure 7.8. A large sediment loss of ~80,000 $m^3 y^{-1}$ (arrows (2), (3) and (4) combined) is seen just after the North Arm jetty. Two large sediment transports are going from SU2 to SU1 (51,799 $m^3 y^{-1}$ southwards) and the second from SU4 to SU3 (13,387 $m^3 y^{-1}$ southwards).

Figure 7.9 shows the contribution of each scenario to the total sediment transports presented in Figure 7.8. The size of each represents the relative contribution of each scenario to the total transport over given boundary. The Figures 7.9a and 7.9b represent the scenarios during non-freshet and freshet period. Both scenario 1 and 5 are the most significant scenarios, which are the scenarios with waves enabled.

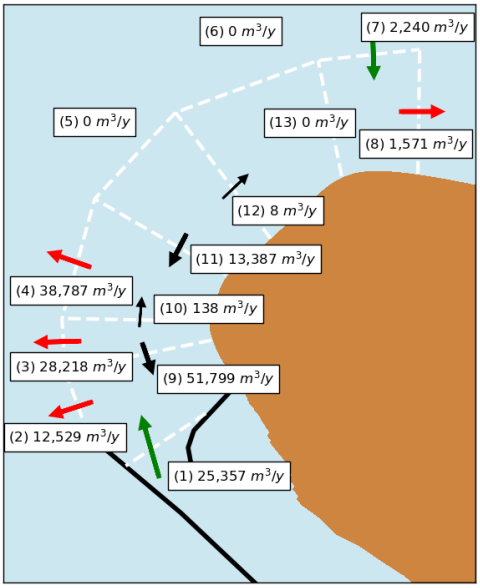

Figure 7.8: Total sediment transports over SU boundaries all scenarios (Table 5.1) combined. Red arrows indicate a loss of sediment. Green arrows indicate sediment input to the system. Black arrows indicate transports between SUs.

7.4. Sediment budget

After the calculation of the total sediment transport per year over the SU boundaries, the change in sediment volume per year can be calculated. This is done by adding all sediment influxes and subtracting all the outgoing sediment fluxes per SU. The result of this is given in Figure 7.10. A large sediment deficit is seen in SU2, SU3, and SU4. For SU2 the sediment leaves the area by both cross-shore and alongshore sediment transports. The transports for SU3 are primarily cross-shore, while for SU4 it is primarily alongshore.

For this sediment budget only the resulting sediment transports from Figure 7.8 are used. No sediment input from the cliffs themselves is considered in this approach.

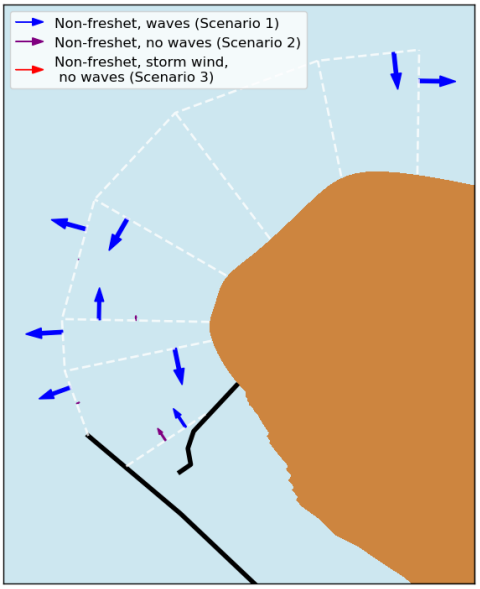

(a) Relative transports of scenarios during the non-freshet period.

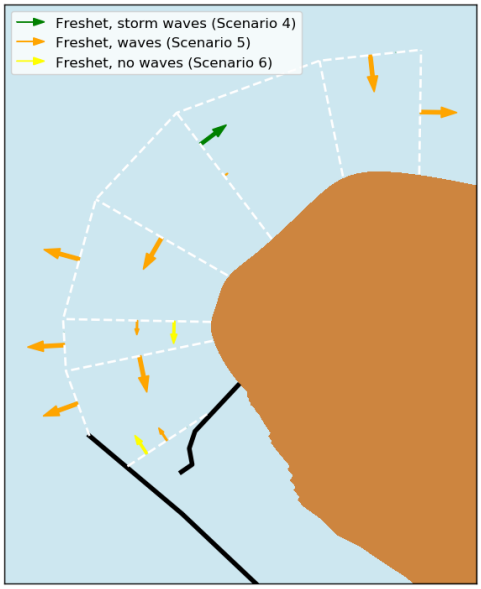

(b) Relative transports of scenarios during the freshet period.

Figure 7.9: The relative contribution of the scenarios to the total sediment transport over the SU boundary during both the non-freshet and freshet period.

7.5. Riverine sediment flux

An additional scenario was to check whether the North Arm of the Fraser River brings sediments to the Point Grey cliffs (Section 5.3.2). To check the sediment transport capacity of the North Arm of the Fraser River has any contribution to the sediment budget, two models were made with sediment concentrations stated in Tables 5.8 and 5.9 and their corresponding river discharges (Table 5.5). The results are given in Figures 7.11. In this figure the instantaneous transport for the three different sediment sizes over SU1 (Figure 6.6) is presented over the simulation. A positive sediment discharge means an influx to the system and negative means a sediment flow towards the sheltered area, Booming Grounds behind the North Arm breakwater and North Arm jetty.

For the sand class <177 µm (see Figure 3.3) the mean transports are in the order of 10^{-15}. For sand class

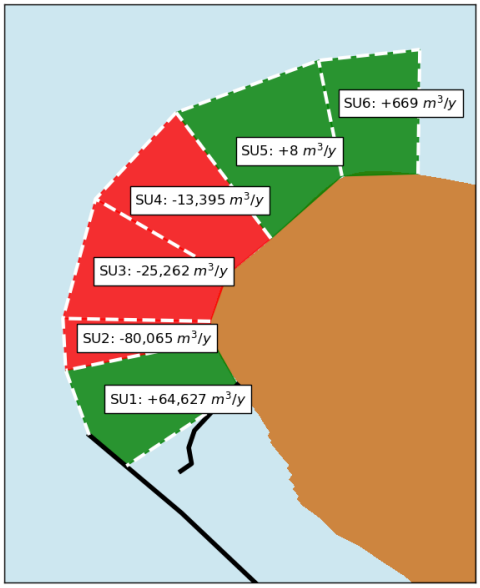

Figure 7.10: SU budgets.

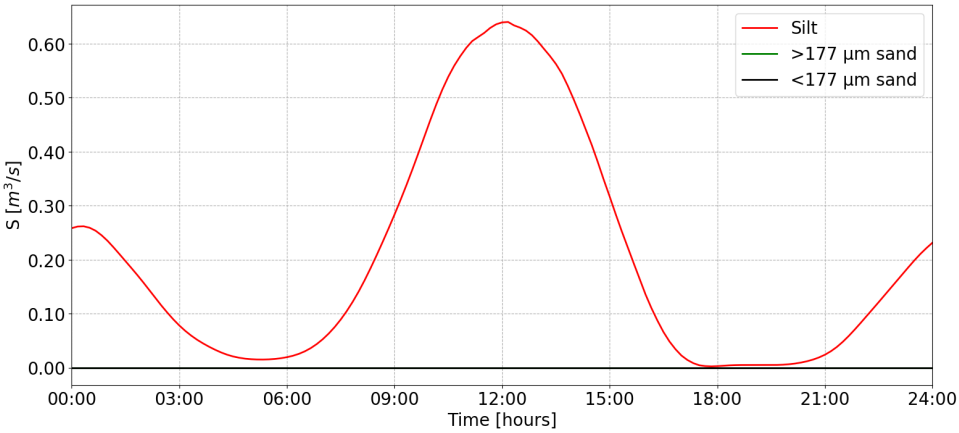

(a) During freshet conditions.

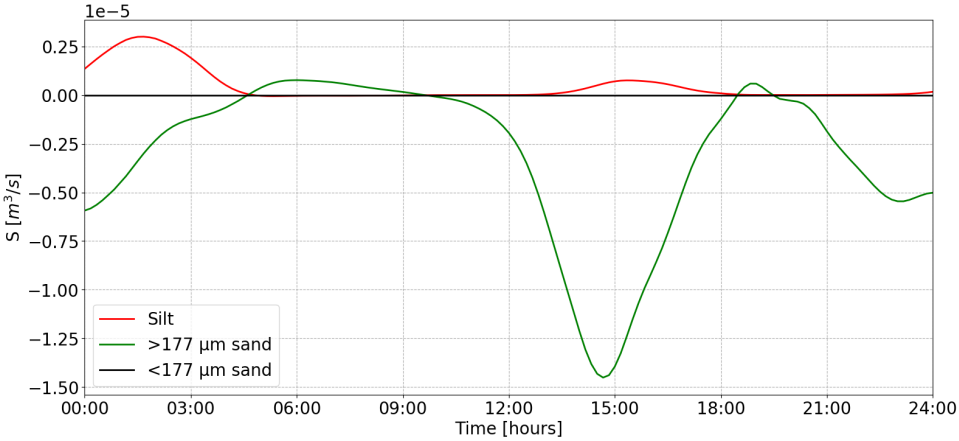

(b) During non-freshet conditions.

Figure 7.11: Fraser River North Arm sediment input during two defining river discharges. Positive numbers indicate sediment flow towards to the Point Grey cliffs. Negative numbers correspond to sediment flows towards the North Arm River.

>177 µm transports are in order 10^{-6}. These transports are considered negligible compared to the sediment transport due to waves presented in Section 7.3. The largest river sediment influx is the silt fraction (Figure 7.11a), which is can reach up to 0.6 $m^3 s^{-1}$. However, this sediment it thought to be transported away from the Point Grey cliffs immediately as the mean diameter of the shoreline material is 380 µm. During non-freshet conditions (Figure 7.11b) the Booming Grounds seems to be importing >177 µm, so transport upstream the North Arm.

7.6. Comparison base cases

As presented in Chapter 5.3 two base cases were run to determine to the effect when either the wind or waves are switched off. To show the effect, the difference in mean total sediment transport over the simulations is shown. The results of both base cases are subtracted from the result of the original scenario 1 to visualize the difference.

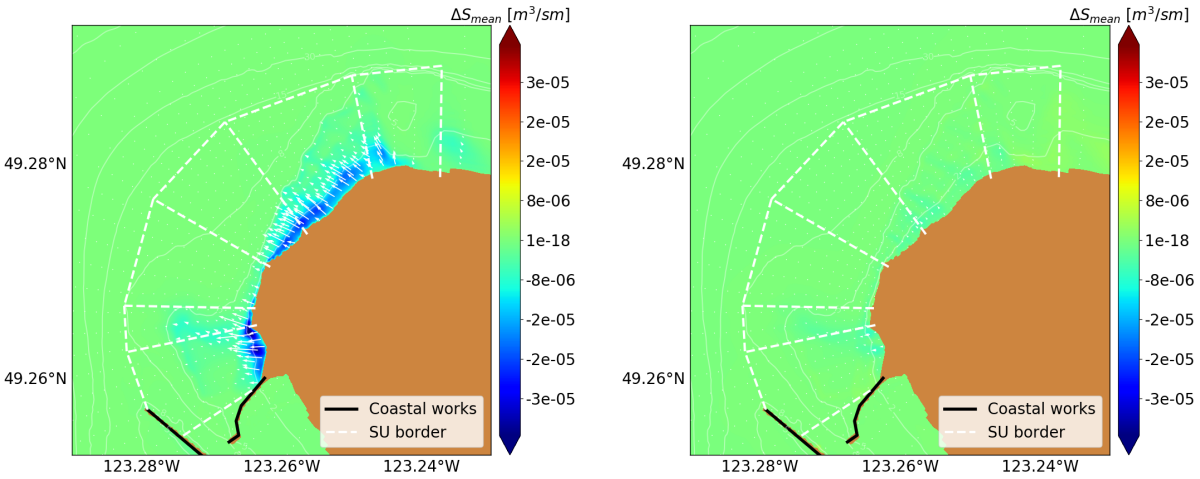

(a) No waves base case.

(b) No wind base case.

Figure 7.12: Difference in mean sediment total transport in scenario 1 (low river discharge, waves enabled) and both base cases (no waves and no wind).

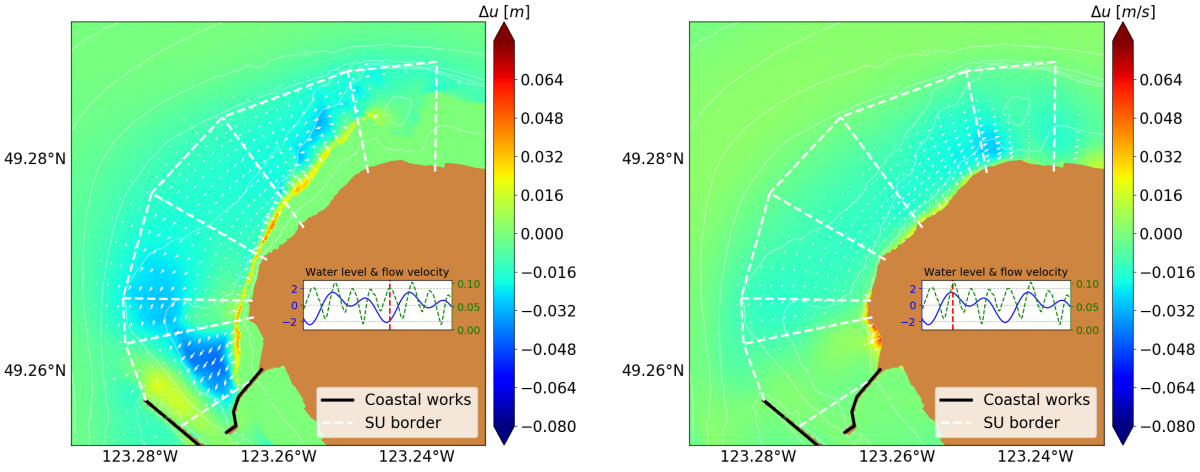

(a) During flood.

(b) During ebb.

Figure 7.13: Difference in flow velocities between scenario 1 (low river discharge, waves enabled) and base case without waves.

For the case when waves are switched off (Figure 7.12a), a significant decrease in the sediment mean total transport can be observed, nearly 100%. While looking at Figure 7.12b, the wind does not affect the transport as the base case without waves does. Besides the difference in sediment transport also the difference in flow

velocity at the same time points as presented in Figure 7.1 between the regular scenario and the one without waves is presented. The effect of wave-induced currents can be seen here. The maximum difference in flow velocities is 7 cm s^{-1} approximately (Figure 7.13), while in the middle of the shelf a decrease of 3 cm s^{-1} is observed.

7.7. Sensitivity analysis

As presented in Chapter 5.3, several sensitivity cases have been executed to visualize the effect of changing parameters of this study. Two main parameters were changed in this analysis, namely the significant wave height and the median sediment diameter. These two main parameters are thought to have the most significant effect on the transport patterns. The third 'parameter' which is changed are the locations of the cross-sections in the model. Important to note is that these runs are only done with one scenario, scenario 1 (non-freshet, waves enabled). Also SU boundaries SU4 top, SU5 top and SU4-5 are excluded in this analysis, since the sediment transports over mentioned cross-sections are and stay negligible.

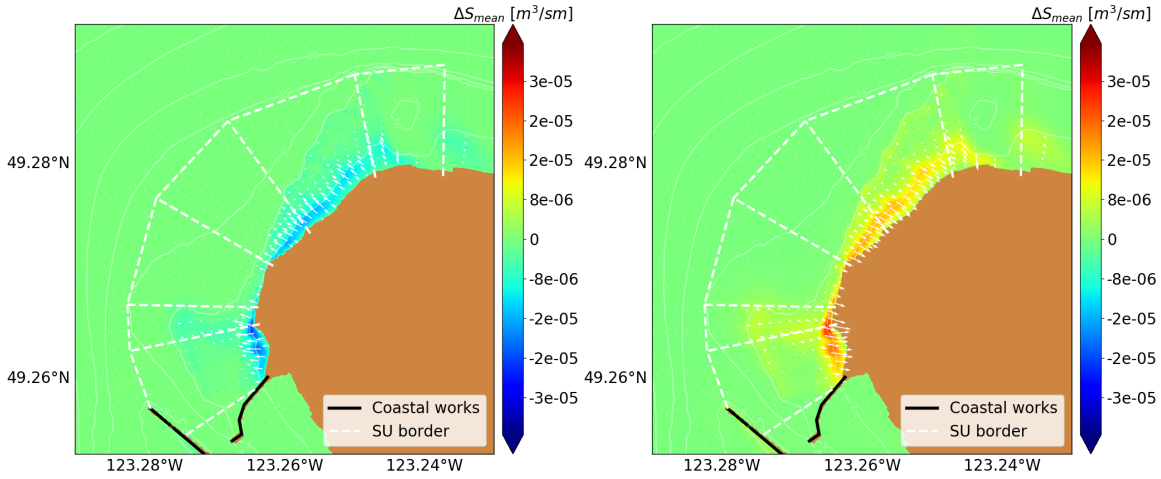

(a) H_s 34% lower. (b) H_s 34% higher.

Figure 7.14: Difference in mean sediment transport between regular scenario 1 (low river discharge, waves enabled) and both wave sensitivity cases.

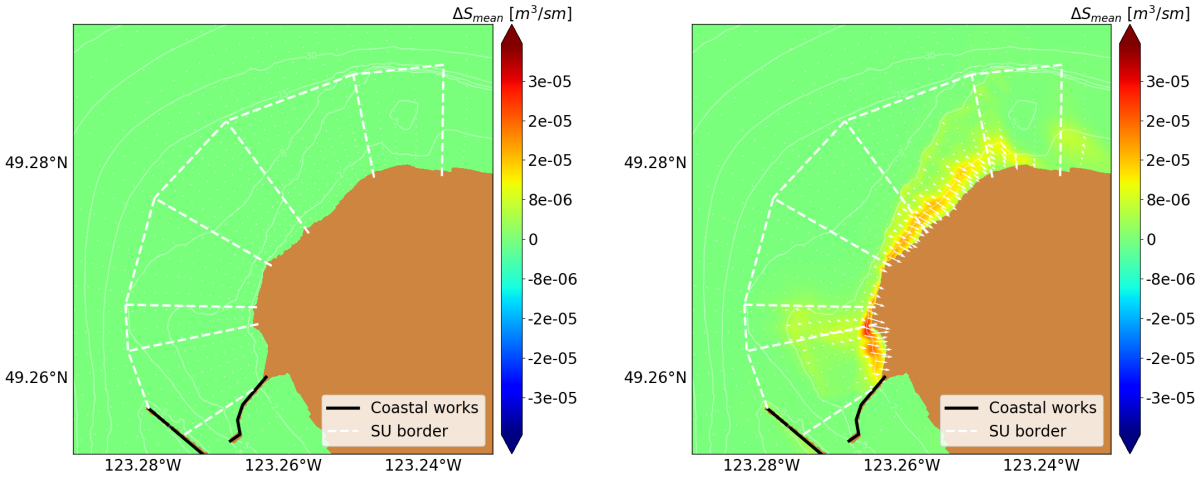

(a) D_{50} 34% lower. (b) D_{50} 34% higher.

Figure 7.15: Difference in mean sediment transport between regular scenario 1 (low river discharge, waves enabled) and both median grain diameter sensitivity cases.

7.7.1. Significant wave height (H_s)

The boundary condition in the Delft3D-WAVE model is increased and decreased by 34%, which means the new significant wave heights are 0.30 m and 0.62 m respectively. Tables G.1 through G.9 show an average increase of the sediment transports of 162%. With a 34% lower H_s the average decrease in sediment transports is 73%. Figure 7.14 shows the difference in mean sediment transport over the whole simulation with respect to the original scenario 1.

7.7.2. Median sediment diameter (D_{50})

The other main parameter changed for the sensitivity analysis is the median sediment diameter D_{50} of the bottom material. The lower value is 250 µm and the higher value is 510 µm, again a difference of ± 34%. The larger mean sediment size shows an average increase of 17% of sediment transport over the cross-sections. The smaller sediment size shows no change in sediment transports (Tables G.1 through G.8). Figure 7.15 illustrates the differences in mean sediment transport, averaged over the whole simulation period.

7.7.3. Other cross-section locations

Another interesting alteration to the model is the location of the cross-sections over where the sediment transports are calculated. This to test whether the results presented in Figure 7.8 are sensitive to changes in locations of the SU borders. In this case the SU borders, SU2-3 and SU3-4 (see Figure 6.6), are both shifted northwards. Figure 7.16 shows the old positions of the SU borders in grey and the new ones in white. The other SU borders did not change location.

The resulting change in sediment transport over these two new boundaries is shown in Table 7.2. The change in sediment transport rates are quite significant. In case of SU boundary between SU2 and SU3 the transport rate increases with a factor 100 and the direction changes as well. For boundary SU3-4 the transport rate even decreases to almost nothing.

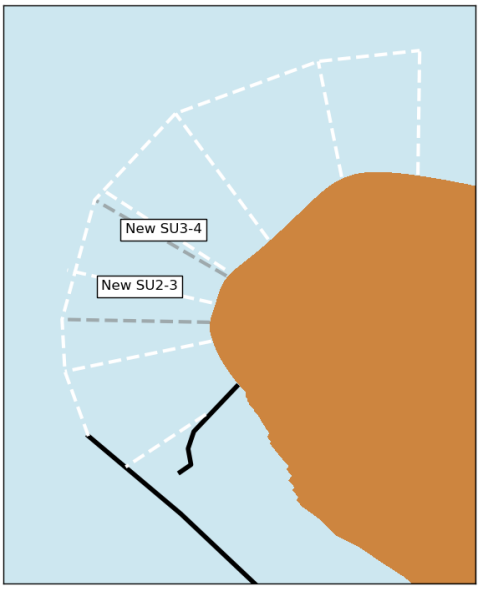

Figure 7.16: The grey boundaries, SU2-3 and SU3-4, are shifted to their new locations.

Table 7.2: New mean sediment transport compared to the initial result from borders SU2-3 and SU3-4.

	Old mean transport $[m^3 s^{-1}]$	**New mean transport** $[m^3 s^{-1}]$
SU2-3	$3.27 \cdot 10^{-5}$	$-2.21 \cdot 10^{-3}$
SU3-4	$8.28 \cdot 10^{-4}$	$0.00 \cdot 10^{-4}$

8

Discussion

8.1. Hydrodynamics

Figure 8.1 is a schematized overview of the flows around the Point Grey cliffs. No relation between the magnitude of the flows and the size of the arrows should be sought. This schematized figure sketches that the flood flow concentrates in the deep Strait of Georgia, while the ebb flow spreads out over the shallow shelf in front of the cliffs. The figure also shows the outflow of the North Arm of the Fraser River and how this outflow is dispersed. A large portion of the flow follows the deep section, while a small section separates north towards the cliffs. This is caused by the flow contraction through the breakwater and North Arm jetty and where the flow afterwards can disperse again. The figure also illustrates the direction of the regular wave- and storm conditions.

The resulting flow velocities are in the range of 12 cms^{-1} maximum on the shallow shelf before the Point Grey cliffs. In the gap between the North Arm breakwater and jetty the flow velocities can reach up to 110 cms^{-1}. During flood the water is pulled outwards from the river and deflected northwards. In ebb conditions the tide and river outflow meet opposite at Point Grey and are then deflected westwards.

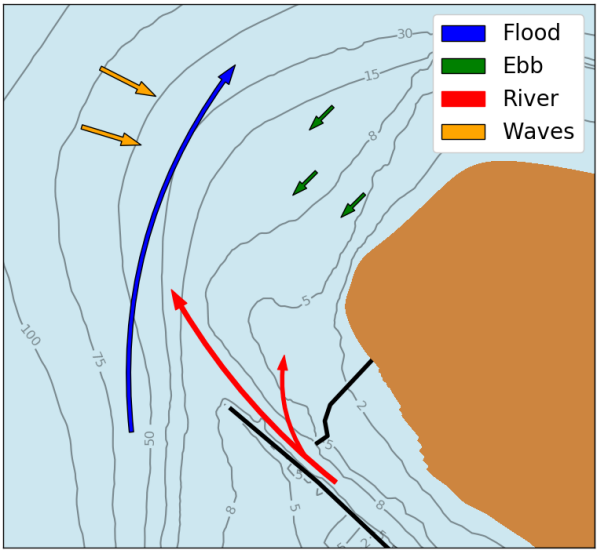

Figure 8.1: Hydrodynamic situation sketch of the Point Grey cliffs.

Representative significant wave heights are in the order of 0.5 m with corresponding peak periods of 7-9 s. Storm conditions with a 5 year Return Period increase the significant wave height to 1 m locally. It can be seen that during regular conditions the undeep spit north of the breakwater stows the waves and during storm conditions it forces the waves to break. The wave conditions are based on a statistical and extreme values analysis where many conditions are transformed into one single condition. As the single condition cannot be validated to measurements an uncertainty is introduced here, which can be significant looking at the sensitivity of the model towards larger wave heights.

8.2. Direct wave attack/wave run-up during extreme water levels

From our model study it can be concluded that waves can reach the cliffs during high water (Figures 7.4b, 7.5b and F.4b), especially below the Museum of Anthropology in SU2 and SU3 (Figure 1.2b). When these conditions meet an extreme water level due to either high tides (Figure A.1a) or storm surges (Section 3.4),

these waves can directly attack the cliff toe. Storm waves with a return period of 5 years in the order of 1 m can propagate towards the shoreline. For regular waves this seems to be in the order of 0.5 m. From the occurrences it is found that Point Grey experiences incoming waves about 35% ($\frac{128 \text{ days}}{365 \text{ days}}$) of the year.

8.3. Sediment transport

According to two sources (Golder Associates Ltd., 2015, Pool, 1975) waves initiate sediment transports in the order of 15,000 to 70,000 $m^3 y^{-1}$ towards the northeast, the Spanish Banks. The model shows about 13,000 $m^3 y^{-1}$ (arrow (11) in Figure 7.8) to the south (SU4 to SU3). Figure 7.6 shows results which correspond to the statements of Golder Associates Ltd. (2015), Pool (1975). Additionally, the model shows sediment transport out southwards from SU2 to SU1, which is from Point Grey towards the North Arm breakwater. Important to note here is that the scenarios with waves coming from the west northwest shows sediment transport, while scenarios with waves disabled do not show any sediment transport. From this we can conclude that under current model setting waves initiate the transportation of the bottom sediment. Figure 7.13 show the residual currents due to waves, such as wave-driven currents and due to set-up differences. The band of velocity difference from the North Arm Breakwater to the Spanish Banks in Figure 7.13a seems to be the reason for initiation of sediment transports. The direction of flows velocity follows the direction of mean sediment transports in Figure 7.6. In the next paragraph additional information is discussed on how the model calculates sediment transports and why the sediment transports follows the propagation direction of the waves.

The model calculates sediment transports in two parts, the suspended- and bed-load transport part (Deltares, 2011a). The suspended transport is calculated by shear stresses induced by flow velocities, by currents wave-orbital motions. The following citation is acquired from the Delft3D manual (Deltares, 2011a) which indicates the computed mean sediment transports are primarily bed-load transports and is computed by the wave transport part ($S_{b,w}$):

> *"The direction of the bed-load transport vector is determined by assuming that it is composed of two parts: part due to current ($S_{b,c}$) which acts in the direction of the near-bed current, and part due to waves ($S_{b,w}$) which acts in the direction of wave propagation."*

Secondly, large sediment transports are observed at the edge of SU1, SU2, and SU3 (arrows (2), (3), and (4) in Figure 7.8). Again, these transports occur during scenarios with waves enabled (Figure 7.9). A probable explanation for this westward transport is the North Arm river outflow and ebb flow directed westward. However, this explanation does not hold as these transports only occur during scenarios with waves enabled while the river discharge stays present. Another explanation may be some sort of slope effects included in the Delft3D model. Results of one new scenario with waves enabled together with no river discharge should be able to answer this question.

All in all, the presented sediment transports are very variable. A conclusion from the model results is that indeed waves are a primary cause of sediment transports by near-bed orbital velocities in this model. The sediment transport are only bed-load transports and the currents are not strong enough to initiate suspended sediment transports. This means that the combined currents of the tide and waves is too weak to initiate sediment transports. A second new observation through the model study is a sediment transport path towards the south, which is not mentioned by found sources. Sources based their findings on empirical formulae with the inclusion of the relative angle between incoming waves and the shoreline. This calculation is done for Wreck Beach at the Museum of Anthropology and northwards. This study is based on a spatial numerical model with the inclusion of refraction of incoming waves. It is expected that the sources did not use any bathymetric information. Due to the more detailed bathymetry in the numerical model, the waves refract by the undeep spit due south. The sediment transport follow the direction of wave propagation, and hence the southward directed transport is found.

8.4. Sediment budgets

Figure 7.10 shows the resulting sediment budget by adding all the sediment fluxes to and from every SU. It is seen that SU2, SU3, and SU4 have a sediment deficit. While SU1, SU5 and SU6 experience accretion. This is exactly what can be expected from the found sources. Golder Associates Ltd. (2015), Mines, and Resources (Canada) Energy (1980), Pool (1975) stated that material is accumulated at the western edge of the Spanish Banks, which this sediment budget shows in very small quantities as well (8 and 669 $m^3 y^{-1}$ in Figure 7.10). It

was also found during the site visit that less sand was found near Tower Beach (the berm and groyne system) and more sand was found near the Spanish Banks (SU5 and SU6).

In Section 7.7.3 the sensitivity of the model to the location of the cross-sections was tested. It proved that the model was very sensitive to alteration of cross-section locations. The sensitivity test shows that the observed sediment transport (~13,000 $m^3 y^{-1}$, arrow (11) in Figure 7.8) diminishes quickly. The implications is the sediment budgets in Figure 7.10 is unreliable and further estimations of sediment budgets should be made with different choices in locations for cross-sections. Another possibility is adding more cross-sections to more accurately follow the differences in sediment transport along the cliffs. Conclusions on sediment budgets are more reliable when based on other sources, such as literature sources etc.

An important subject of the Point Grey sediment budget is the Fraser River. Golder Associates Ltd. (2015) stated that no sediment inflow from the North Arm Fraser River can be expected, because any sediment will be pushed outward into the deep Strait of Georgia. Pool (1975) states ~68,000 $m^3 y^{-1}$ of sand coming in (Table 3.5). The model states that the North Arm is only capable of transporting silt particles towards the Point Grey cliff area. Sometimes the sheltered area imports >177 µm sands behind the North Arm breakwater (Figure 7.11), which in reality is unlikely when compared to sources.

The flushing of sediment described by Golder Associates Ltd. (2015) can be explained by the construction of the North Arm jetty and breakwater. Due to the flow contraction between the two works an channelization high velocities are reached, blasting out the sediments before the sediment can divert the northeast. The trifurcation works, constructed from 1973 and 1975, altered the division of sediment between the North Arm and Main Arm. Since the model shows that the river is not able to transport any sediment towards the Point Grey cliffs, the trifurcation works would not be partly responsible for the lack of sediment. The same holds for the dredging in the Fraser Main Arm as these sediments are not able to travel from the Main Arm mouth all the way north to the Point Grey cliffs. The main point is that it seems that the Fraser River, due to human interventions, seems unable to transport sand towards the Point Grey coastal system. The only source of sediment will therefore be the Point Grey cliffs themselves. No other data could be found about natural historical changes in annual sediment load of the Fraser River to suggest long-term trends in sediment supply to the system.

During the collection of sediment, it was difficult to find loose sand between the hard rock bottom in front of Tower Beach (SU3/SU4). This points towards a structural sediment deficit in front of the Tower Beach area. This means that neighboring areas will not receive material to build up a natural protective beach. At transect T and M, within these SUs, it can be seen that the material is in the intertidal area is coarser than the cliff material. This can mean that the finer material is transported away. At transect N, P, and S this is not the case. Here the intertidal samples are finer than the cliff material. This may indicate that finer material from Tower Beach is deposited at the North Arm breakwater and near the Spanish Banks up north.

8.5. Sea-level rise and increased storm intensity

The changes in climate force the mean sea-level to rise and increases storm intensities (Johannessen and Macdonald, 2009, Shaw et al., 1998). Expected sea-level rise in 2099 can amount to ~1 m (Environmental Reporting British Columbia, 2017). The rise of the sea can accelerate the erosion of the Point Grey cliffs as it enables waves to propagate further towards the cliffs. The increased storm intensities give rise to higher waves with more energy being formed. The change in climate also affects the general wave climate (Lee, 2008). Any intervention should be designed with the aforementioned mechanisms in mind to the fact that an intervention has a design lifetime during which the effect of sea-level rise and changes in wave climate can be significant.

8.6. The model - Assumptions & limitations

In this study a Delft3D-FLOW and WAVE model is used with conditions found in governmental databases, literature or field work. With the use of this data several scenarios were constructed. Results presented in this study are based on a continuous situation with all sorts of conditions prevailing reduced to discrete scenarios. Although the scenarios represent characteristic conditions of the coastal system, errors are introduced by turning a continuous system into a discrete one. E.g. the model uses averaged values which may vary yearly and information about extreme events are lost. Additionally singular wave conditions are used in the scenarios. These singular wave conditions are approximations of many summed wave conditions. The averaging

and approximation of representative conditions result in errors in modelled flow velocities, wave heights and propagation and finally in the computation of sediment transports. The process of reaching the scenarios is therefore important and should be done correctly. The mean Fraser River discharge varies during the summer and the rest of year from 2000 $m^3 s^{-1}$ to 8000 $m^3 s^{-1}$, which was the main factor to divide to scenarios over two periods over the year. The second division of scenarios is based on the wind and wave direction. The main directions are the west northwest and east southeast (Figure 3.7). For each scenario a single representative wave condition is sought by means of a statistical analysis. The storm wave climates are found by means of an extreme value analysis (Appendix C). The Fraser River sediment input (concentrations) is calculated with the use of average values found in the literature. The median sediment diameters of different sediment fractions are assumed by numbers found in literature or expert judgment. The bottom sediment is based on a sieving analysis done on the sediment acquired on the shoreline in front of the Point Grey cliffs.

The first part of the model was the propagation of the tide through the basin of the Strait of Georgia. The water levels in the model are calibrated fairly well (RMSE of 0.15 m) with the use of tidal stations as presented in Figures 6.9, E.1 and E.2. The leading calibration reference point is Point Atkinson tidal station is ~7 km away from the project area, which means calibration is not done on local scale.

Furthermore, the tidal propagation is not fully captured in the finer models. In Figures 6.3c and 6.4c can be seen that the numerical grid is cut-off early on inside the North Arm. Ages and Woollard (1976) states that the tide influence reaches all the way to Chilliwack, almost 100 km upstream. Missing this influence can affect the magnitude of the river discharge significantly. It is expected that modelled flow velocities will change for both flood and ebb. Expected is that during flood the flow velocities are lower as the tide wants to travel up the river, counteracting the direction of the river discharge. During ebb the flow velocities are believed to be larger as extra water will out of the river. The lower flood velocity will decrease the sediment transport capability of the river, while during ebb this capability is increased. Increased ebb velocities may bring sediment further out, while during flood sediment will settle nearer to the mouth. The effect on the estimated is unclear. This depends whether the change in flow magnitude for flood is greater (decreased sediment transport) or the changes in ebb velocities (increased sediment transport). It may affect the sediment transport magnitudes over arrows (1), (2), (3) and maybe (4) in Figure 7.8, how exactly remains to be seen.

The second hydrodynamic component of the model is the propagation of the short wave climate. This model is based on a statistical wave analysis and reduced to one single climate. Additionally, since the analysis is done on a time series offshore it can be very uncertain how the waves propagate through the basin. The wave climate could not be calibrated since no nearshore wave data was available. Therefore the error in the results can be large due to the non-linear relationship between significant wave heights and sediment transport, as shown in the sensitivity analysis. A 34% increase of the significant wave height at the boundary has a mean increase of 162% of the sediment transport over the cross-sections. A 34% lower significant wave height results in an average decrease of 73%. The change of model results can be found in Figure 7.14.

The model uses the standard non-cohesive transport approximations of Delft3D-FLOW presented by van Rijn et al. (2000). The approximations are valid for the following ranges:

- Sands with median grain diameter between 100 μm and 500 μm.
- Depths between 0.25 and 20 m.
- Flow velocities between 0 and 2 $m\,s^{-1}$.
- Relative wave heights ($\frac{H_s}{h}$) between 0 and 0.5.

For the scenario model runs, the bottom material is set within the applicable range. In reality the material at Tower Beach is closer to boulders, which means other transport formulae must be chosen in this area. This will result in smaller sediment transports coming from Tower Beach directed elsewhere, because less sand is available for transport creating a supply-limited situation. However, for the goal of this study it is sufficient to assume sand everywhere. The numerical depth is set to 0.2 m, which means the second requirement is not met as transport calculations are done at depths of 0.2 m. The flow velocities never exceed the 2 $m\,s^{-1}$. Relative wave heights are generally around 0.25, which is in the application range of the model.

The modelling of the sediment transports are based on a single median sediment diameter found on the shoreline. However, it is uncertain what the grain sizes are in deeper parts of water. After the sensitivity analysis the model does not seem too sensitive to changes in median grain diameter. An increase of 34%, shows an average increase of 17% in the sediment transports. Decreasing the median grain diameter of 34% shows no change in transports. One would think that the sediment transports will be larger when the sediment size

is smaller, but the model contradicts this expectation. That a higher sediment transport is expected, may be due to the fact that a higher median grain diameter is chosen (510 µm) than the limit of the used transport formula (500 µm). However, it is expected when the sediment becomes even smaller, closer to silt, this observation may not hold and that the sediment transports will increase. However, other transport formulae compatible with silt fractions must be used. A second assumption is that the sediment is abundantly available, while this might not be true. During the field work little sediment seemed to be available in front of the constructed berm (SU3) in the intertidal area. A supply-limited situation is thus more likely and will result in lower sediment transports, especially transports coming to and away Tower Beach. The difference in sediment transports between the regular case and the sensitivity case can be found in Figure 7.15.

The results of the sediment transports over the initial cross-sections (Figure F.5) show bounded instabilities (spikes) with an interval which is equal to the coupling interval between the Delft3D FLOW and WAVE programs. The signal to noise ratio ranges from 0 to about 0.5 of the solutions (Figure F.5). A possible explanation of the instabilities may be the sudden changes of the water level in between two wave calculations. These instabilities will most probably diminish when a lower coupling interval is chosen. However, this will significantly increase the computational time. In the calculations for transports and budgets the mean values of the transports over the simulation period are used, the means are sufficient for this analysis[1]. The sediment transport follows an average peak function during the simulation period, which alternatively undershoots and overshoots. By averaging over the simulation period the overshoots and undershoots are thought to be cancelled against each other.

Locations of the cross-sections in the model can also have a significant impact on the calculated transports as seen by the last sensitivity case as shown in Table 7.2. The changes made to two SU borders (Figure 7.16) showed that the transport over from SU2 to SU3 changed from direction and that no transport was visible over from SU3 to SU4 while there was before. This means that the transports and budgets presented in this study are highly sensitive to the chosen locations. A possible explanation is that the cross-section is near a turning point of shoreline orientation as with the case of boundary SU3-4. For boundary SU2-3 the possible explanation for it reaching zero sediment transport is that the cross-section in its new position is almost parallel to the incoming wave direction. This forces the sediment transport to be parallel to the cross-section as well, resulting in no transport over the cross-section. For further sediment budget calculations a critical look must be taken toward the location of the cross-sections with current knowledge.

Did the model agree with the conceptual sediment budgets from Figure 3.12 and Table 3.5? No, the model did not find the northeasterly directed wave-induced transports in the same order of as Golder Associates Ltd. (2015), Pool (1975), which are based on calculations with empirical formulae of Castanho (Pool, 1975, Silvester, 1974), Kamphuis and CERC (Golder Associates Ltd., 2015, Kamphuis, 2000, U.S. Army Corps of Engineers, 2002) with single representative values for wave conditions. Golder Associates Ltd. (2015) also used a smaller median grain diameter of 300 µm compared to this study's 380 µm. This model did find the qualitative direction presented by the mean sediment transports (see Figure 7.6). However, this is not captured by the sediment budgets using the model cross-sections. Besides, this numerical model did not include any sediment input from the cliffs as these processes are not included in the Delft3D model.

8.7. Further steps

This research tried to give a first overview in the local hydrodynamics, sediment transports and budgets of the Point Grey cliffs and its coastal system. All information in this thesis should therefore serve as a basis to continue the search for the missing parts of the story as well as the final goal this project has: the generation of potential solutions to mitigate the marine erosion of the Point Grey cliffs. In this section an overview for next research steps is given:

1. **Extra data collection.**
   One outcome of the sensitivity analysis was that the significant wave height can have a profound effect on the modelled sediment transports. Therefore it is preferable to collect nearshore wave data to the Point Grey cliffs to be able to validate the Delft3D-WAVE results. Additionally currents and water levels can be measured at the same time, with additional equipment, to be able to validate the model on a local scale. Secondly, a more detailed bathymetry is needed to be able to correctly model the propagation of the waves to the shoreline, which can function as a basis for future morphological change

[1] Following personal communication with Pieter Koen Tonnon (Senior Advisor Coastal Morphology at Deltares).

study as well. A sediment collection and study is beneficial as it is assumed that the bottom of the shelf is sand, based on the sieving analysis done in this study. Whether this assumption is correct can be proved by the third study. Also, measuring sediment transports at locations can be used for calibration of the model at local scales.

The locations where these studies or collection should be performed is elaborated in the recommendations (Section 9.2).

2. **Detailed study to the direct wave attack and wave run-up during regular conditions and storms.**
   A more detailed study is needed on the degree of exposure of the Point Grey cliffs to direct wave attack and wave run-up in regular and extreme storm conditions. For this an XBeach model is proposed for this study. In this study the amount sediments taken from the cliffs can be studied as well, since geological processes such as avalanching is included as well. Boundary conditions for this model can be extracted from the presented study and Delft3D model. The extra data collection from the previous step can greatly improve the results of the existing model and the proposed XBeach model.

3. **Detailed study towards the effects of sea-level rise and future wave conditions.**
   In this study no future scenarios were run. To study the effects of sea-level rise and intensified wave conditions future scenarios have to be set-up and studied how these affect the sediment transports at the Point Grey cliffs. From both studies extra requirements will arise which have to be met by the proposed coastal measure during its lifetime.

4. **Further calibrate and validate the model.**
   After the data collection and deeper studies into the two other marine erosion mechanisms the model can be calibrated and validated even further. The goal is to improve the certainty of the model results which then can act as a source for data for technical design criteria.

5. **Set-up program of requirements for coastal interventions.**
   After further model calibration and validation extra technical design criteria can be extracted from the model, such as flow velocities, water levels, (storm) wave conditions, sediment sizes and bathymetry. All these factors can be used to set-up technical design criteria to which the coastal intervention has to comply. Besides that the coastal interventions also has to meet other criteria as well. One design strategy is the Building with Nature (BwN) concept explained by the list below directly taken from de Vriend et al. (2015):

Step 1: Understanding the system (including the ecosystem).
Step 2: Identify realistic alternatives that use and/or provide ecosystem services.
Step 3: Evaluate the qualities of each and preselect an integral solution.
step 4: Fine-tune the selected solution (practical restrictions and the governance context).
Step 5: Prepare the solution for implementation in the next project phase.

   Another possible, more parallel, design strategy is defined by U.S. Army Corps of Engineers (2002) and state the following design criteria:

   - Economical (costs, benefits, etc.).
   - Environmental (impact surroundings).
   - Institutional, political, and legal (policies, social well-being, laws).
   - Aesthetics.

   For the environmental, institutional, political and legal criteria, a start for the Living Breakwater project has been made by Cantoni et al. (2019). Said report tries to map the environmental conditions at the Point Grey cliffs as well as the relevant policies and laws at the Point Grey cliffs area.

6. **Testing effectiveness of proposed solutions in model study.**
   After the generation of the interventions model studies can be performed on the effectiveness of the proposed solutions. At the same time the designs can be compared on the secondary design criteria listed before such as costs, environmental impact, constructability etc.

8.8. First solution thoughts

In coastal management there are four main strategies with each their solution as given in Table 8.1. The *Protect* is the preferred strategy for the UBC. Coastal works within this strategy can be divided into hard-, hybrid-, and soft solutions. The hard structures force the shoreline to stay in place. These structures can affect the natural dynamics in its own coastal system or adjacent systems. Hybrid solutions do not result in a fixed shoreline. Soft solutions are activities which do not interfere with the natural dynamics of the system. These solutions mostly consist out of supplements of natural assets (Cantoni et al., 2019).

Table 8.1: Coastal Management Strategies (CMS) with example solutions. From Cantoni et al. (2019), Golder Associates Ltd. (2015).

Protect	**Accommodate**	**Avoid**	**Retreat**
Hard solutions	Raising buildings	Potential development area in low-risk lands	Relocation
Hybrid solutions	Flood insurance	Land acquisition	Resettlement
Soft solutions	Flood-proofing structures		Managed retreat

Examples of the hard-, hybrid- and soft solutions will be discussed. A revetment is a perfect example of a hard solution as it fixes the shorelines. Another example is the berm and groyne system already present at the Point Grey cliffs. Another example for an hard structure is a breakwater. A breakwater might not be the preferred solution here since it obstructs natural currents and sediment transports in the system. A sub-merged breakwater might solve this problem. However, it will be difficult to design a fully submerged breakwater with the large tidal variations. The interventions in such a way that it causes the waves to break. Cantoni et al. (2019) present several hybrid solutions, such as hydraulic piling, clam gardens, or artificial reefs. These structures primarily limit the wave energy and add environmental value. In the last category, the soft solutions, the most promising are the engineered beach and foreshore nourishment solutions. Following the BwN approach a soft solution will be preferred as these solution work together with nature in stead of obstruct natural processes.

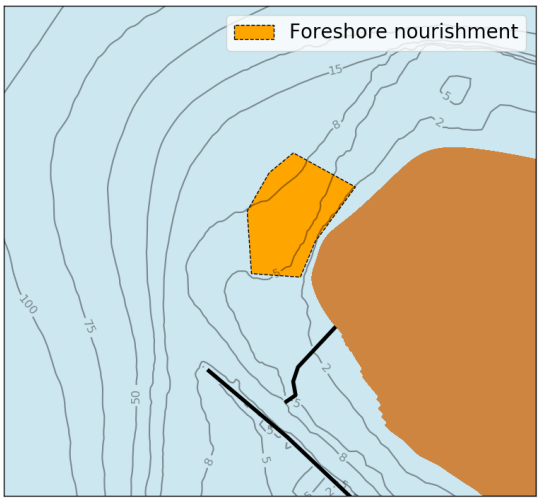

Figure 8.2: Impression sketch of the location of a foreshore nourishment at the Point Grey cliffs.

- *Revetment*
  A revetment is an example of an hard solution for a direct wave attack problem. With a revetment the cliff toe is directly protected. However, it has a significant impact on the aesthetics of the area. An artist impression is shown Figure 8.3.
- *Foreshore nourishment*
  A foreshore nourishment can potentially feed the area by means of the alongshore sediment transport.

Besides that the dredged material from the Fraser Main Arm can be a potential source. The downside of this intervention that it does not provide protection against direct wave attack directly. It takes time for the nourished sand to be transported towards locations where it needs to settle and grow a protective beach. The proposed location is in front of Tower Beach.

- *Engineered beach*
  An engineered beach is a soft solution to the direct wave attack on cliff toe and is a more direct approach than the foreshore nourishment. The beach can elevate the cliff toe which protect it from wave attack and run-up (Ruggiero et al., 2001, Sunumura, 2015). Again, the potential source could be the dredged material from the Fraser River. An impression is given in Figure 8.4.

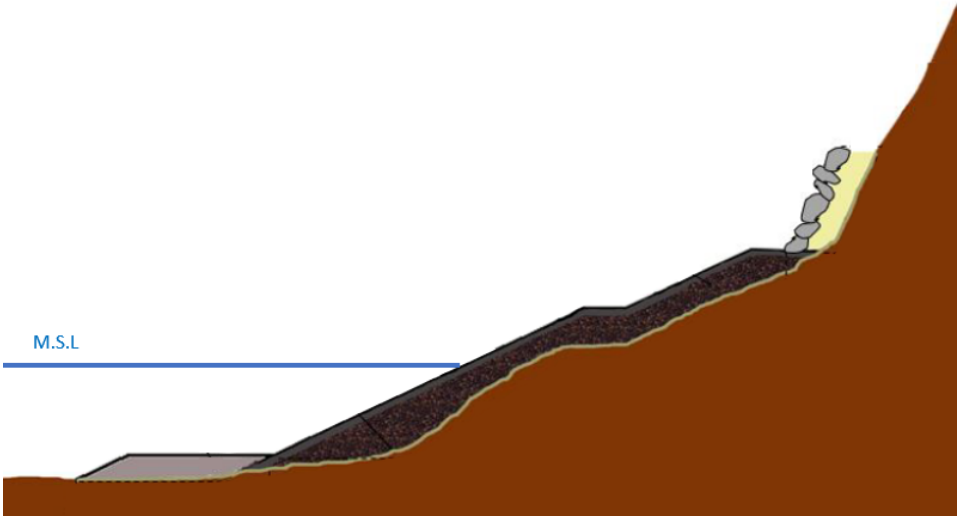

Figure 8.3: Impression sketch of a revetment at the toe of the Point Grey cliffs. Adapted from Cantoni et al. (2019).

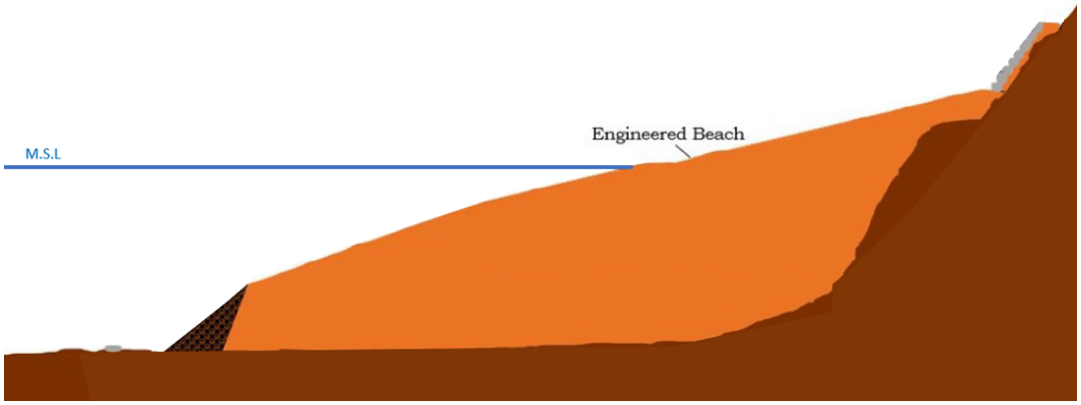

Figure 8.4: Impression sketch of an engineered beach at the toe of the Point Grey cliffs. Adapted from Cantoni et al. (2019).

After this study a combined solution of an engineered beach and nourishment is preferred. The reason is that the combined solution can accommodate all four of the erosion mechanisms. The engineered beach can protect the cliff toe by wave dissipation and can be heightened to adjust for future sea-level rise. The foreshore nourishment feeds Wreck Beach with sediment. This way Wreck Beach can expand the engineered beach in a natural way. A second argument is the potential source of the material: the dredged sand from the Fraser River which is normally dumped in the Strait of Georgia. This material is naturally present in the system, but is not able to reach the Point Grey cliffs. However, the dredged material should be checked for any

pollution before being laid down at the project area. The major downside is the need for period maintenance and monitoring of this combined solution due to its dynamic nature.

8.9. Relevance of study

In this study an attempt was made to put the erosion of the Point Grey cliffs into the general context of coastal cliff erosion. Wave-induced alongshore sediment transported is one of the mechanisms responsible for the marine erosion of the Point Grey cliffs. Three others were identified: direct wave attack during extreme water levels, potential sediment budget deficits, and sea-level rise together with intensified wave conditions. This study tried to diverge to reach a full overview of all marine cliff erosion mechanism. Indicators were found that wave-driven alongshore sediment transport is not the only responsible marine erosion mechanism. These new insights can be used to determine an appropriate solution to the marine erosion of the Point Grey cliffs.

Besides, this study presented case-study to map the current hydrodynamics for the Strait of Georgia and at a local scale near the Point Grey cliffs. The mapping was done by means of data collection together with the construction and analysis of a numerical model. It gathered the data into one report and constructed representative scenarios for the coastal system. The model gave new insights and proved statements regarding the hydrodynamics and sediment transports. Additionally, a hydrodynamic Delft3D model is presented. The Delft3d model can be used for further hydrodynamic research and numerical testing of the interventions designs. Recommendations are discussed to improve the quality of the model and new models. This report can be used by further work on a coastal interventions design to save the work- and living space of many people on the UBC campus.

9

Conclusions & Recommendations

9.1. Key findings

In Section 1.2 the objectives of this study were presented. Deduced from the objectives are the research questions presented in the same section. In the sections below the research questions will be answered.

1. & 2. ***How do soft coastal cliffs erode and which marine erosion mechanisms are important for the Point Grey cliff's erosion?***

Soft coastal cliffs erode first by detachment of cliff material. This happens due to groundwater seepage, water run-off, direct wave attack and/or wave run-up. The second step transports the material down the cliff slope by surface water run-off, wind or gravity. Material is then deposited on the foreshore. After time this material is transported away by sediment transports either induced by tidal- or wave-induced currents.

Over several timescales erosion mechanisms can be indicated. Time scale $\mathcal{O}$(1 s - 1 h) describes erosion at seconds to days. Direct wave attack during extreme events (high tides or storms) is the relevant marine erosion mechanism. The second marine erosion mechanism, time scale $\mathcal{O}$(1 d - 1 m) is the alongshore sediment transport, which according to sources is the prominent marine erosion mechanism at the Point Grey cliffs. Time scale $\mathcal{O}(1-10$ y) belongs to sediment budgets. In this time scale, from years to decades, structural sediment deficits can be a cause of marine erosion. The fourth, time scale $\mathcal{O}(100-1000$ y), belongs to the effects of climate change, namely sea-level rise and increased intensity in wave conditions enabling and increasing the erosion potential of the other three time scales.

3. ***What are the current hydrodynamics, sediment properties, sediment transport patterns, and human interventions around coastal system at the Point Grey cliffs?***

The tide at the Point Grey cliffs has a mean tidal range between 3 to 4 m (Figure 3.6) with maximum flow velocities equal to 12 cm s^{-1}. Only one main wave direction is relevant for the Point Grey cliffs, namely the west northwest (~35% of the year), because the shoreline is facing this direction and is sheltered for the waves from the east southeast. From the model results it was found that the representative significant wave height is approximately 0.5 meters just before breaking for regular wave conditions. The North Arm of the Fraser River jets 80% of the yearly discharge, about 1200 m^3 s^{-1}, during freshet (May-July) into the coastal area. During freshet the outflow velocities can reach 110 cm s^{-1}. With non-freshet conditions the discharge decreases to 375 m^3 s^{-1} and the flow velocities decreases to 70 cm s^{-1}. The flood currents pulls the river outflow outwards reaching higher flow velocities. Ebb counteracts the river outflow at Point Grey where it pushes the river flow westwards.

For storm conditions the significant storm wave heights with a Return Period of five years are approximately 1.1 m at breaking. The 1.3 year Return Period storm surge computed by Tinis (2017) amounts to 0.6 m.

The cliff material generally has a median sediment diameter of 300 µm. The sieving analysis in this study shows the shoreline material with a median grain diameter of 380 µm.

4. ***Which physical process initiates the sediment transports at the Point Grey cliffs and how do they influence the sediment budgets?***
   The model, with the assumptions presented in this report, shows that the alongshore sediment transports are initiated by waves. Cases with waves disabled show almost no sediment transports at all. The tide alone seems unable to mobilize sediment. However, the tide affects the water level, thus how far the waves can propagate onshore. And thus where the sediment transport due to other mechanisms occur.

   The results show that the sediment is transported by model calculations of wave-orbital velocities near the bottom. The transports are mainly bed-load transports. Other wave-driven currents and currents originated from differences in spatial wave set-up seem unable transported sediment in suspension.

   In the model another transportation direction is indicated. Sediment is moved southwards from Point Grey towards the North Arm breakwater. In mean values the model shows sediment transported directed northeast. However, using sediment budgets this model study fails to show this transportation northeast.

   The model shows that the North Arm seems unable to transport any sediment towards the Point Grey cliffs other than silts. Golder Associates Ltd. (2015) assumes no input as well, but due to another reason: the channelization of the North Arm. It seems reasonable that there is no other sediment source than the Point Grey cliffs themselves. The system misses sediments to build a natural protection against the erosion, indicating a structural sediment deficit. This sediment deficit hypothesis is primarily applicable to the area of Tower Beach.

5. ***What further steps need to be taken to reach a solution for the marine erosion at the Point Grey cliffs?***
   The present study acts as a basis with its found current (boundary) data and relevant cliff erosion processes. Additional data can improve the model results greatly. Subsequent studies into direct wave attack, wave run-up and influences of climate change will generate additional technical specifications for a potential solution to the marine erosion. The future steps are presented in Section 8.7 and elaborated in the recommendations section hereafter.

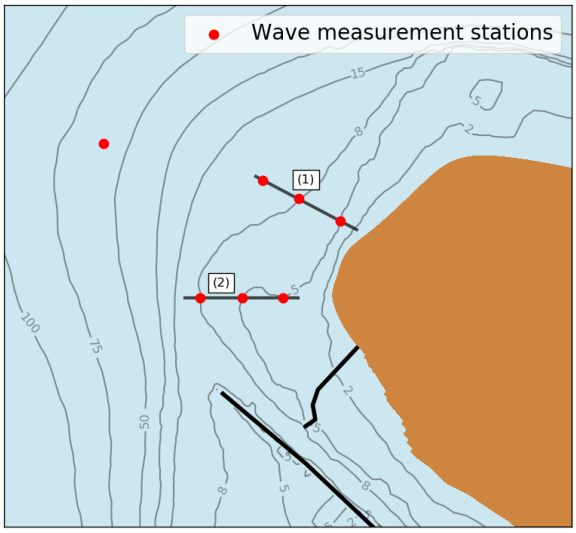

Figure 9.1: Locations of proposed wave measuring stations.

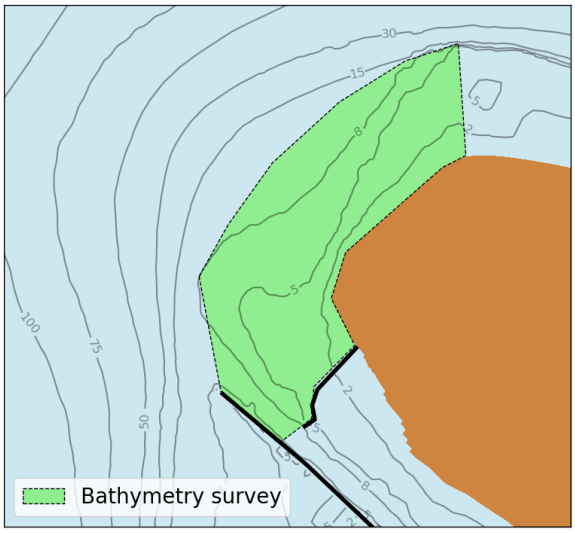

Figure 9.2: Proposed area of bathymetric survey.

9.2. Recommendations

For further studies at the Point Grey cliffs several recommendations can be done to either improve the current study or what is needed for the further steps presented in Chapter 8.

1. ***Further data collection***
   The current model was shown to be sensitive to the significant wave height of the modelled wave con-

ditions. The model can be improved greatly with accurate wave data. Therefore it is recommended to collect nearshore wave data. The proposed locations of the measurement stations are given in Figure 9.1. Two transects are proposed with each three sensors to be able to study the propagation of the waves to the nearshore. Additionally one sensor is placed in deeper water to measure offshore wave data closer to our project site. The offshore station should be placed carefully as it might interfere with the shipping lane towards Vancouver Harbour. Different options are available as measuring devices, e.g. wave buoys or bottom-mounted pressure sensors. Pressure sensors may be the better choice as they are generally cost less than buoys. Together with the pressure sensors additional water level or flow velocity sensor can be applied for extra calibration data.

A second need of data is more detailed bathymetry. The bathymetry used in this study is coarse, as it is retrieved from nautical charts. Detailed bathymetry is of importance as it can alter wave propagation in the nearshore greatly. This detailed bathymetry can then be combined with the LiDAR data of the cliff transects and serve as depth files for new numerical models. Secondly, a surveyed bathymetry can serve as a base case for future morphological studies. The proposed area is roughly 4 km^2 shown in Figure 9.2. The bathymetry survey can be repeated once per year for morphological change data. Performing the surveys yearly excludes seasonal variability and additionally fits the period of the sediment budgets presented in this study.

Extra studies to bottom sediment at the Point Grey cliffs are preferred. The studies in this report assumed a sandy bottom with median grain diameter found from shoreline sediments. This may not be representative for the bottom sediment underwater on the shelf and should therefore be checked. In Figure 9.3 the additional underwater sediment samples are shown. The transects are chosen to complement the already existing locations presented in Figure 4.2. Additional locations inside the North Arm channel to study the bottom material there and potential sediment transport in the river channel. New insights can then be processed into new model bottom compositions. From the samples behind the breakwater an indication can be made what kind of sediment are located there.

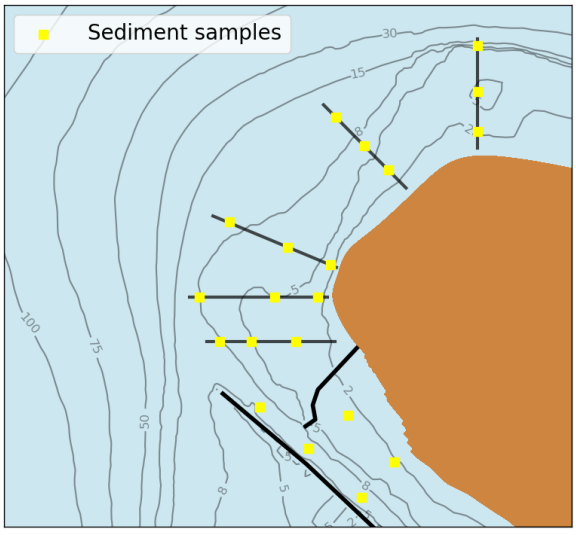

Figure 9.3: Proposed locations of additional sediment samples.

Sediment transport readings in the water at the Point Grey cliffs are of help. This can be done by means of optical or acoustic probes. This data can be used to calibrate sediment transport and help to calibrate the sediment transport factors for the model (Table 6.7).

Lastly, an ecological survey of the nearshore area is needed to determine the environmental boundary conditions. Within the BwN process the ecological design components can be incorporated to reach an optimal final cliff marine protection design.

2. ***Improve assessment of sediment transports and sediment budgets by the current model.***
With new data gathered in foregoing steps and improving model settings by calibration and validation,

such as wave boundaries and cross-section placement, the sediment transports per scenario can be calculated more accurately. In the sensitivity analysis it came to light that the model was sensitive to several parameters.

3. ***Determine magnitude of direct wave attack and wave run-up at the Point Grey cliffs.***
   In this report an approach is chosen appropriate to study the general hydrodynamics and sediment transports. The first erosion mechanism, direct wave attack and wave run-up, is not studied in detail although this mechanism is apparent following the wave model results. For further studies digging deeper in these mechanisms a XBeach (Roelvink et al., 2009) is recommended, together with newly acquired wave and bathymetry data, to check the exposure of the cliff toe to mentioned direct wave attack and wave run-up during extreme tides and storms. The XBeach model is better in resolving drying and flooding. The model includes geological processes as well such as avalanching.

4. ***Assess impact of sea-level rise and intensified wave conditions on the recession of the Point Grey cliffs.***
   Future sea-level rise and wave conditions will affect the rate the Point Grey cliff recede. In further studies future scenarios need to be set-up to predict the changes in erosion rate of the Point Grey cliffs in light of climate change and sea-level rise.

5. ***Reach an integral solution for the marine and sub-aerial erosion.***
   After a successful solution to the marine erosion of Point Grey cliffs the sub-aerial processes described in Chapter 2 still pose risks of the erosion. Although it is more likely that the cliffs will reach a more stable state, it can not be said that the overall recession will be surely stopped. A reduction of sub-aerial erosion is still needed, even with the mitigation of marine erosion.

By means of this study as a basis for following development activities in the 'Living Breakwater' project an integral resilient coastal intervention design will be found, grinding the marine erosion to a halt and save the Point Grey cliffs.

A

Cliff transects

The Living Breakwater project identified several cross-sections were of particular interest. These transects are highlighted in Figure A.1b. These locations are used for the visualization of the cliff cross-sections from the LiDAR data in Figure A.1a.

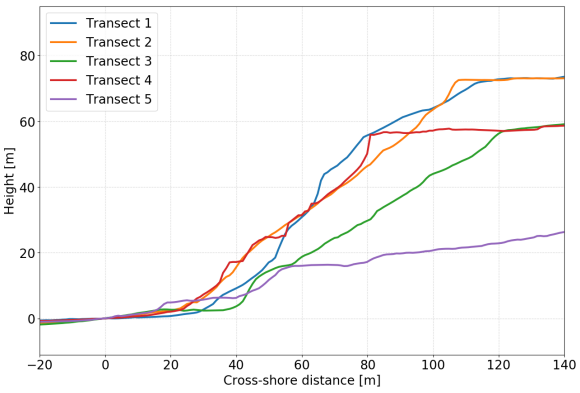

(a) Cross-sections from cliffs at locations highlighted in Figure A.1b.

(b) Locations of transects.

Figure A.1: Point Grey cliff transects acquired from 2015 LiDAR data together with the location of these transects along Wreck Beach.

Figure A.2 shows the division of different LiDAR survey areas. The data used in this example (Figure A.3) is the survey from area 480-5457. Other tiles used for the cliff cross-sections are 480-5456, 481-5457, 481-5458, and 482-5458.

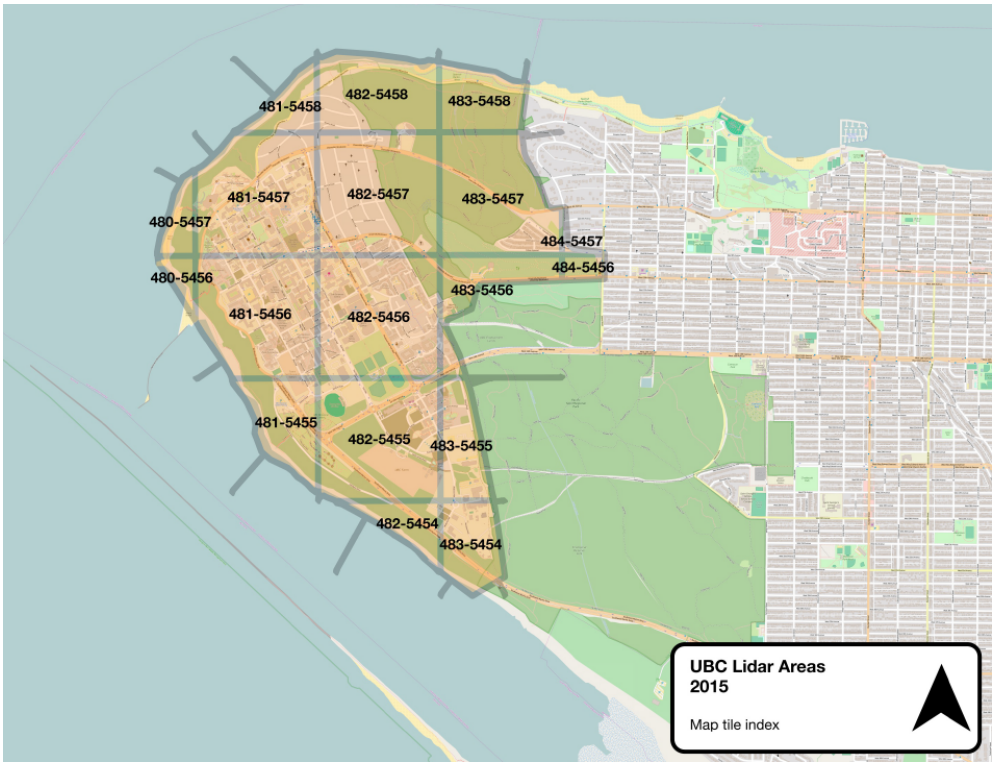

Figure A.2: Tile codes LiDAR survey.

A GIS program is used to process the LiDAR data points. Figure A.3a shows the regular LiDAR data points. From these data points the ground data points can be extracted. The result of the ground level extraction is given in Figure A.3b.

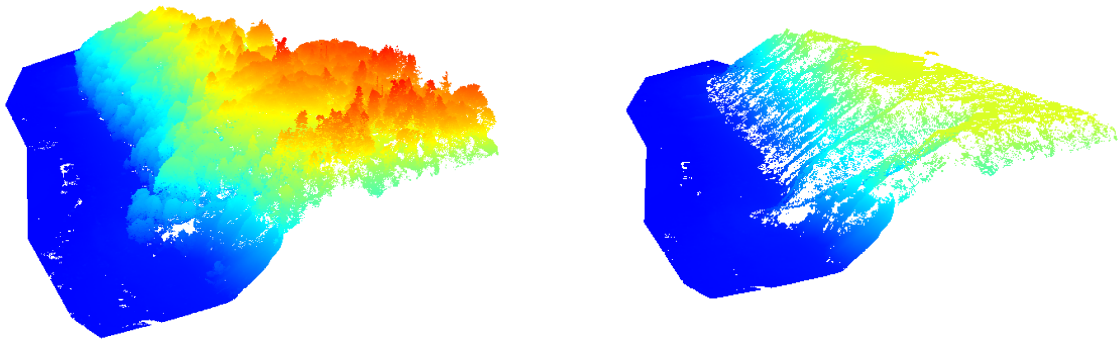

(a) Raw LiDAR.

(b) Ground elevation.

Figure A.3: Raw and processed LiDAR data points of tile 480-5457.

The processed (ground) data points can be used to construct a Digital Elevation Model (DEM) with the same GIS program. From these models cross-section elevations can be read. The resulting cross-section elevations can be found in Figure A.1a.

B

Pebble counts

Besides the volumetric sampling described in Chapter 4 additional pebble counts were carried out at two locations on Tower Beach. The reason for this is to get an idea of the size of the stones on the berm constructed in 1980's. The pebble counts are done at two locations of Tower Beach, one at the start near Tower 1 and the second at the end near Tower 2. The locations can be seen in Figure 4.1.

The pebble counting is done by the use of a gravelometer (Figure B.1). At the location two lines on different beach levels are chosen along which pebbles are sampled. On sight the largest pebble is chosen on which the sample interval is determined, two times the diameter of this largest stone. One rock is picked up at this sampling interval and its smallest passing sieve is ticked (see Tables B.1 & B.2).

Figure B.1: Gravelometer used during the pebble counting on 06/11/2018.

Figure B.3 shows the resulting grading diagram for the material found on the berms. This diagram is constructed with the data found in Tables B.1 & B.2. At the first location (Table B.1) the median grain diameter (D_{50}) is $25.2 \cdot 10^3$ µm. The D_{50} at location 2 (Table B.2) is $43.6 \cdot 10^3$ µm. These values can be seen as indicative, since the error of this sampling method is assumed to be large.

(a) First pebble count.

(b) Second pebble count.

Figure B.2: Two illustrative photos of pebble counting done on Tower Beach. Completed on 06/11/2018.

Table B.1: Results of pebble count at location 1.

Location 1			
Date:	06/11	**Coord.**:	49.269612
Year:	2018		-123.262979
Max. size:	128 mm	**Interval:**	250 mm
Size [mm]	**Line 1**	**Line 2**	**Total**
<128			
<91	4		4
<64	4	4	8
<45	11	9	20
<32	18	22	40
<22.5	6	17	23
<16	8	6	14
<11.3	5		5
<8	4		4
Total	60	58	118

Table B.2: Results of pebble count at location 2.

Location 2			
Date:	06/11	**Coord.:**	49.273854
Year:	2018		-123.256790
Max. size:	128 mm	**Interval:**	250 mm
Size [mm]	**Line 1**	**Line 2**	**Total**
<128	2	2	4
<91	7	7	14
<64	20	22	42
<45	20	29	49
<32	9	8	17
<22.5	3		3
<16			
<11.3			
<8			
Total	61	68	129

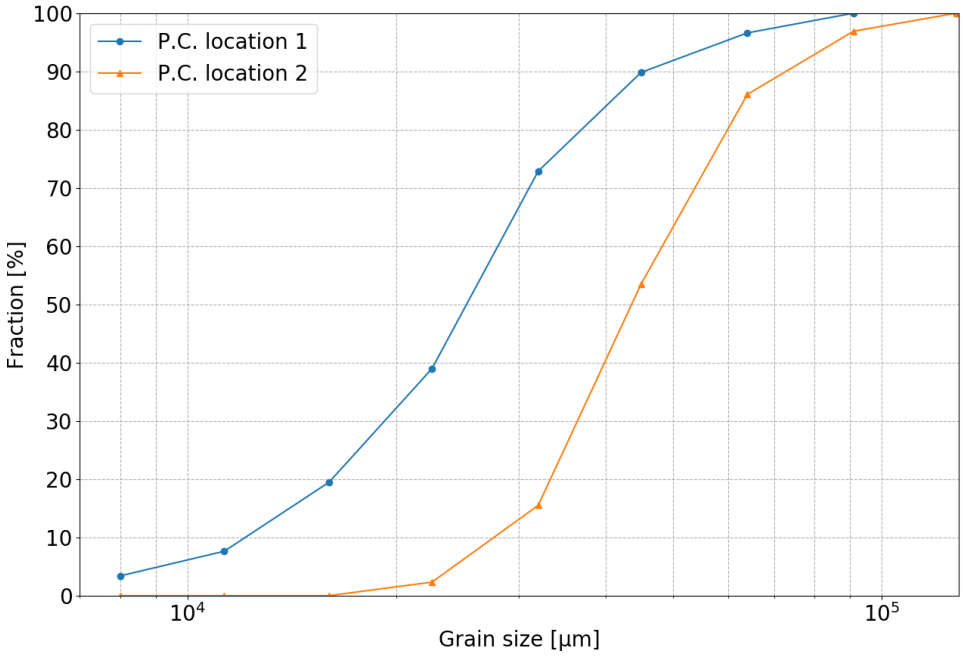

Figure B.3: Grading diagrams following pebble counts with resulting D_{50}.

C

Wave & wind data processing

C.1. Waves

The waves originate from two main directions at the Halibut Bank buoy: WNW and ESE. This part covers the generation of a single wave condition for both directions during freshet and non-freshet periods. Below the significant wave height (H_s) over the years 2008 to 2017 is shown.

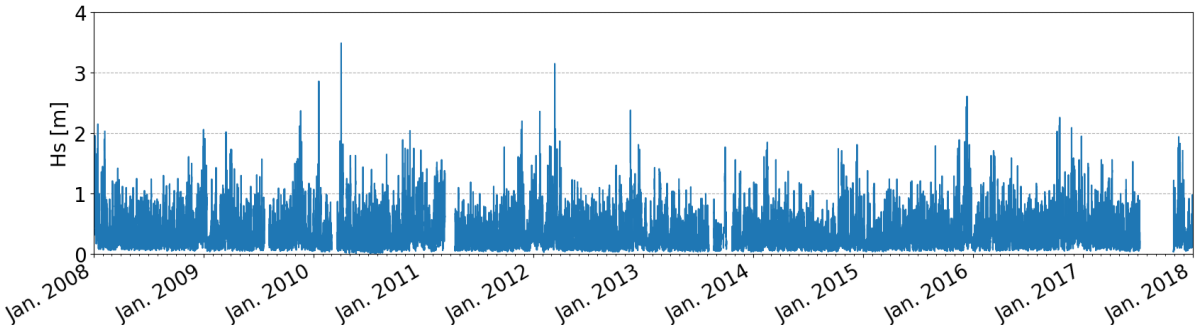

Figure C.1: Signal of significant wave height over the years 2008 through 2017 with data gaps.

The processing of the wave data consists of two parts. The first part is to construct representative wave climates under regular conditions and an extreme value analysis to calculate storm conditions.

C.1.1. Regular wave climates

Firstly, the data is divided into the two periods: freshet (May - July) and non-freshet (August - April). The directions of interest lie between 240° to 330° (WNW) and 60° to 150° (ESE). In the end this analysis results in four single wave conditions.

Table C.1: Occurrence of significant wave heights from every direction at Halibut Bank (2008 - 2017) during non-freshet.

H_s [m]		Wind direction [°]												
Lower limit	Upper limit	-15 to 15	15 to 45	45 to 75	75 to 105	105 to 135	135 to 165	165 to 195	195 to 225	225 to 255	255 to 285	285 to 315	315 to 345	Total
0	0.25	0.036	0.015	0.017	0.066	0.071	0.037	0.014	0.009	0.012	0.038	0.068	0.039	0.422
0.25	0.50	0.010	0.004	0.005	0.081	0.066	0.026	0.008	0.004	0.004	0.033	0.058	0.015	0.313
0.50	0.75	0.001	0.001	0.002	0.053	0.037	0.011	0.003	0.001	0.001	0.013	0.029	0.004	0.157
0.75	1.00	0.000	0.000	0.000	0.022	0.020	0.005	0.001	0.000	0.000	0.003	0.011	0.001	0.064
1.00	1.25	0.000	0.000	0.000	0.009	0.008	0.002	0.000	0.000	0.000	0.001	0.004	0.001	0.024
1.25	1.50	0.000	0.000	0.000	0.003	0.003	0.001	0.000	0.000	0.000	0.000	0.001	0.000	0.010
1.50	>	0.000	0.000	0.000	0.003	0.003	0.001	0.000	0.000	0.000	0.000	0.001	0.000	0.007
Total		0.047	0.019	0.025	0.237	0.208	0.083	0.026	0.015	0.018	0.088	0.172	0.061	0.998

Table C.2: Weighted mean significant wave heights from every direction at Halibut Bank (2008 - 2017) during non-freshet.

H_s [m]		Wind direction [°]												
Lower limit	Upper limit	-15 to 15	15 to 45	45 to 75	75 to 105	105 to 135	135 to 165	165 to 195	195 to 225	225 to 255	255 to 285	285 to 315	315 to 345	Total
0	0.25	0.15	0.14	0.14	0.16	0.16	0.16	0.15	0.15	0.14	0.15	0.15	0.15	
0.25	0.50	0.33	0.34	0.36	0.37	0.37	0.36	0.36	0.35	0.35	0.37	0.37	0.35	
0.50	0.75	0.58	0.59	0.59	0.61	0.61	0.61	0.59	0.60	0.60	0.60	0.60	0.60	
0.75	1.00	0.88	0.82	0.83	0.85	0.85	0.86	0.85	0.87	0.85	0.84	0.85	0.86	
1.00	1.25	1.08	1.05	1.07	1.10	1.11	1.11	1.13	1.14	1.04	1.09	1.10	1.09	
1.25	1.50	0.00	0.00	0.00	1.35	1.35	1.36	1.36	1.25	1.29	1.27	1.35	1.35	
1.50	>	0.00	0.00	0.00	1.72	1.89	1.90	1.86	1.51	0.00	1.74	1.65	1.61	

Table C.3: Average wave direction of significant wave heights from every direction at Halibut Bank (2008 - 2017) during non-freshet.

H_s [m]		Wind direction [°]												
Lower limit	Upper limit	-15 to 15	15 to 45	45 to 75	75 to 105	105 to 135	135 to 165	165 to 195	195 to 225	225 to 255	255 to 285	285 to 315	315 to 345	Total
0	0.25	-2	29	62	93	119	148	178	211	241	274	299	329	
0.25	0.50	-3	29	65	94	117	147	176	209	242	277	297	329	
0.50	0.75	-5	29	66	94	116	147	176	209	242	278	296	325	
0.75	1.00	-6	29	70	95	116	147	175	210	242	278	299	322	
1.00	1.25	-12	29	72	97	115	147	174	210	243	280	301	320	
1.25	1.50	0	0	0	98	116	147	173	202	253	279	305	320	
1.50	>	0	0	0	98	118	146	173	206	0	275	306	317	

Table C.4: Average peak period of significant wave heights from every direction at Halibut Bank (2008 - 2017) during non-freshet.

H_s		Wind direction [°]												
[m]		-15	15	45	75	105	135	165	195	225	255	285	315	
Lower limit	Upper limit	to 15	to 45	to 75	to 105	to 135	to 165	to 195	to 225	to 255	to 285	to 315	to 345	Total
0	0.25	9.66	8.97	9.39	9.94	9.24	8.88	8.63	8.11	8.68	10.30	10.02	10.03	
0.25	0.50	7.60	7.07	9.07	8.26	7.23	7.05	6.72	7.57	8.41	7.56	7.22	7.26	
0.50	0.75	5.14	5.80	10.32	5.72	5.02	4.94	4.10	4.60	4.95	5.96	5.45	4.85	
0.75	1.00	4.75	4.87	6.86	4.66	4.22	4.50	4.71	6.63	6.88	5.01	4.76	4.32	
1.00	1.25	4.79	5.08	4.62	4.57	4.34	4.67	4.99	4.80	4.44	4.61	4.76	4.64	
1.25	1.50	0.00	0.00	0.00	4.77	4.69	5.09	5.41	5.89	5.06	4.80	4.89	4.98	
1.50	>	0.00	0.00	0.00	5.12	5.52	5.67	6.32	5.89	0.00	5.34	5.24	5.28	

Table C.5: Average wind speeds of significant wave heights from every direction at Halibut Bank (2008 - 2017) during non-freshet.

H_s		Wind direction [°]												
[m]		-15	15	45	75	105	135	165	195	225	255	285	315	
Lower limit	Upper limit	to 15	to 45	to 75	to 105	to 135	to 165	to 195	to 225	to 255	to 285	to 315	to 345	Total
0	0.25	2.3	1.6	1.8	3.5	3.4	2.9	2.2	1.7	1.8	2.9	3.2	2.6	
0.25	0.50	3.3	2.3	3.9	6.1	5.7	5.0	4.3	3.4	3.6	5.3	5.4	4.0	
0.50	0.75	4.1	3.5	5.8	8.2	7.7	6.8	5.6	5.8	5.5	7.2	7.2	5.8	
0.75	1.00	3.8	3.5	7.8	9.9	9.2	8.3	7.1	6.2	7.0	8.7	9.1	7.8	
1.00	1.25	7.0	2.8	8.5	11.5	10.9	9.3	7.8	7.4	5.0	10.0	10.7	10.0	
1.25	1.50	0.0	0.0	0.0	12.4	11.9	10.1	8.3	5.5	7.0	11.1	12.3	11.0	
1.50	>	0.0	0.0	0.0	14.1	13.8	12.1	9.1	7.6	0.0	11.6	13.8	12.6	

Table C.6: Occurrence of significant wave heights from every direction at Halibut Bank (2008 - 2017) during freshet.

H_s [m]		Wind direction [°]												
Lower limit	Upper limit	-15 to 15	15 to 45	45 to 75	75 to 105	105 to 135	135 to 165	165 to 195	195 to 225	225 to 255	255 to 285	285 to 315	315 to 345	Total
0	0.25	0.028	0.012	0.015	0.060	0.114	0.080	0.026	0.017	0.019	0.052	0.057	0.028	0.508
0.25	0.50	0.004	0.001	0.002	0.029	0.081	0.036	0.004	0.003	0.005	0.064	0.061	0.008	0.298
0.50	0.75	0.000	0.000	0.000	0.010	0.041	0.010	0.001	0.000	0.001	0.041	0.035	0.001	0.140
0.75	1.00	0.000	0.000	0.000	0.003	0.012	0.002	0.000	0.000	0.000	0.010	0.014	0.000	0.041
1.00	1.25	0.000	0.000	0.000	0.001	0.002	0.000	0.000	0.000	0.000	0.001	0.005	0.000	0.009
1.25	1.50	0.000	0.000	0.000	0.000	0.000	0.000	0.000	0.000	0.000	0.000	0.001	0.000	0.002
1.50	>	0.000	0.000	0.000	0.000	0.000	0.000	0.000	0.000	0.000	0.000	0.000	0.000	0.000
Total		0.031	0.014	0.018	0.102	0.250	0.128	0.031	0.020	0.025	0.170	0.173	0.037	0.999

Table C.7: Weighted mean significant wave heights from every direction at Halibut Bank (2008 - 2017) during freshet.

H_s		Wind direction [°]												
[m]		-15	15	45	75	105	135	165	195	225	255	285	315	
Lower limit	Upper limit	to 15	to 45	to 75	to 105	to 135	to 165	to 195	to 225	to 255	to 285	to 315	to 345	Total
0	0.25	0.14	0.14	0.14	0.15	0.16	0.16	0.15	0.15	0.15	0.16	0.16	0.15	
0.25	0.50	0.32	0.32	0.34	0.37	0.37	0.34	0.34	0.34	0.34	0.38	0.37	0.34	
0.50	0.75	0.54	0.55	0.55	0.60	0.61	0.60	0.58	0.56	0.59	0.60	0.61	0.61	
0.75	1.00	0.80	0.00	0.83	0.85	0.83	0.82	0.80	0.00	0.88	0.84	0.85	0.84	
1.00	1.25	0.00	0.00	0.00	1.12	1.10	1.09	1.02	0.00	1.17	1.08	1.11	1.14	
1.25	1.50	0.00	0.00	0.00	1.34	1.34	1.40	1.42	0.00	0.00	0.00	1.35	0.00	
1.50	>	0.00	0.00	0.00	0.00	1.58	1.58	0.00	0.00	0.00	0.00	1.54	0.00	

Table C.8: Average wave direction of significant wave heights from every direction at Halibut Bank (2008 - 2017) during freshet.

H_s		Wind direction [°]												
[m]		-15	15	45	75	105	135	165	195	225	255	285	315	
Lower limit	Upper limit	to 15	to 45	to 75	to 105	to 135	to 165	to 195	to 225	to 255	to 285	to 315	to 345	Total
0	0.25	-2	30	62	93	121	148	178	209	241	274	297	330	
0.25	0.50	-2	28	61	96	121	145	177	211	244	276	294	328	
0.50	0.75	-6	19	68	97	120	142	177	210	247	278	293	325	
0.75	1.00	5	0	62	99	120	140	189	0	246	279	294	319	
1.00	1.25	0	0	0	96	119	140	189	0	238	280	296	317	
1.25	1.50	0	0	0	102	118	140	194	0	0	0	299	0	
1.50	>	0	0	0	0	116	142	0	0	0	0	296	0	

Table C.9: Average peak period of significant wave heights from every direction at Halibut Bank (2008 - 2017) during freshet.

H_s [m]		Wind direction [°]												
Lower limit	Upper limit	-15 to 15	15 to 45	45 to 75	75 to 105	105 to 135	135 to 165	165 to 195	195 to 225	225 to 255	255 to 285	285 to 315	315 to 345	Total
0	0.25	10.31	9.07	8.83	10.82	10.34	9.61	9.44	10.70	10.17	11.26	11.01	10.84	
0.25	0.50	8.82	9.64	9.24	9.35	9.30	8.20	7.71	9.73	7.02	11.13	8.89	6.89	
0.50	0.75	3.57	4.27	7.44	6.40	5.44	4.97	3.67	3.58	3.51	7.82	6.34	6.58	
0.75	1.00	5.86	0.00	3.74	3.71	4.86	3.89	4.54	0.00	4.27	4.46	4.80	3.94	
1.00	1.25	0.00	0.00	0.00	4.37	4.86	4.70	5.33	0.00	4.27	6.47	4.58	5.20	
1.25	1.50	0.00	0.00	0.00	4.50	4.56	5.52	5.33	0.00	0.00	0.00	4.96	0.00	
1.50	>	0.00	0.00	0.00	0.00	4.62	5.01	0.00	0.00	0.00	0.00	5.20	0.00	

Table C.10: Average wind speeds of significant wave heights from every direction at Halibut Bank (2008 - 2017) during freshet.

H_s [m]		Wind direction [°]												
Lower limit	Upper limit	-15 to 15	15 to 45	45 to 75	75 to 105	105 to 135	135 to 165	165 to 195	195 to 225	225 to 255	255 to 285	285 to 315	315 to 345	Total
0	0.25	1.9	1.5	1.7	3.2	3.3	2.9	2.1	1.6	1.9	3.1	3.1	2.6	
0.25	0.50	3.4	2.3	2.7	5.8	5.6	4.7	3.4	3.0	3.1	5.4	5.2	3.5	
0.50	0.75	4.7	3.2	5.9	7.7	7.5	6.7	4.4	3.9	6.0	7.2	6.9	5.8	
0.75	1.00	6.7	0.0	6.7	9.5	9.0	7.8	3.7	0.0	8.6	8.6	8.6	9.4	
1.00	1.25	0.0	0.0	0.0	11.1	11.0	9.4	8.7	0.0	10.9	10.2	10.0	9.0	
1.25	1.50	0.0	0.0	0.0	11.5	11.5	11.1	6.9	0.0	0.0	0.0	11.0	0.0	
1.50	>	0.0	0.0	0.0	0.0	12.1	12.4	0.0	0.0	0.0	0.0	11.3	0.0	

Each data point is divided in a certain significant wave height bin and direction bin. Tables C.1 & C.6 both show the occurrences for the all the combinations of bins. Both Tables C.2 & C.7 shows the morphological weighted significant wave height, calculated by:

$$\sqrt{\sum \frac{{H_s}^{2.5}}{\text{no. waves in bin}}} \tag{C.1}$$

The wind/wave direction, peak wave period and wind speeds are averaged within a certain bin and are given in Tables C.3 to C.8 and C.5 to C.10.

In Figure C.2 the final result of the construction of wave conditions is shown. These vectors are calculated by using the data shown in the occurrence, weighted significant wave height and mean wave directions tables. The factor 2.5 comes from the proportionality of significant wave height to sediment transports. The length of every vector is the product is given by:

$$occurance \times {H_s}^{2.5} \tag{C.2}$$

The angle of a certain vector is the average wave direction. The dotted lines in the graph show resulting representative wave climates. From the length of these dotted lines follows the H_s and the angle is the direction of this incoming wave.

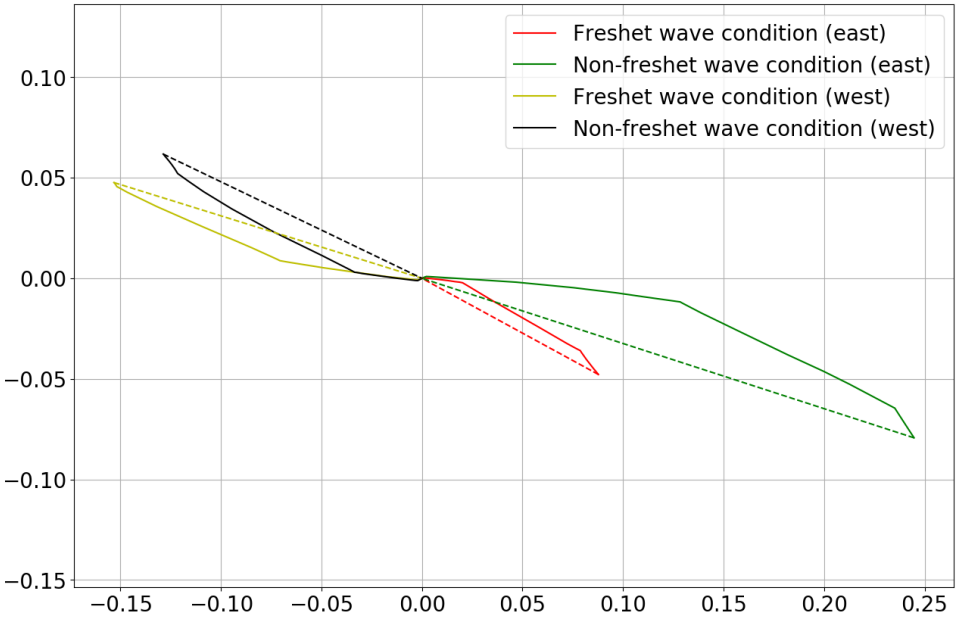

Figure C.2: Calculating representative wave conditions.

Another important factor is the peak wave period. As there is no clear relation between H_s and this peak wave period, an estimation is made. This is done by taking the H_s bin where the representative H_s fall into.

Table C.11: Resulting representative wave conditions.

Wave climate	**Color**	H_s [m]	**Dir.** [°]	T_p [s]	u_w [m s^{-1}]
West (non-freshet)	Black	0.46	295	7.22	5.3
East (non-freshet)	Green	0.58	108	5.02	7.7
West (freshet)	Yellow	0.48	287	8.89	5.2
East (freshet)	Red	0.40	119	9.30	5.6

C.1.2. Extreme value analysis

The extreme value analysis for storms is done by following Appendix A from van den Bos and Verhagen (2018). Again, the data is divided into the same two directions as in the last section. The first step is then to determine a threshold value above which the storms are distinguished from regular conditions. A first assumption is that only one storm per day is allowed. The second is that approximately ten storms per year (N_s) are sought (van den Bos and Verhagen, 2018).

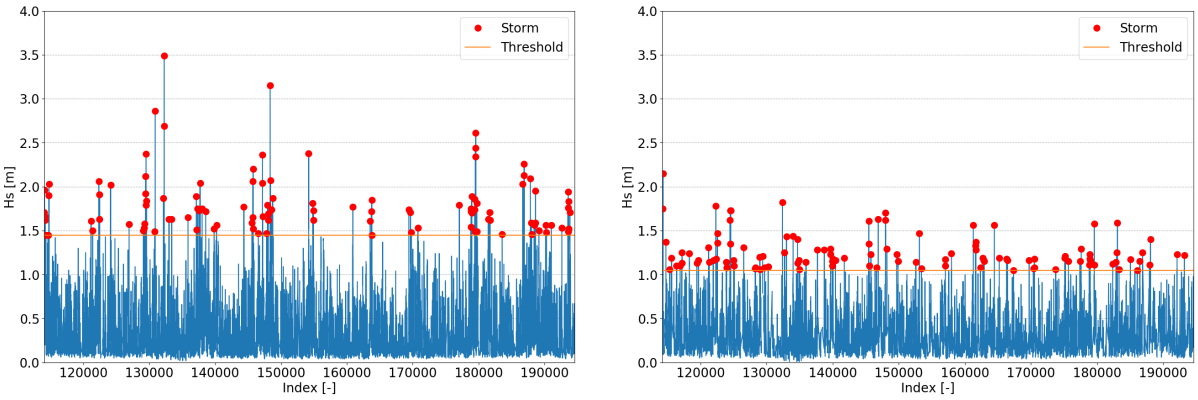

(a) Western storms.

(b) Eastern storms.

Figure C.3: Identifying storms from significant wave height signal.

The used threshold values and number of storms are given in Table C.12. Then, the storms are sorted in ascending order and given a rank (i). Afterwards the non-exceedence (P) and exceedance (Q) probabilities of the individual storms are calculated by means of Equation C.3.

Table C.12: Resulting values from peak-over-threshold method.

Direction	**West**	**East**
Threshold [m]	1.05	1.45
N_s [-]	11.2	10.9
N [-]	112	109

$$P_i = \frac{i}{N+1}$$
$$Q_i = 1 - P_i \tag{C.3}$$

The non-exceedence probability can be rewritten into the a so-called return period, which more often used in an extreme value analysis. The return period actually is the interval between two events of the same magnitude.

$$R_i = \frac{1}{Q_i \cdot N_s} \tag{C.4}$$

Then, a best fit is sought from four different extreme value distributions: Exponential-, Gumbel-, General Pareto-, and Weibull distributions. This is done by estimating the distribution variables to the data by means of linear regression. The equations for linear progression per distribution are listed below (Equation C.5)

$$
\begin{aligned}
\text{Exponential: } H_s &= \gamma + \beta \cdot -\log(\frac{1}{R_i \cdot N_s}) \\
\text{Gumbel: } H_s &= \gamma + \beta \cdot -\log(-\log(1 - \frac{1}{R_i \cdot N_s})) \\
\text{General Pareto: } H_s &= \gamma + \beta(\frac{(\frac{1}{R_i \cdot N_s})^{-\alpha} - 1}{\alpha}) \\
\text{Weibull: } H_s &= \gamma + \beta \cdot -\log((\frac{1}{R_i \cdot N_s})^{1/\alpha})
\end{aligned}
\tag{C.5}
$$

By minimizing the Root Mean Squared Error (RMSE) the parameters for every distribution can be obtained. The equation of the RMSE is given in Equation C.6.

$$
RMSE = \sqrt{\frac{1}{N}\sum_{i=1}^{N}(H_{ss,i} - H_{ss,pred,i})^2} \tag{C.6}
$$

After an initial guess the parameters (γ, β, α) for different distributions the best fit is generated. The results are in Tables C.13 & C.14 and the green-highlighted distributions are the best fits.

Table C.13: Results linear regression (West).

	γ	β	α	**RMSE**
Expon.	1.044	0.217	-	0.027
Gumbel	1.166	0.162	-	0.052
GPD	1.051	0.202	0.043	0.026
Weibull	1.060	0.195	0.922	0.026

Table C.14: Results linear regression (East).

	γ	β	α	**RMSE**
Expon.	1.438	0.375	-	0.048
Gumbel	1.648	0.280	-	0.093
GPD	1.483	0.278	0.167	0.027
Weibull	1.500	0.282	0.817	0.035

In Figure C.4a the best fits for each distribution is visualized. Then in Figure C.4b the 90% confidence interval is shown for the best fits highlighted in green in Tables C.13 & C.14.

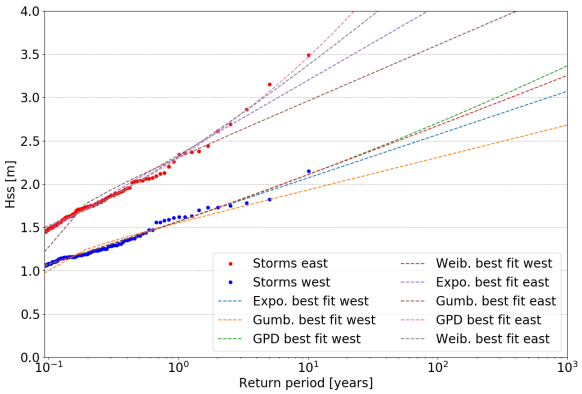

(a) Different extreme value distribution fits to both western and eastern storms.

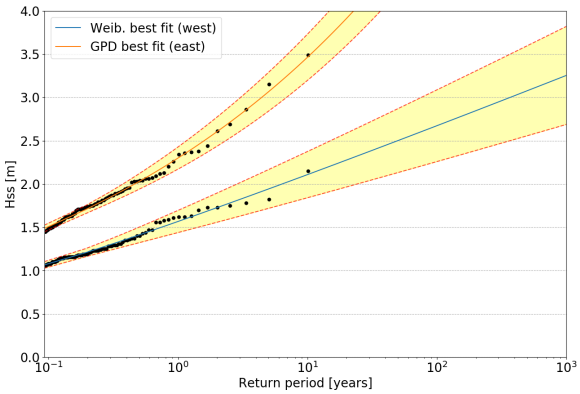

(b) The 90% confidence intervals for both best fit distributions.

Figure C.4: Left: Different extreme value distribution fits to data points. Right: Visualized 90% confidence intervals of the two best fits.

Table C.15 shows the outcomes of using the extreme value distributions to calculate a storm's H_{ss}. The last three important factors, the peak wave period (T_p), direction and wind speed (u_w) are still unknown. Since

no clear relations between mentioned factors and H_{ss}, the mean value of the storm data set is used. This results in a $T_p = 4.71$ s, coming from 297° under $u_w = 11.2\,\mathrm{m\,s^{-1}}$ conditions for western storms. For eastern storms these values becomes: $T_p = 5.48$ s, 117°, and $u_w = 13.4\,\mathrm{m\,s^{-1}}$.

Table C.15: Storm parameters corresponding to different Return Periods.

RP	**1 y**	**5 y**	**10 y**	**100 y**	**500 y**
H_{ss} [m] **(west)**	1.57	1.94	2.11	2.71	3.16
H_{ss} [m] **(east)**	2.32	3.04	3.37	4.55	5.44

C.2. Wind

Note that the corresponding wind speeds to different wave climates are already found in the last section. Therefore Figure C.5 functions for visual reference only.

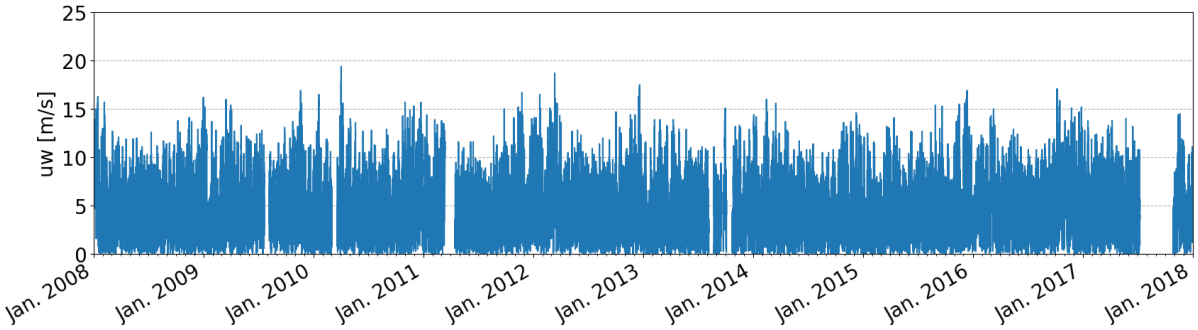

Figure C.5: Signal of u_w over the years 2008 through 2017 with data gaps.

D

Nautical charts

On the next two pages the nautical charts are presented which are used to construct the bathymetry for the model. This is done with a GIS program to copy the depth lines and extract the isolines with their corresponding coordinates. The first chart in Figure D.1 is of the Point Grey and its surroudings (no. 4962). The second chart, Figure D.2 is of the lower Fraser Main Arm (no. 4961a).

The nautical charts are given depths relative to the Chart Datum (CD), which is approximately the level of Lowest Astronomical Tide (LAT). Canada uses two other vertical datums: CGVD28 and CGVD2013. CGVD2013 is approximated as MSL and +3.1 meters higher than CD according to Golder Associates Ltd. (2015). Therefore all depths extracted from the nautical charts are adjusted accordingly.

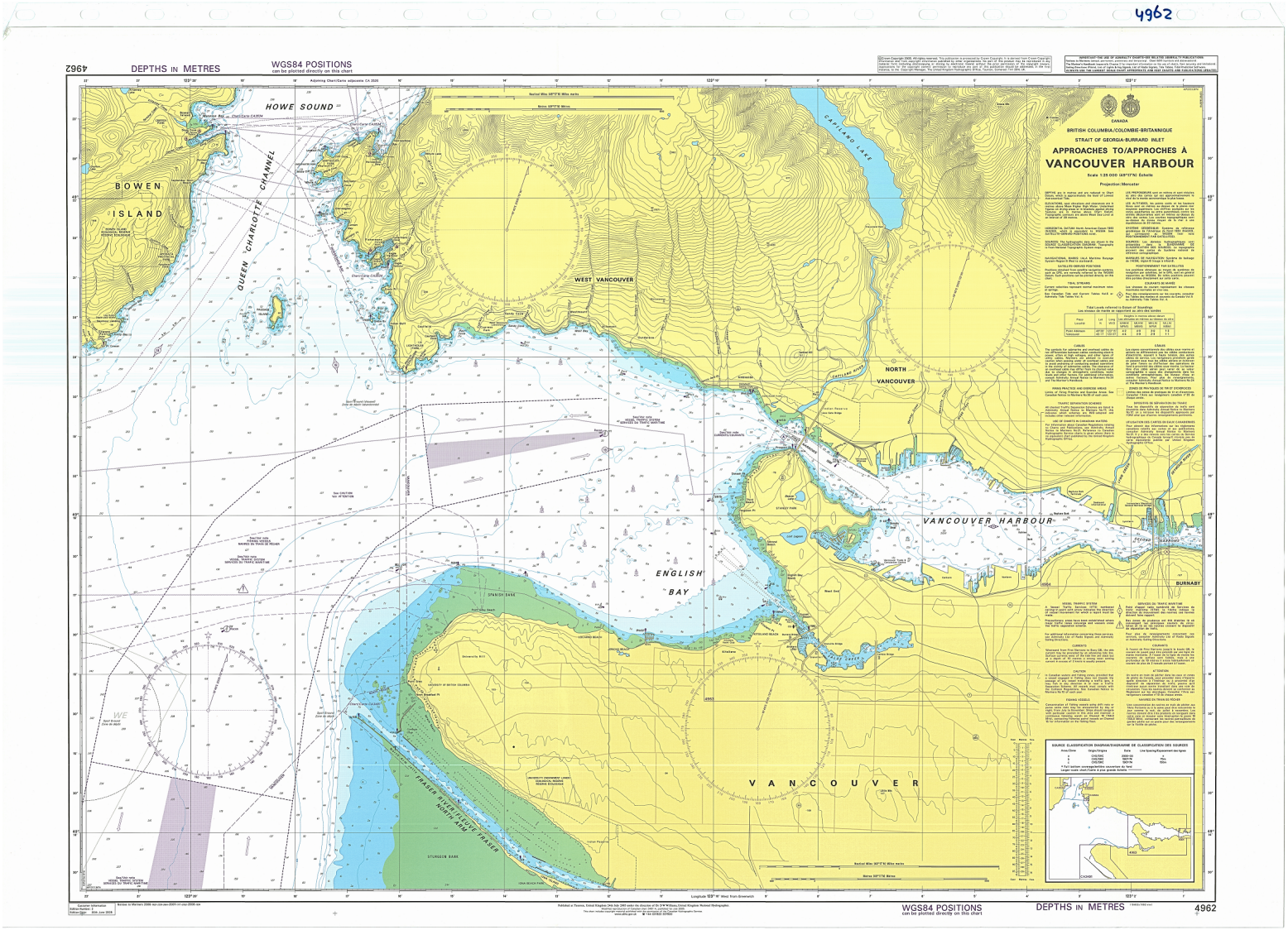

Figure D.1: Digitized nautical chart of Point Grey and surroundings (No. 4962).

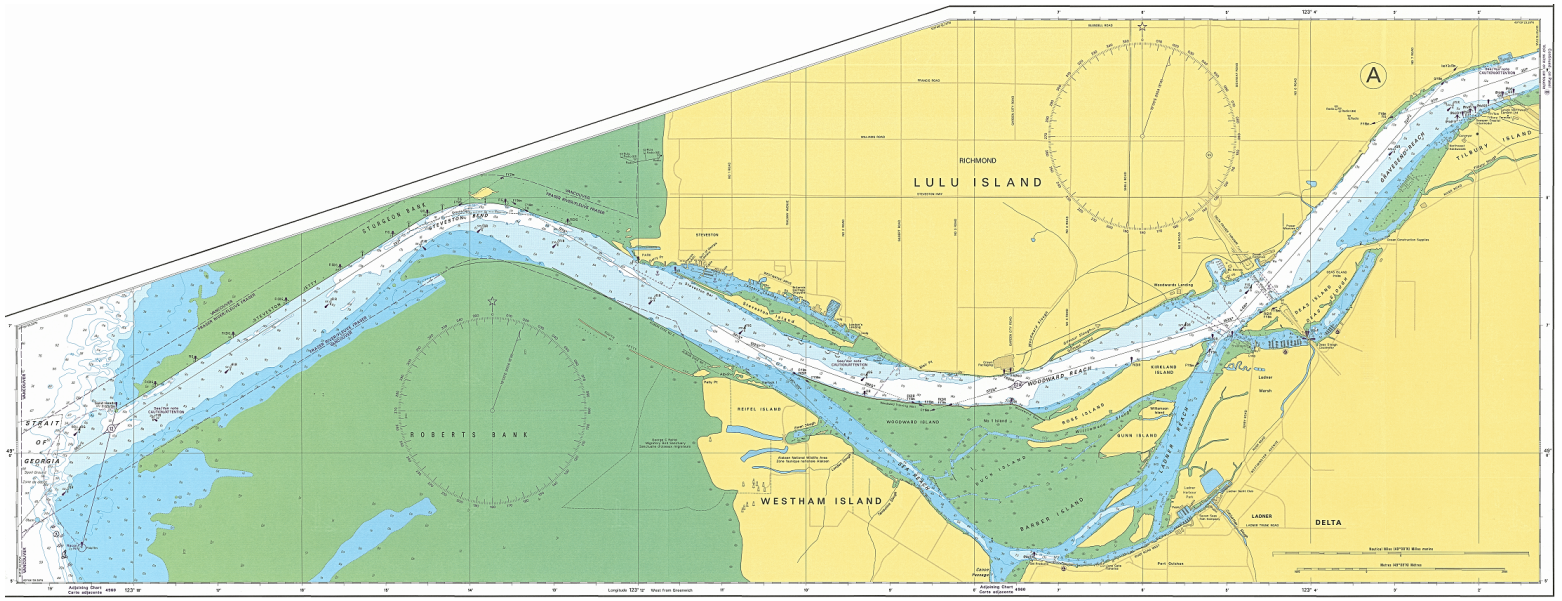

Figure D.2: Digitized nautical chart of the Fraser River Main Arm (No. 4961a).

E

Model calibration results

In the last section of Chapter 6 the model was calibrated to water levels. In that chapter the best and worst fit of this calibration was already shown. In the first section the remaining water level comparisons are shown. In the second section in this appendix the remaining comparisons of the amplitudes and phases of the modeled tidal constituents are given.

E.1. Water levels of the large model during calibration

In Figure E.1 the remaining water level comparisons are given following the water level calibration of the Delft3D-FLOW model in Chapter 6.

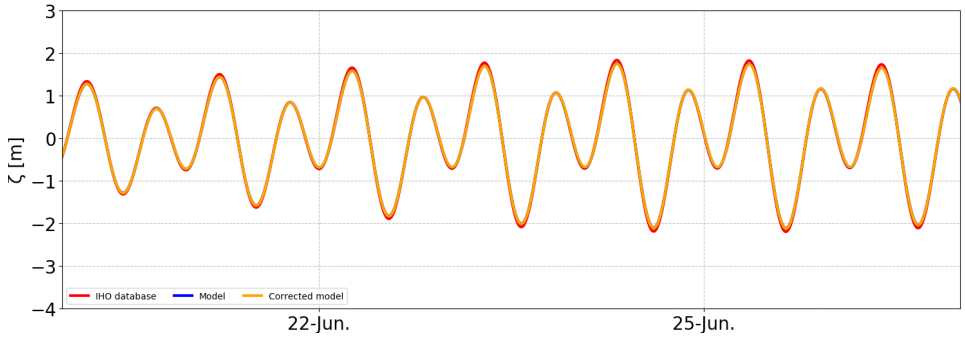

(a) IAPSO#-30.2.1.2

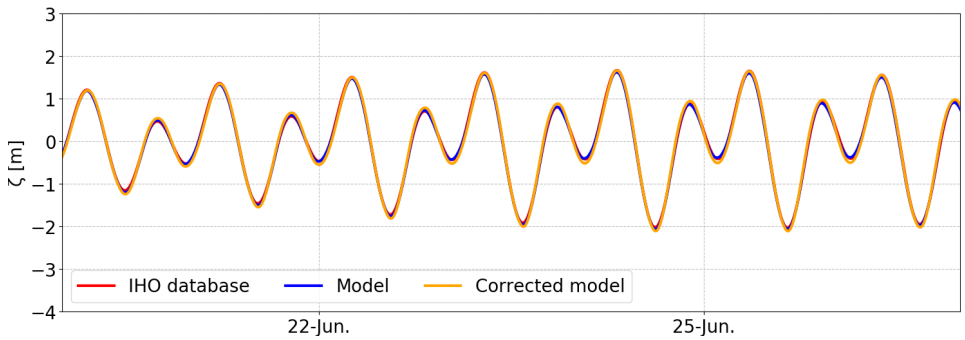

(b) Neah Bay

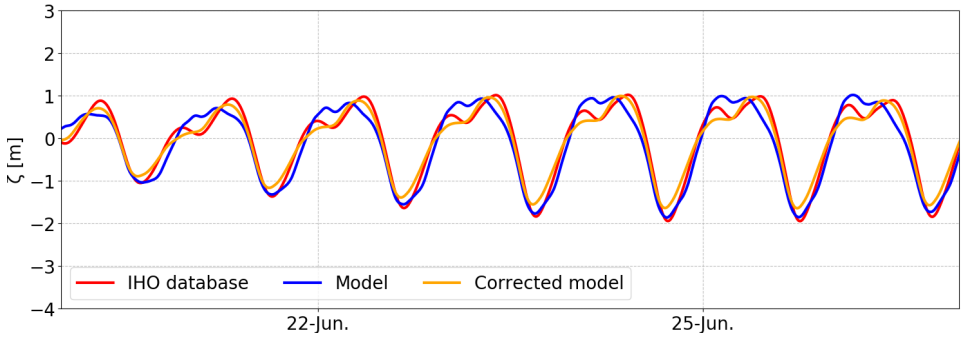

(c) Oak Bay

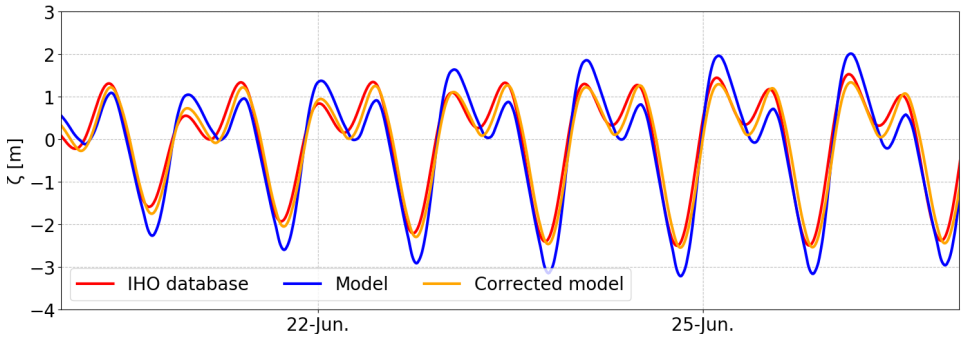

(d) Porlier Pass

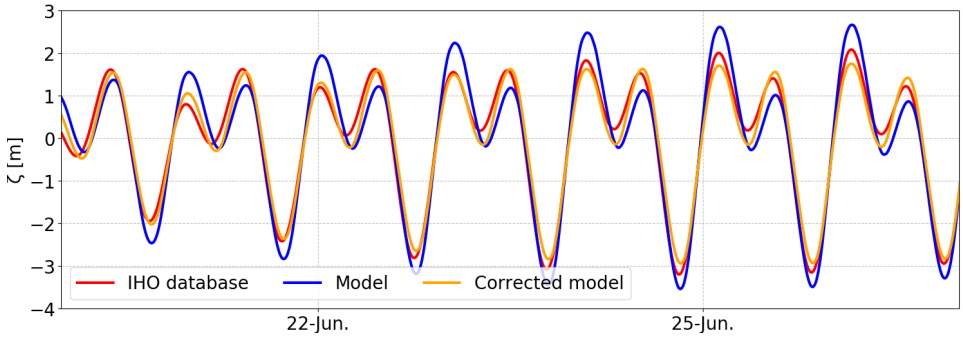

(e) Whaletown Bay

Figure E.1: Water level variations of several tidal stations chosen to analyse the propagation of the tidal wave through the Strait of Georgia.

E.2. Tidal amplitudes and phases during calibration

In Figure E.2 the remaining amplitude and phase comparisons of the tidal constituents are given following the water level calibration of the Delft3D-FLOW model in Chapter 6.

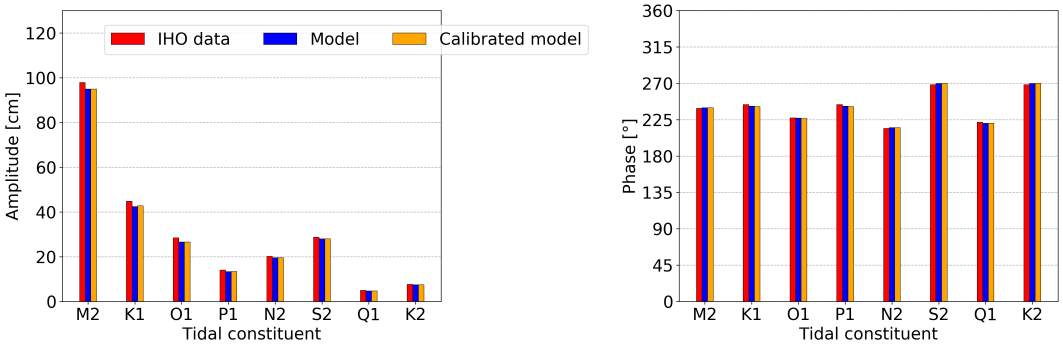

(a) IAPSO#-30.2.1.2

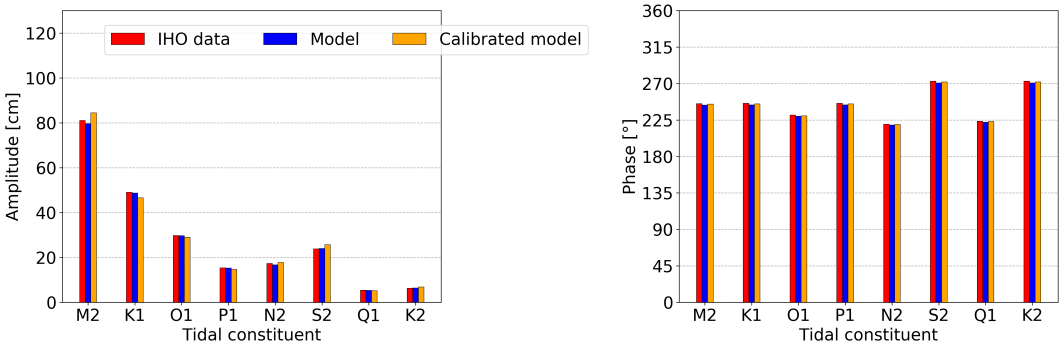

(b) Neah Bay

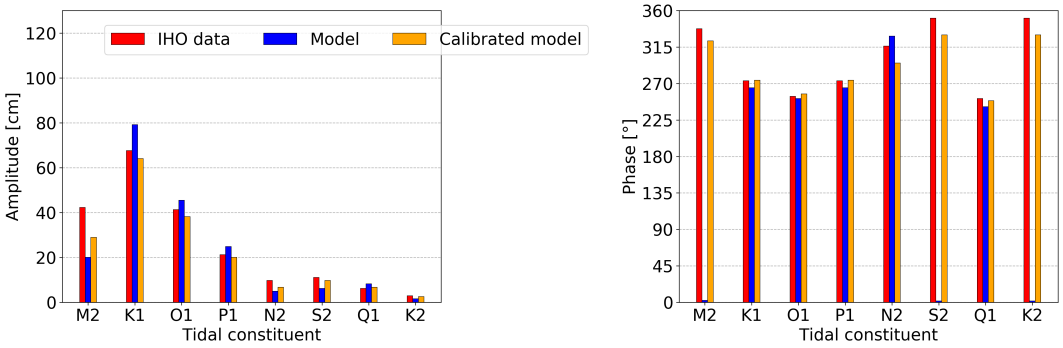

(c) Oak Bay

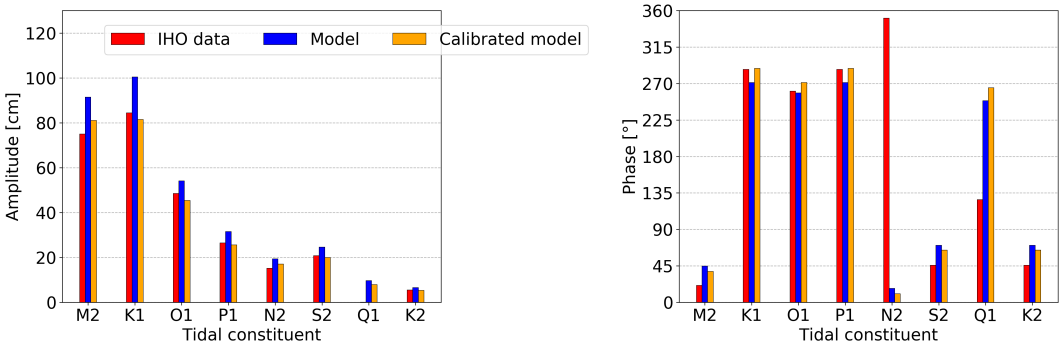

(d) Porlier Pass

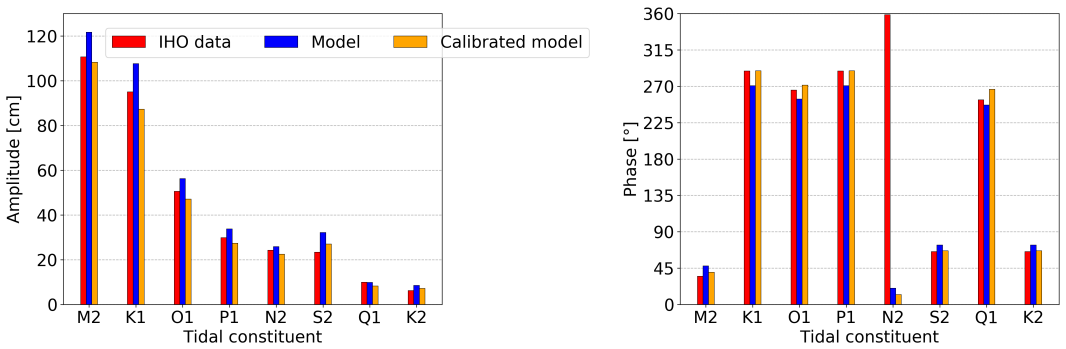

(e) Whaletown Bay

Figure E.2: Amplitudes and phases of most important tidal constituents at several tide stations along Strait of Georgia.

F

Additional model results

F.1. Flow- and wave fields

In this section the the additional flow fields of the model scenarios as a supplement to Section 7.1. In this section mainly the flow fields of the two storm scenarios (Figures F.1 and F.2). The flow fields are not that interesting for this study's scope and is there presented here as extra information. These scenarios mainly show the influence of higher storm winds and in case of scenario 4 (Figure F.2) the influence of representative 5-year Return Period storm waves.

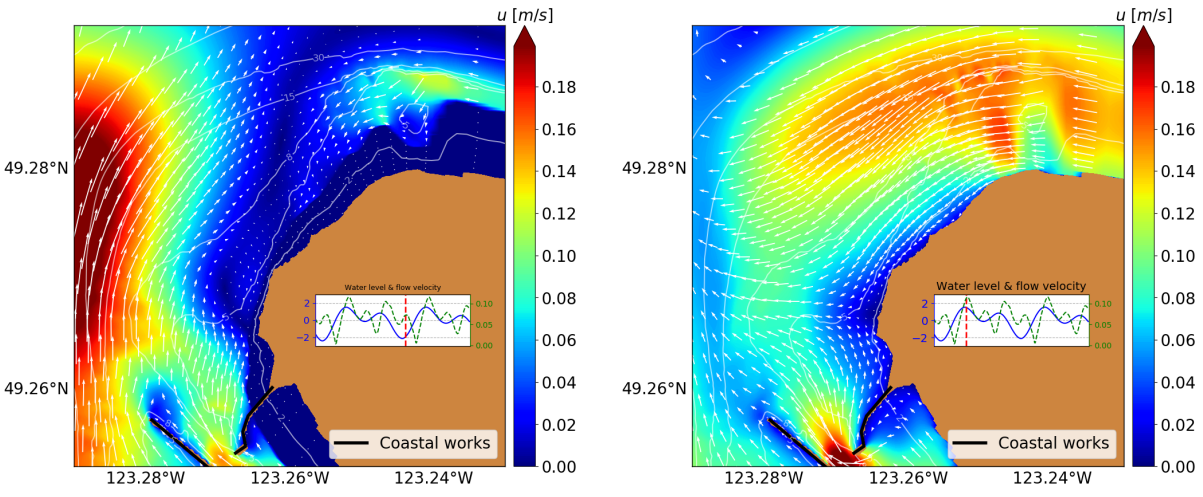

(a) During flood.

(b) During ebb.

Figure F.1: Difference in flow pattern during flood and ebb conditions of scenario 3 (low river discharge, storm wind enabled, waves disabled).

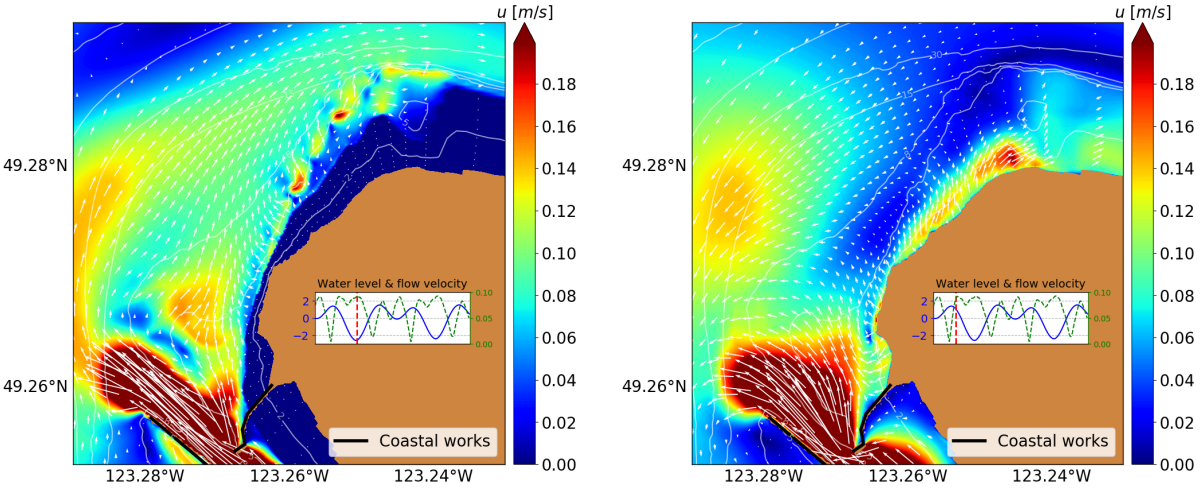

(a) During flood.

(b) During ebb.

Figure F.2: Difference in flow pattern during flood and ebb conditions of scenario 4 (high river discharge, storm wind and waves enabled).

Lastly Figure F.3 is presented here. This scenarios results are comparable the results of scenario 5 in Figure 7.2.

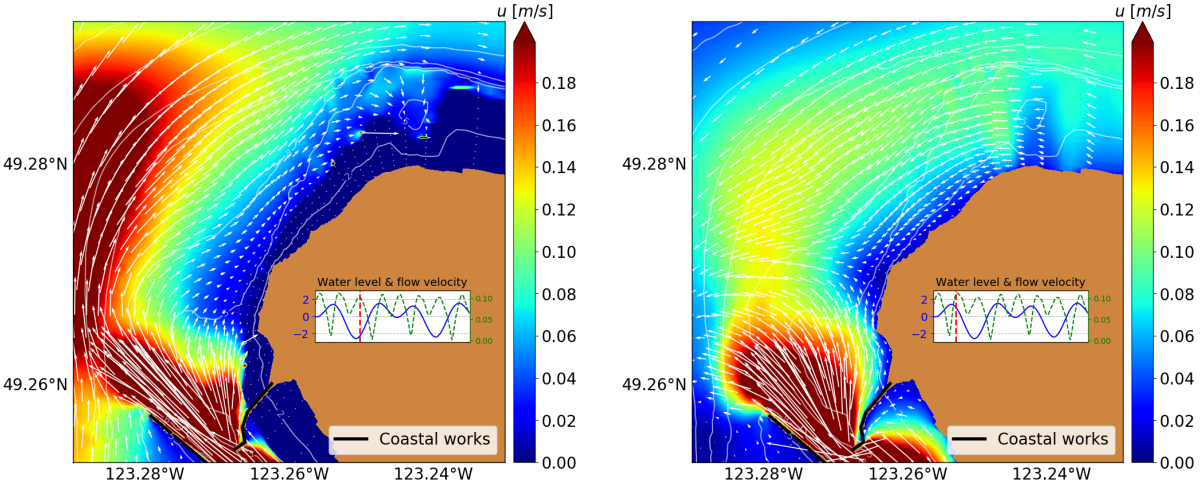

(a) During flood.

(b) During ebb.

Figure F.3: Difference in flow pattern during flood and ebb conditions of scenario 12 (high river discharge, waves disabled).

The wave field of scenario 5 (Figure F.4) is also presented here, since it very similar to the results of scenario 1 (Figure 7.4) and seems unnecessary to present them together in the same section.

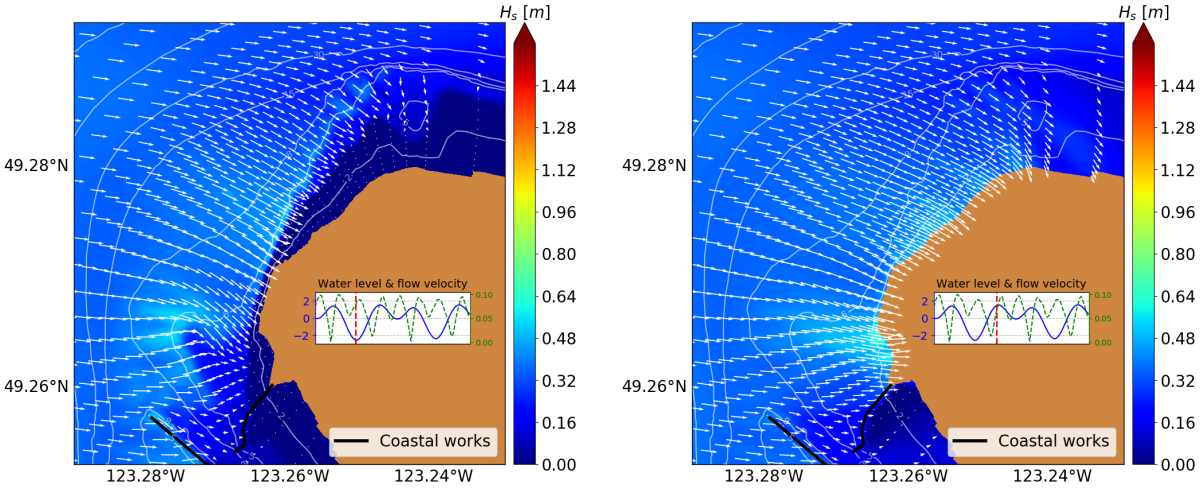

(a) During low water.

(b) During high water.

Figure F.4: Difference in significant wave heights during high and low waters of scenario 5 (high river discharge, waves enabled).

F.2. Model sediment transport results

In this appendix the modeled sediment transports over the cross-sections due to different scenarios from Table 5.1. These results represent a two-day simulation. From these figures the mean sediment transport are used further in the calculation of sediment transport in Tables F.1 through F.12.

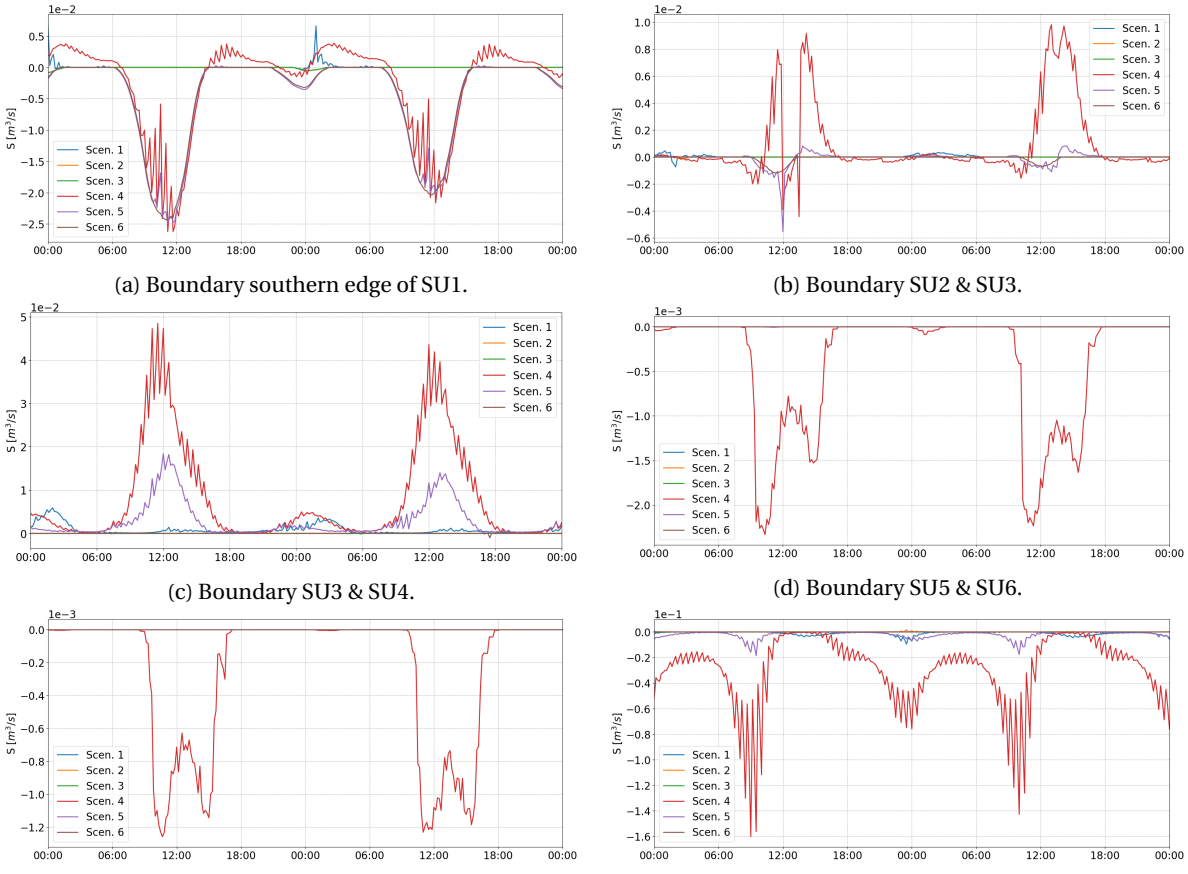

(a) Boundary southern edge of SU1.

(b) Boundary SU2 & SU3.

(c) Boundary SU3 & SU4.

(d) Boundary SU5 & SU6.

(e) Boundary SU6 & SU7.

(f) Boundary SU1 top.

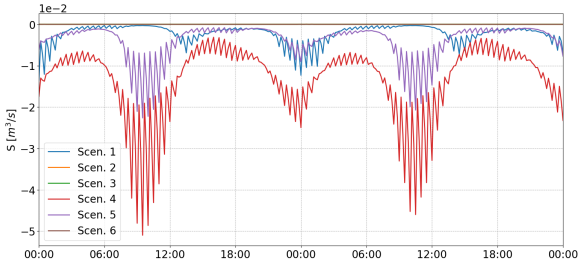

(g) Boundary SU2 top.

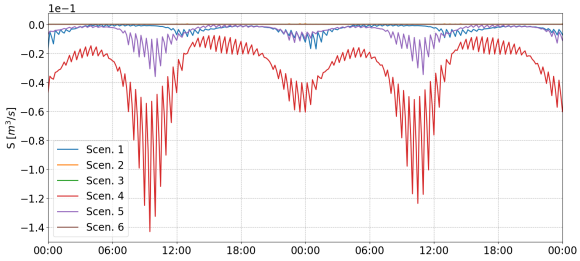

(h) Boundary SU3 top.

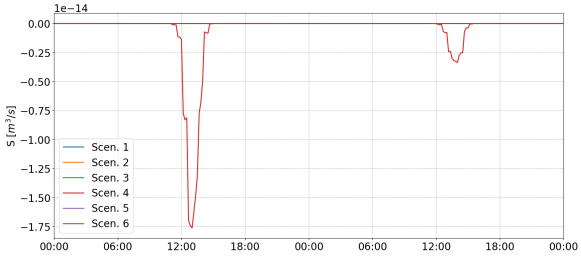

(i) Boundary SU4 top.

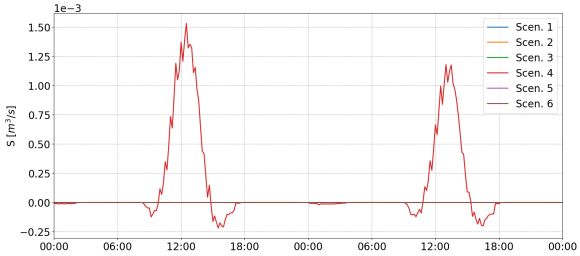

(j) Boundary SU5 top.

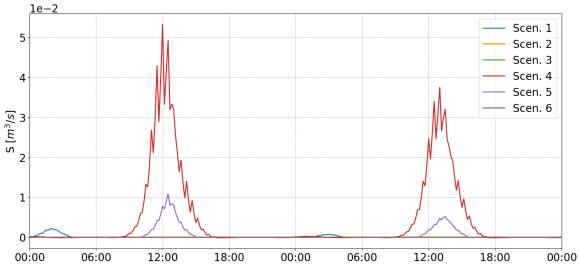

(k) Boundary SU6 top.

Figure F.5: Sediment transport through all boundaries of the proposed SUs calculated by the model during all the scenarios.

Tables F.1 through F.12 shows usage of the computed mean sediment transports mentioned above. The results are the sediment transport of each cross-section from all scenarios presented in Figure 7.8.

Table F.1: Yearly sediment transport computation over cross-section SU1 south.

	Mean transport $[m^3 s^{-1}]$	**Days**	**Coefficient**	**Occur.**	**Total transport** $[m^3 y^{-1}]$
Scenario 1	$1.11 \cdot 10^{-4}$	302	1	0.339	-982
Scenario 2	$-3.70 \cdot 10^{-5}$	302	1	0.661	-638
Scenario 3	$-3.53 \cdot 10^{-5}$	0.083	0.2	-	0
Scenario 4	$-2.63 \cdot 10^{-3}$	0.083	0.2	-	-4
Scenario 5	$-4.39 \cdot 10^{-3}$	63	1	0.405	-9,678
Scenario 6	$-4.34 \cdot 10^{-3}$	63	1	0.595	-14,055
Total	-	-	-	-	-25,357

Table F.2: Yearly sediment transport computation over cross-section SU1 top.

	Mean transport $[m^3 s^{-1}]$	**Days**	**Coefficient**	**Occur.**	**Total transport** $[m^3 y^{-1}]$
Scenario 1	$-1.01 \cdot 10^{-3}$	302	1	0.339	-8,934
Scenario 2	$5.09 \cdot 10^{-5}$	302	1	0.661	878
Scenario 3	$1.11 \cdot 10^{-8}$	0.083	0.2	-	0
Scenario 4	$-2.93 \cdot 10^{-2}$	0.083	0.2	-	-42
Scenario 5	$-2.01 \cdot 10^{-3}$	63	1	0.405	-4,431
Scenario 6	$-2.64 \cdot 10^{-9}$	63	1	0.595	0
Total	-	-	-	-	-12,529

Table F.3: Yearly sediment transport computation over cross-section SU2-3.

	Mean transport $[m^3 s^{-1}]$	**Days**	**Coefficient**	**Occur.**	**Total transport** $[m^3 y^{-1}]$
Scenario 1	$3.27 \cdot 10^{-5}$	302	1	0.339	289
Scenario 2	$-2.60 \cdot 10^{-6}$	302	1	0.661	45
Scenario 3	$-1.61 \cdot 10^{-14}$	0.083	0.2	-	0
Scenario 4	$8.56 \cdot 10^{-5}$	0.083	0.2	-	0
Scenario 5	$-8.39 \cdot 10^{-5}$	63	1	0.405	-185
Scenario 6	$-8.87 \cdot 10^{-5}$	63	1	0.595	-287
Total	-	-	-	-	-138

Table F.4: Yearly sediment transport computation over cross-section SU2 top.

	Mean transport [$m^3 s^{-1}$]	**Days**	**Coefficient**	**Occur.**	**Total transport** [$m^3 y^{-1}$]
Scenario 1	$-2.21 \cdot 10^{-3}$	302	1	0.339	-19,548
Scenario 2	$7.40 \cdot 10^{-7}$	302	1	0.661	13
Scenario 3	$3.40 \cdot 10^{-8}$	0.083	0.2	-	0
Scenario 4	$-1.34 \cdot 10^{-2}$	0.083	0.2	-	-19
Scenario 5	$-3.93 \cdot 10^{-3}$	63	1	0.405	-8,664
Scenario 6	$-1.04 \cdot 10^{-7}$	63	1	0.595	0
Total	-	-	-	-	-28,218

Table F.5: Yearly sediment transport computation over cross-section SU3-4.

	Mean transport [$m^3 s^{-1}$]	**Days**	**Coefficient**	**Occur.**	**Total transport** [$m^3 y^{-1}$]
Scenario 1	$8.28 \cdot 10^{-4}$	302	1	0.339	7,324
Scenario 2	$8.41 \cdot 10^{-8}$	302	1	0.661	1
Scenario 3	$-9.75 \cdot 10^{-9}$	0.083	0.2	-	0
Scenario 4	$8.00 \cdot 10^{-3}$	0.083	0.2	-	12
Scenario 5	$2.75 \cdot 10^{-3}$	63	1	0.405	6,062
Scenario 6	$-3.61 \cdot 10^{-6}$	63	1	0.595	-12
Total	-	-	-	-	13,387

Table F.6: Yearly sediment transport computation over cross-section SU3 top.

	Mean transport [$m^3 s^{-1}$]	**Days**	**Coefficient**	**Occur.**	**Total transport** [$m^3 y^{-1}$]
Scenario 1	$-3.09 \cdot 10^{-3}$	302	1	0.339	-27,332
Scenario 2	$2.50 \cdot 10^{-5}$	302	1	0.661	431
Scenario 3	$7.99 \cdot 10^{-8}$	0.083	0.2	-	0
Scenario 4	$-3.32 \cdot 10^{-2}$	0.083	0.2	-	-48
Scenario 5	$-5.37 \cdot 10^{-3}$	63	1	0.405	-11,838
Scenario 6	$4.72 \cdot 10^{-8}$	63	1	0.595	0
Total	-	-	-	-	-38,787

Table F.7: Yearly sediment transport computation over cross-section SU4-5.

	Mean transport $[m^3 s^{-1}]$	**Days**	**Coefficient**	**Occur.**	**Total transport** $[m^3 y^{-1}]$
Scenario 1	$-1.19 \cdot 10^{-19}$	302	1	0.339	0
Scenario 2	$-2.92 \cdot 10^{-21}$	302	1	0.661	0
Scenario 3	$-1.42 \cdot 10^{-23}$	0.083	0.2	-	0
Scenario 4	$-4.08 \cdot 10^{-4}$	0.083	0.2	-	-7
Scenario 5	$-1.64 \cdot 10^{-7}$	63	1	0.405	-1
Scenario 6	$-3.23 \cdot 10^{-9}$	63	1	0.595	0
Total	-	-	-	-	-8

Table F.8: Yearly sediment transport computation over cross-section SU4 top.

	Mean transport $[m^3 s^{-1}]$	**Days**	**Coefficient**	**Occur.**	**Total transport** $[m^3 y^{-1}]$
Scenario 1	$-3.68 \cdot 10^{-39}$	302	1	0.339	0
Scenario 2	$-7.65 \cdot 10^{-36}$	302	1	0.661	0
Scenario 3	$-4.88 \cdot 10^{-36}$	0.083	0.2	-	0
Scenario 4	$-6.09 \cdot 10^{-16}$	0.083	0.2	-	0
Scenario 5	$-3.46 \cdot 10^{-39}$	63	1	0.405	0
Scenario 6	$-9.36 \cdot 10^{-36}$	63	1	0.595	0
Total	-	-	-	-	0

Table F.9: Yearly sediment transport computation over cross-section SU5-6.

	Mean transport $[m^3 s^{-1}]$	**Days**	**Coefficient**	**Occur.**	**Total transport** $[m^3 y^{-1}]$
Scenario 1	$-2.68 \cdot 10^{-28}$	302	1	0.339	0
Scenario 2	$-2.99 \cdot 10^{-32}$	302	1	0.661	0
Scenario 3	$-2.42 \cdot 10^{-33}$	0.083	0.2	-	0
Scenario 4	$-2.50 \cdot 10^{-4}$	0.083	0.2	-	0
Scenario 5	$4.64 \cdot 10^{-23}$	63	1	0.405	0
Scenario 6	$-3.64 \cdot 10^{-20}$	63	1	0.595	0
Total	-	-	-	-	0

Table F.10: Yearly sediment transport computation over cross-section SU5 top.

	Mean transport [$m^3 s^{-1}$]	**Days**	**Coefficient**	**Occur.**	**Total transport** [$m^3 y^{-1}$]
Scenario 1	$-3.15 \cdot 10^{-15}$	302	1	0.339	0
Scenario 2	$-1.59 \cdot 10^{-24}$	302	1	0.661	0
Scenario 3	$-1.16 \cdot 10^{-22}$	0.083	0.2	-	0
Scenario 4	$1.16 \cdot 10^{-4}$	0.083	0.2	-	0
Scenario 5	$-1.13 \cdot 10^{-13}$	63	1	0.405	0
Scenario 6	$-4.44 \cdot 10^{-22}$	63	1	0.595	0
Total	-	-	-	-	0

Table F.11: Yearly sediment transport computation over cross-section SU6 east.

	Mean transport [$m^3 s^{-1}$]	**Days**	**Coefficient**	**Occur.**	**Total transport** [$m^3 y^{-1}$]
Scenario 1	$-1.20 \cdot 10^{-4}$	302	1	0.339	-1,061
Scenario 2	$2.57 \cdot 10^{-8}$	302	1	0.661	1
Scenario 3	$1.45 \cdot 10^{-8}$	0.083	0.2	-	0
Scenario 4	$-2.63 \cdot 10^{-3}$	0.083	0.2	-	-4
Scenario 5	$-2.30 \cdot 10^{-4}$	63	1	0.405	-507
Scenario 6	$-9.17 \cdot 10^{-9}$	63	1	0.595	0
Total	-	-	-	-	-1,571

Table F.12: Yearly sediment transport computation over cross-section SU6 top.

	Mean transport [$m^3 s^{-1}$]	**Days**	**Coefficient**	**Occur.**	**Total transport** [$m^3 y^{-1}$]
Scenario 1	$1.03 \cdot 10^{-4}$	302	1	0.339	911
Scenario 2	$-2.28 \cdot 10^{-13}$	302	1	0.661	0
Scenario 3	$-4.52 \cdot 10^{-18}$	0.083	0.2	-	0
Scenario 4	$4.37 \cdot 10^{-3}$	0.083	0.2	-	6
Scenario 5	$6.00 \cdot 10^{-4}$	63	1	0.405	1,323
Scenario 6	$-5.76 \cdot 10^{-16}$	63	1	0.595	0
Total	-	-	-	-	2,240

G

Model sensitivity analysis results

In Figure G.1 the results of the sensitivity cases are shown and compared to its original scenario 1. Again the mean sediment transport are calculated from these results and compared to the original mean sediment transport from Tables F.1 through F.12.

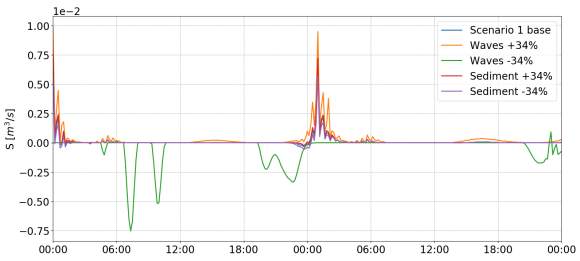

(a) Cross-section SU1 south.

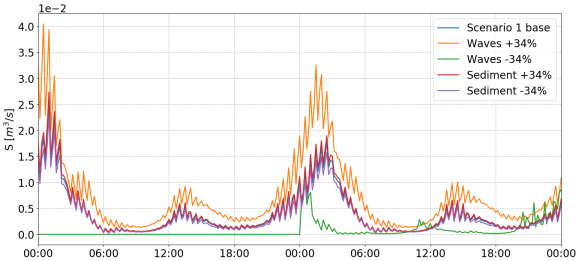

(b) Cross-section SU1-2.

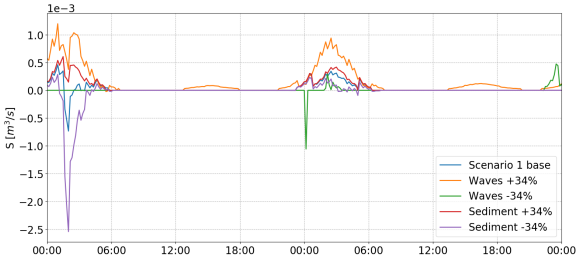

(c) Cross-section SU2-3.

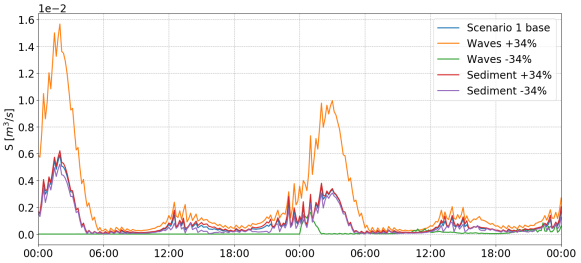

(d) Cross-section SU3-4.

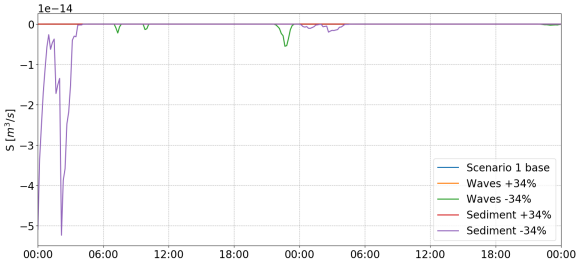

(e) Cross-section SU4-5.

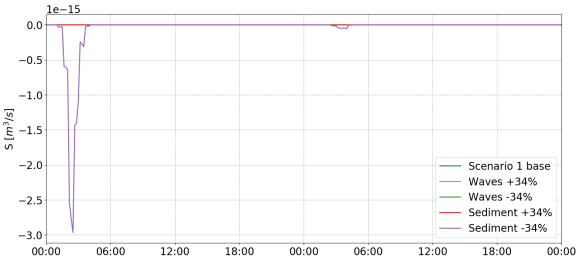

(f) Cross-section SU5-6.

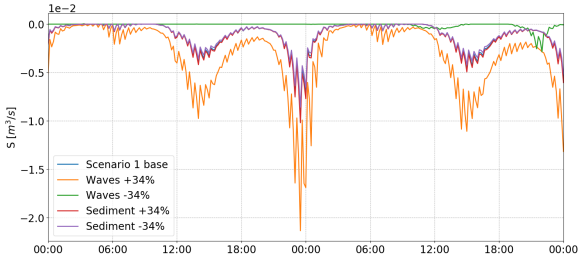

(g) Cross-section SU1 top.

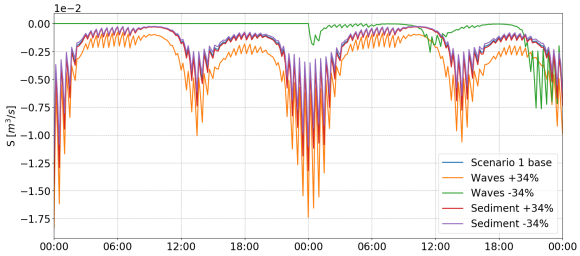

(h) Cross-section SU2 top.

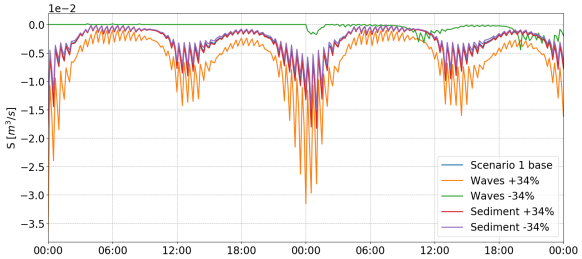

(i) Cross-section SU3 top.

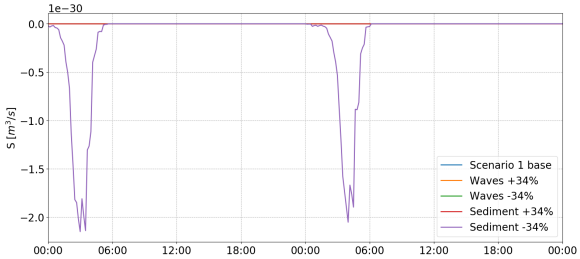

(j) Cross-section SU4 top.

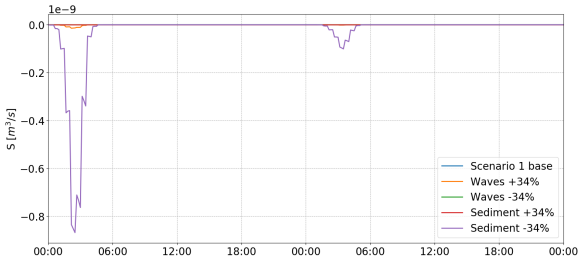

(k) Cross-section SU5 top.

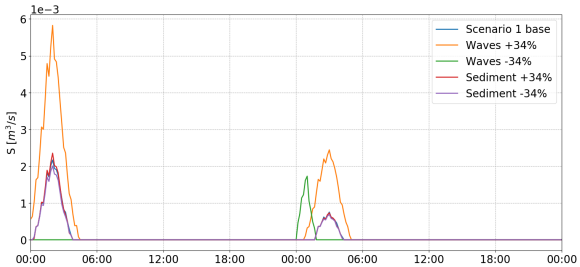

(l) Cross-section SU6 top.

Figure G.1: Sediment transport through all boundaries of the proposed SUs calculated by the model during the sensitivity analysis.

Tables G.1 through G.9 show the resulting mean sediment transport of each of the sensitivity cases and compared to the original result. Not all cross-sections are included here, the cross-sections with zero transport (Tables F.8, F.7, and F.10) are thus excluded.

Table G.1: Comparison between sediments transport of regular and sensitivity cases for cross-section SU1 south.

	Mean transport $[m^3 s^{-1}]$	**Base case** $[m^3 s^{-1}]$	**Relative in- or decrease**
Waves +34%	$2.94 \cdot 10^{-4}$	$1.11 \cdot 10^{-4}$	+120%
Waves -34%	$-1.10 \cdot 10^{-5}$	$1.11 \cdot 10^{-4}$	-109%
Sediment +34%	$1.31 \cdot 10^{-4}$	$1.11 \cdot 10^{-4}$	+18%
Sediment -34%	$1.10 \cdot 10^{-4}$	$1.11 \cdot 10^{-4}$	0%

Table G.2: Comparison between sediments transport of regular and sensitivity cases for cross-section SU1 top.

	Mean transport $[m^3 s^{-1}]$	**Base case** $[m^3 s^{-1}]$	**Relative in- or decrease**
Waves +34%	$-3.06 \cdot 10^{-3}$	$-1.10 \cdot 10^{-3}$	+178%
Waves -34%	$-2.14 \cdot 10^{-4}$	$-1.10 \cdot 10^{-3}$	-81%
Sediment +34%	$-1.15 \cdot 10^{-3}$	$-1.10 \cdot 10^{-3}$	+5%
Sediment -34%	$-1.10 \cdot 10^{-3}$	$-1.10 \cdot 10^{-3}$	0%

Table G.3: Sediments transports during the sensitivity cases over the SU1 to SU2 cross-section.

	Mean transport $[m^3 s^{-1}]$	**Base case** $[m^3 s^{-1}]$	**Relative in- or decrease**
Waves +34%	$7.31 \cdot 10^{-3}$	$3.97 \cdot 10^{-3}$	+84%
Waves -34%	$1.37 \cdot 10^{-3}$	$3.97 \cdot 10^{-3}$	-65%
Sediment +34%	$4.29 \cdot 10^{-3}$	$3.97 \cdot 10^{-3}$	+8%
Sediment -34%	$3.97 \cdot 10^{-3}$	$3.97 \cdot 10^{-3}$	0%

Table G.4: Comparison between sediments transport of regular and sensitivity cases for cross-section SU2 top.

	Mean transport $[m^3 s^{-1}]$	**Base case** $[m^3 s^{-1}]$	**Relative in- or decrease**
Waves +34%	$-3.81 \cdot 10^{-3}$	$-2.21 \cdot 10^{-3}$	+72%
Waves -34%	$-9.46 \cdot 10^{-4}$	$-2.21 \cdot 10^{-3}$	-57%
Sediment +34%	$-2.36 \cdot 10^{-3}$	$-2.21 \cdot 10^{-3}$	+7%
Sediment -34%	$-2.21 \cdot 10^{-3}$	$-2.21 \cdot 10^{-3}$	0%

Table G.5: Comparison between sediments transport of regular and sensitivity cases for cross-section SU2-3.

	Mean transport [$m^3 s^{-1}$]	**Base case** [$m^3 s^{-1}$]	**Relative in- or decrease**
Waves +34%	$1.52 \cdot 10^{-4}$	$3.27 \cdot 10^{-5}$	+365%
Waves -34%	$2.61 \cdot 10^{-5}$	$3.27 \cdot 10^{-5}$	-20%
Sediment +34%	$6.07 \cdot 10^{-5}$	$3.27 \cdot 10^{-5}$	+85%
Sediment -34%	$3.27 \cdot 10^{-4}$	$3.27 \cdot 10^{-5}$	0%

Table G.6: Comparison between sediments transport of regular and sensitivity cases for cross-section SU3 top.

	Mean transport [$m^3 s^{-1}$]	**Base case** [$m^3 s^{-1}$]	**Relative in- or decrease**
Waves +34%	$-6.41 \cdot 10^{-3}$	$-3.09 \cdot 10^{-3}$	+107%
Waves -34%	$-8.30 \cdot 10^{-4}$	$-3.09 \cdot 10^{-3}$	-73%
Sediment +34%	$-3.28 \cdot 10^{-3}$	$-3.09 \cdot 10^{-3}$	+6%
Sediment -34%	$-3.09 \cdot 10^{-3}$	$-3.09 \cdot 10^{-3}$	0%

Table G.7: Comparison between sediments transport of regular and sensitivity cases for cross-section SU3-4.

	Mean transport [$m^3 s^{-1}$]	**Base case** [$m^3 s^{-1}$]	**Relative in- or decrease**
Waves +34%	$2.27 \cdot 10^{-3}$	$8.28 \cdot 10^{-4}$	+174%
Waves -34%	$1.45 \cdot 10^{-4}$	$8.28 \cdot 10^{-4}$	-82%
Sediment +34%	$9.04 \cdot 10^{-4}$	$8.28 \cdot 10^{-4}$	+9%
Sediment -34%	$8.28 \cdot 10^{-4}$	$8.28 \cdot 10^{-4}$	0%

Table G.8: Comparison between sediments transport of regular and sensitivity cases for cross-section SU6 east.

	Mean transport [$m^3 s^{-1}$]	**Base case** [$m^3 s^{-1}$]	**Relative in- or decrease**
Waves +34%	$-2.64 \cdot 10^{-4}$	$-1.20 \cdot 10^{-4}$	+120%
Waves -34%	$-3.40 \cdot 10^{-5}$	$-1.20 \cdot 10^{-4}$	-72%
Sediment +34%	$-1.34 \cdot 10^{-4}$	$-1.20 \cdot 10^{-4}$	+12%
Sediment -34%	$-1.20 \cdot 10^{-4}$	$-1.20 \cdot 10^{-4}$	0%

Table G.9: Comparison between sediments transport of regular and sensitivity cases for cross-section SU6 top.

	Mean transport $[m^3 s^{-1}]$	**Base case** $[m^3 s^{-1}]$	**Relative in- or decrease**
Waves +34%	$3.50 \cdot 10^{-4}$	$1.03 \cdot 10^{-4}$	+239%
Waves -34%	$5.76 \cdot 10^{-6}$	$1.03 \cdot 10^{-4}$	-94%
Sediment +34%	$1.05 \cdot 10^{-3}$	$1.03 \cdot 10^{-4}$	+1%
Sediment -34%	$1.03 \cdot 10^{-4}$	$1.03 \cdot 10^{-4}$	0%

Bibliography

Ages, A. and Woollard, A. (1976). The tides in the fraser estuary. *Pacific Marine Science Report*, pages 76–5.

Armstrong, J. E. (1990). *Vancouver Geology*.

Atkins, R. J., Tidd, M., and Ruffo, G. (2016). Sturgeon bank, fraser river delta, bc, canada: 150 years of human influences on salt marsh sedimentation. *Journal of Coastal Research*, 75(sp1):790–794.

Attard, M. E., Venditti, J. G., and Church, M. (2014). Suspended sediment transport in fraser river at mission, british columbia: New observations and comparison to historical records. *Canadian Water Resources Journal*, 39(3):356–371.

Ayranci, K. (2014). Facies Modelling of a Tide-Influenced, River-Dominated Delta, Fraser River Delta, British Columbia, Canada.

Barrie, J. V. and Currie, R. G. (2000). Human impact on the sedimentary regime of the fraser river delta, canada. *Journal of Coastal Research*, pages 747–755.

Booij, N., Ris, R. C., and Holthuijsen, L. H. (1999). A third-generation wave model for coastal regions: 1. Model description and validation. *Journal of Geophysical Research: Oceans*, 104(C4):7649–7666.

Bosboom, J. and Stive, M. J. F. (2015). *Lecture notes Coastal Dynamics 1*. VSSD.

Bros, W. J. (2007). Sustainable Dredging Program on the Lower Fraser River.

Cantoni, I., Gaido, C., Jonker, T., and van Gijzen, L. (2019). Cliff erosion at point grey ubc.

CBC News (2013). Landslide hits Vancouver nudist beach.

CBC News (2014). Wreck Beach: man's body found in debris below cliffs.

Church, J. A., Clark, P. U., Cazenave, A., Gregory, J. M., Jevrejeva, S., Levermann, A., Merrifield, M. A., Milne, G. A., Nerem, R. S., Nunn, P. D., Payne, A. J., Pfeffer, W. T., Stammer, D., and Unnikrishnan, A. S. (2013). 2013: Sea Level Change. *Climate Change 2013: The Physical Science Basis. Contribution of Working Group I to the Fifth Assessment Report of the Intergovernmental Panel on Climate Change*, pages 1137–1216.

Church, M. (2010). Sustaining Fraser Estuary; Bases for a sediment management plan.

Clague, J. J. (1976). Quadra sand and its relation to the late wisconsin glaciation of southwest british columbia. *Canadian Journal of Earth Sciences*, 13(6):803–815.

Collins, B. D. and Sitar, N. (2008). Processes of coastal bluff erosion in weakly lithified sands, Pacifica, California, USA. *Geomorphology*, 97(3-4):483–501.

de Vriend, H. J., van Koningsveld, M., Aarninkhof, S. G. J., de Vries, M. B., and Baptist, M. J. (2015). Sustainable hydraulic engineering through building with nature. *Journal of Hydro-environment Research*, 9(2):159–171.

Deltares (2011a). *Delft3D FLOW: User Manual*.

Deltares (2011b). *Delft3D TIDE: User Manual*.

Deltares (2011c). *Delft3D WAVE: User Manual*.

Downie, K. A. and Saaltink, H. (1983). An Artificial Cobble Beach for Erosion Control.

Doyle, D. (2018). private communcation.

Dronkers, J. (2005). *Dynamics of Coastal Systems*. WORLD SCIENTIFIC PUB CO INC.

Edil, T. B. and Vallejo, L. E. (1980). Mechanics of coastal landslides and the influence of slope parameters. *Engineering Geology*, 16(1-2):83–96.

Einsele, G. (2013). *Sedimentary Basins*.

Emery, K. O. and Kuhn, G. G. (1982). Sea cliffs: Their processes, profiles, and classification. *Geological Society of America Bulletin*, 93(7):644.

Environmental Reporting British Columbia (2017). Change in Sea Level in B.C.

Ferguson, A. (1991). Navigation, dredging and environment in the Fraser River Estuary.

Fraser Estuary Management Program (2006). Fraser River Estuary Management Plan.

FREMP (2007). Sediment Budget & Dredging Activities Annual Report.

French, T. D. and Chambers, P. A. (1997). Reducing flows in the Nechako River (British Columbia, Canada): potential response of the macrophyte community. *Canadian Journal of Fisheries and Aquatic Sciences*, 54(10):2247–2254.

Galloway, W. E. (1975). Process framework for describing the morphologic and stratigraphic evolution of deltaic depositional systems. *Deltas: Models for Exploration*.

Golder Associates Ltd. (2015). Point Grey Cliff Erosion Study. techreport, Golder Associates Ltd.

Gracia, F. J., Anfuso, G., Benavente, J., Río, L. D., Domínguez, L., and Martínez, J. A. (2005). Monitoring coastal erosion at different temporal scales on sandy beaches: Application to the spanish gulf of cadiz coast. *Journal of Coastal Research*, (SPEC. ISSUE 49):22–27. Cited By :4.

Hampton, M. A., Griggs, G. B., Edil, T. B., Guy, D. E., Kelley, J. T., Komar, P. D., Mickelson, D. M., and Shipman, H. M. (2004). Processes that govern the formation and evolution of coastal cliffs. *US Geological Survey Professional Paper*, (1693):7–38. Cited By 19.

Hart, D. (2018). personal communcation.

Howard, A. D. and McLane, C. F. (1988). Erosion of cohesionless sediment by groundwater seepage. *Water Resources Research*, 24(10):1659–1674.

Howes, D., Harper, J., and Owens, E. (2018). Physical shore-zone mapping system for british columbia.

Isfeld, E. O., Stepchuk, F., and Atkins, R. J. (1996). A Channel Maintenance Management Study: Lower Fraser Sandheads to Patullo Bridge including North and Middle Arms. *CWRA*, pages 191–196.

Johannessen, S. C. and Macdonald, R. W. (2009). Effects of local and global change on an inland sea: the strait of georgia, british columbia, canada. *Climate Research*, 40:1–21.

Johannessen, S. C., Macdonald, R. W., and Paton, D. W. (2003). A sediment and organic carbon budget for the greater Strait of Georgia. *Estuarine, Coastal and Shelf Science*, 56(3-4):845–860.

Kamphuis, J. W. (2000). *Introduction to Coastal Engineering and Management*. Advanced Series on Ocean Engineering (Hardcover) Series. World Scientific.

Lau, A. (2015). Connecting communities: principles for musqueam-ubc collaboration.

Lee, E. M. (2008). Coastal cliff behaviour: Observations on the relationship between beach levels and recession rates. *Geomorphology*, 101(4):558–571.

Lee, E. M. and Clark, A. R. (2002). *Investigation and Management of Soft Rock Cliffs*. Thomas Telford Publishing.

Lem, G. N. (1974). Shore changes and sand movementat the south shore of english bay, vancouver, canada.

Levings, C. D. (1980). Consequences of training walls and jetties for aquatic habitats at two British Columbia estuaries. *Coastal Engineering*, 4:111–136.

Luijendijk, A. P. (2001). Validation, calibration and evaluation of Delft3D-FLOW model with ferry measurements.

Lum, K. (1975). Erosion of the point grey cliffs.

McLaren, P. and Ren, P. (1995). Sediment transport and its environmental implications in the lower Fraser River and Fraser delta.

McLean, D. (1975). Marine erosion at towers beach, university of british columbia.

McLean, D. G., Church, M., and Tassone, B. (1999). Sediment transport along lower Fraser River: 1. Measurements and hydraulic computations. *Water Resources Research*, 35(8):2533–2548.

Milliman, J. D. (1980). Sedimentation in the Fraser River and its estuary, southwestern British Columbia (Canada). *Estuarine and Coastal Marine Science*, 10(6):609–633.

Mines, and Resources (Canada) Energy (1980). *The Coastline of Canada: Littoral Processes and Shore Morphology*. Canadian Government Publishing Centre.

Moore, R. and Davis, G. (2014). Cliff instability and erosion management in England and Wales. *Journal of Coastal Conservation*, 19(6):771–784.

nhc (2008). Comprehensive Review of Fraser River at Hope, Flood Hydrology and Flowss - Scoping Study.

Northwest Hydraulic Consultants (2002). Review of the lower Fraser River sediment budget: Final report.

Pawlowicz, R., Costanzo, R. D., Halverson, M., Devred, E., and Johannessen, S. (2017). Advection, Surface Area, and Sediment Load of the Fraser River Plume Under Variable Wind and River Forcing. *Atmosphere-Ocean*, 55(4-5):293–313.

Piteau Associates (2002). Hydrogeological and geotechnical assessment of northwest area ubc campus, vancouver. Technical report, Piteau Associates.

Pool, M. I. (1975). Sand sources, volumes and movement patterns on wreck beach, vancouver, british columbia.

R. A. Spence Ltd. (1967). Investigation of foundation conditions for proposed residences and stability of cliff against seismic forces - fort camp area, u.b.c.

Richmond (2000). City of Richmond Dyke System.

Roelvink, D., Reniers, A., van Dongeren, A., van Thiel de Vries, J., McCall, R., and Lescinski, J. (2009). Modelling storm impacts on beaches, dunes and barrier islands. *Coastal Engineering*, 56(11-12):1133–1152.

Ruggiero, P., Komar, P. D., McDougal, W. G., Marra, J. J., and Beach, R. A. (2001). Wave runup, extreme water levels and the erosion of properties backing beaches. *Journal of Coastal Research*, 17(2):407–419. cited By 186.

Sandwell, Pitaeu Associates, and Trow (2004). Comprehensive Hydrogeology and Cliff Erosion Assessment of Point Grey.

Shaw, J., Taylor, R. B., Forbes, D. L., Ruz, M. H., and Solomon, S. (1998). Sensitivity of the coasts of canada to sea-level rise.

Silvester, R. (1974). *Coastal Engineering*. Number v. 1 in Developments in Sedimentology. Elsevier Scientific Publishing Company.

Sunumura, T. (2015). Rocky coast processes: with special reference to the recession of soft rock cliffs. *Proceedings of the Japan Academy, Series B*, 91(9):481–500.

Thomas, C. A. and Bendell-Young, L. I. (1999). The Significance of Diagenesis versus Riverine Input in Contributing to the Sediment Geochemical Matrix of Iron and Manganese in an Intertidal Region. *Estuarine, Coastal and Shelf Science*, 48(6):635–647.

Thomson, R. E. (1981). *Oceanography of the British Columbia Coast*. Gordon Soules Book Pub.

Tinis, S. (2017). BC Storm Surge Forecasting System.

UBC (2004). North campus neighbourhood plan.

UBC/Pacific Spirit Regional Park Cliff Management (2000). Point grey cliffs need your help. 2210 West Mall Vancouver, B.C. V6T 1Z4.

U.S. Army Corps of Engineers (2002). *CEM: Coastal Engineering Manual*. U.S. Army Corps of Engineers.

van den Bos, J. P. and Verhagen, H. J. (2018). *Lecture Notes CIE5308*.

Van Osch, E. (1990). Coastal bluff erosion in the Strait of Georgia region: Geomorphology and management.

van Rijn, L. C., Roelvink, J. A., and Horst, W. T. (2000). Approximation formulae for sand transport by currents and waves and implementation in DELFT-MOR.